

CITATION REPORT

List of articles citing

Discovery of a three-dimensional topological Dirac semimetal, Na₃Bi

DOI: 10.1126/science.1245085
Science, 2014, 343, 864-7.

Source: <https://exaly.com/paper-pdf/59014066/citation-report.pdf>

Version: 2024-04-17

This report has been generated based on the citations recorded by exaly.com for the above article. For the latest version of this publication list, visit the link given above.

The third column is the impact factor (IF) of the journal, and the fourth column is the number of citations of the article.

#	Paper	IF	Citations
1749	Topological insulator to Dirac semimetal transition driven by sign change of spin-orbit coupling in thallium nitride. 2014 , 90,		35
1748	Chiral anomaly and diffusive magnetotransport in Weyl metals. 2014 , 113, 247203		170
1747	Chiral viscoelastic response in Weyl semimetals. 2014 , 108, 37007		13
1746	Holographic interaction effects on transport in Dirac semimetals. 2014 , 90,		10
1745	Tunable line node semimetals. 2014 , 90,		101
1744	Quantum transport of disordered Weyl semimetals at the nodal point. 2014 , 113, 026602		133
1743	Long-range interaction induced phases in Weyl semimetals. 2014 , 89,		20
1742	Three-dimensional massless Dirac fermions in carbon schwarzites. 2014 , 90,		27
1741	Weyl semimetals with short-range interactions. 2014 , 90,		58
1740	Molecular beam epitaxial growth of a three-dimensional topological Dirac semimetal Na ₃ Bi. 2014 , 105, 031901		31
1739	Topological tuning in three-dimensional dirac semimetals. 2014 , 113, 256403		45
1738	Thermoelectric properties of Weyl and Dirac semimetals. 2014 , 90,		143
1737	Stability of multinode Dirac semimetals against strong long-range correlations. 2014 , 90,		20
1736	Migdal's theorem and electron-phonon vertex corrections in Dirac materials. 2014 , 89,		22
1735	Interdimensional effects in systems with quasirelativistic dispersion relations. 2014 , 89,		2
1734	Classification of reflection-symmetry-protected topological semimetals and nodal superconductors. 2014 , 90,		200
1733	Probing the Chiral Anomaly with Nonlocal Transport in Three-Dimensional Topological Semimetals. 2014 , 4,		250

1732	Quantum transport evidence for the three-dimensional Dirac semimetal phase in Cd ₃ As ₂ . 2014 , 113, 246402	309
1731	Rare region effects dominate weakly disordered three-dimensional Dirac points. 2014 , 89,	104
1730	Lorentz invariance in chiral kinetic theory. 2014 , 113, 182302	144
1729	Topological response in ferromagnets. 2014 , 89,	17
1728	The crystal and electronic structures of Cd ₃ As ₂ , the three-dimensional electronic analogue of graphene. 2014 , 53, 4062-7	149
1727	A stable three-dimensional topological Dirac semimetal Cd ₃ As ₂ . 2014 , 13, 677-81	1010
1726	Observation of a three-dimensional topological Dirac semimetal phase in high-mobility Cd ₃ As ₂ . 2014 , 5, 3786	938
1725	Superconducting properties and electronic structure of NaBi. 2014 , 26, 212201	10
1724	Time-reversal-invariant topological superconductivity in doped Weyl semimetals. 2014 , 90,	91
1723	Anomalous Hall effect in Weyl metals. 2014 , 113, 187202	206
1722	Electric transport of a single-crystal iron chalcogenide FeSe superconductor: Evidence of symmetry-breakdown nematicity and additional ultrafast Dirac cone-like carriers. 2014 , 90,	67
1721	Quantum oscillations from surface Fermi arcs in Weyl and Dirac semimetals. 2014 , 5, 5161	346
1720	Superconducting properties of BaBi ₃ . 2014 , 27, 105001	24
1719	Marginal Fermi liquid versus excitonic instability in three-dimensional Dirac semimetals. 2014 , 90,	20
1718	Exploration and prediction of topological electronic materials based on first-principles calculations. 2014 , 39, 849-858	65
1717	Topological zero modes and Dirac points protected by spatial symmetry and chiral symmetry. 2014 , 90,	40
1716	Dirac materials. 2014 , 63, 1-76	589
1715	Condensed matter realization of the axial magnetic effect. 2014 , 89,	94

1714	Coulomb disorder in three-dimensional Dirac systems. 2014 , 90,	46
1713	Landau quantization and quasiparticle interference in the three-dimensional Dirac semimetal Cd ₃ As ₂ . 2014 , 13, 851-6	357
1712	Classification of stable three-dimensional Dirac semimetals with nontrivial topology. 2014 , 5, 4898	519
1711	Condensed-matter physics: Catching relativistic electrons. 2014 , 513, 319-20	7
1710	Quantum oscillations as a probe of interaction effects in Weyl semimetals in a magnetic field. 2014 , 90,	11
1709	Experimental realization of a three-dimensional Dirac semimetal. 2014 , 113, 027603	813
1708	Density response in Weyl metals. 2014 , 89,	38
1707	Ground-state phase in the three-dimensional topological Dirac semimetal Na ₃ Bi. 2014 , 89,	31
1706	Weyl and Dirac semimetals with Z ₂ topological charge. 2014 , 89,	66
1705	Dispersion of Fermi arcs in Weyl semimetals and their evolutions to Dirac cones. 2014 , 89,	97
1704	Diffusive quantum criticality in three-dimensional disordered Dirac semimetals. 2014 , 90,	65
1703	Quantum transport in Dirac materials: Signatures of tilted and anisotropic Dirac and Weyl cones. 2015 , 91,	92
1702	Probing the Fermi surface of three-dimensional Dirac semimetal Cd ₃ As ₂ through the de Haas-van Alphen technique. 2015 , 91,	35
1701	Weyl semimetal from spontaneous inversion symmetry breaking in pyrochlore oxides. 2015 , 91,	28
1700	Breakdown of three-dimensional Dirac semimetal state in pressurized Cd ₃ As ₂ . 2015 , 91,	30
1699	Topologically protected Dirac cones in compressed bulk black phosphorus. 2015 , 91,	74
1698	Dirac metal to topological metal transition at a structural phase change in Au ₂ Pb and prediction of Z ₂ topology for the superconductor. 2015 , 91,	37
1697	Correlation effects in double-Weyl semimetals. 2015 , 91,	47

1696	Surface Fermi arcs in Z2 Weyl semimetals A3Bi (A=Na, K, Rb). 2015, 91,	21
1695	Plasmon signature in Dirac-Weyl liquids. 2015, 91,	58
1694	Surface versus bulk Dirac state tuning in a three-dimensional topological Dirac semimetal. 2015, 91,	12
1693	Weak antilocalization and localization in disordered and interacting Weyl semimetals. 2015, 92,	75
1692	Interacting Dirac liquid in three-dimensional semimetals. 2015, 92,	28
1691	Topological node-line semimetal in three-dimensional graphene networks. 2015, 92,	488
1690	High-field magnetoconductivity of topological semimetals with short-range potential. 2015, 92,	83
1689	Collective modes, ac response, and magnetic properties of the three-dimensional Dirac semimetal in the triplet superconducting state. 2015, 92,	2
1688	Optical spectroscopy study of the three-dimensional Dirac semimetal ZrTe5. 2015, 92,	155
1687	Lifshitz transition and Van Hove singularity in a three-dimensional topological Dirac semimetal. 2015, 92,	28
1686	Axial anomaly and longitudinal magnetoresistance of a generic three-dimensional metal. 2015, 92,	139
1685	Large-gap two-dimensional topological insulator in oxygen functionalized MXene. 2015, 92,	169
1684	Topological nodal line semimetals with and without spin-orbital coupling. 2015, 92,	485
1683	Patterns of electromagnetic response in topological semimetals. 2015, 92,	38
1682	Chiral degeneracies and Fermi-surface Chern numbers in bcc Fe. 2015, 92,	56
1681	Many-body effects and ultraviolet renormalization in three-dimensional Dirac materials. 2015, 92,	40
1680	Quantum critical exponents for a disordered three-dimensional Weyl node. 2015, 92,	53
1679	Chiral electromagnetic waves in Weyl semimetals. 2015, 92,	29

1678	Kondo effect in three-dimensional Dirac and Weyl systems. 2015, 92,	45
1677	Phase diagram of the quantum electrodynamics of two-dimensional and three-dimensional Dirac semimetals. 2015, 92,	26
1676	Electronic cooling in Weyl and Dirac semimetals. 2015, 92,	33
1675	Magnetic catalysis and axionic charge density wave in Weyl semimetals. 2015, 92,	60
1674	Combined fast reversible liquidlike elastic deformation with topological phase transition in Na ₃ Bi. 2015, 92,	8
1673	Topological charges of three-dimensional Dirac semimetals with rotation symmetry. 2015, 92,	45
1672	Magnetic impurity in a Weyl semimetal. 2015, 92,	26
1671	Transversal magnetoresistance in Weyl semimetals. 2015, 92,	41
1670	Electron-hole compensation effect between topologically trivial electrons and nontrivial holes in NbAs. 2015, 92,	59
1669	Ruderman-Kittel-Kasuya-Yosida interaction in Weyl semimetals. 2015, 92,	43
1668	Optical evidence for a Weyl semimetal state in pyrochlore Eu ₂ Ir ₂ O ₇ . 2015, 92,	119
1667	Unidirectional transport in electronic and photonic Weyl materials by Dirac mass engineering. 2015, 92,	23
1666	Conductance fluctuations in chaotic bilayer graphene quantum dots. 2015, 92, 012918	8
1665	Topological Node-Line Semimetal and Dirac Semimetal State in Antiperovskite Cu ₃ PdN. 2015, 115, 036807	524
1664	Magnetic Field-Induced Insulator-Semimetal Transition in a Pyrochlore Nd ₂ Ir ₂ O ₇ . 2015, 115, 056402	66
1663	Helical Spin Order from Topological Dirac and Weyl Semimetals. 2015, 115, 076802	19
1662	Magnetoinfrared Spectroscopy of Landau Levels and Zeeman Splitting of Three-Dimensional Massless Dirac Fermions in ZrTe ₅ . 2015, 115, 176404	135
1661	Angular-Dependent Phase Factor of Shubnikov-de Haas Oscillations in the Dirac Semimetal Cd ₃ As ₂ . 2015, 115, 226401	51

1660	Universality of Plasmon Excitations in Dirac Semimetals. 2015 , 115, 236402	25
1659	Observation of the Chiral-Anomaly-Induced Negative Magnetoresistance in 3D Weyl Semimetal TaAs. 2015 , 5,	752
1658	Anisotropic Fermi Surface and Quantum Limit Transport in High Mobility Three-Dimensional Dirac Semimetal Cd3As2. 2015 , 5,	92
1657	Three-dimensional Dirac semimetals: Design principles and predictions of new materials. 2015 , 91,	163
1656	Floquet dynamics in two-dimensional semi-Dirac semimetals and three-dimensional Dirac semimetals. 2015 , 91,	39
1655	Superconductivity in Weyl metals. 2015 , 92,	89
1654	On the origin of minimal conductivity at a band crossing. 2015 , 92,	32
1653	Density of states and magnetotransport in Weyl semimetals with long-range disorder. 2015 , 92,	19
1652	Effects of anisotropy and disorder on the conductivity of Weyl semimetals. 2015 , 92,	6
1651	First-principles study of the large-gap three-dimensional topological insulators M3Bi2 (M=Ca, Sr, Ba). 2015 , 92,	7
1650	Temperature-dependent many-body effects in Dirac-Weyl materials: Interacting compressibility and quasiparticle velocity. 2015 , 92,	5
1649	RKKY interaction of magnetic impurities in Dirac and Weyl semimetals. 2015 , 92,	72
1648	Chiral separation and chiral magnetic effects in a slab: The role of boundaries. 2015 , 92,	14
1647	Collisions in Chiral Kinetic Theory. 2015 , 115, 021601	90
1646	Evidence for Half-Metallicity in n-type HgCr2Se4. 2015 , 115, 087002	52
1645	Dirac Semimetals in Two Dimensions. 2015 , 115, 126803	348
1644	Topological Superconductivity in Dirac Semimetals. 2015 , 115, 187001	94
1643	Experimental Discovery of Weyl Semimetal TaAs. 2015 , 5,	1167

1642	Current at a Distance and Resonant Transparency in Weyl Semimetals. 2015 , 5,	51
1641	Dirac and Weyl Semimetal in XYBi (X = Ba, Eu; Y = Cu, Ag and Au). 2015 , 5, 14423	43
1640	Observation of Fermi Arcs in Non-Centrosymmetric Weyl Semi-Metal Candidate NbP. 2015 , 32, 107101	52
1639	Structural and Transport Properties of the Weyl Semimetal NbAs at High Pressure. 2015 , 32, 097102	16
1638	Theory of Kerr and Faraday rotations and linear dichroism in Topological Weyl Semimetals. 2015 , 5, 12683	66
1637	Photoconductivity in Dirac materials. 2015 , 5, 117213	8
1636	Electric control of topological phase transitions in Dirac semimetal thin films. 2015 , 5, 14639	58
1635	Large single crystal growth, transport property, and spectroscopic characterizations of three-dimensional Dirac semimetal Cd ₃ As ₂ . 2015 , 5, 12966	27
1634	Semimetal-semiconductor transition and giant linear magnetoresistances in three-dimensional Dirac semimetal Bi _{0.96} Sb _{0.04} single crystals. 2015 , 107, 112101	19
1633	Strong-coupling phases of 3D Dirac and Weyl semimetals. A renormalization group approach. 2015 , 2015, 1	13
1632	Emergent gravity and chiral anomaly in Dirac semimetals in the presence of dislocations. 2015 , 360, 655-678	42
1631	Topological Surface States: Hybridization and Transport from Theoretical Approaches. 2015 , 36, 135-140	
1630	Synthesis and Photovoltaic Properties of Cd ₃ As ₂ Faceted Nanoplates and Nano-Octahedrons. 2015 , 15, 3264-3270	13
1629	Topological metal of NaBi with ultralow lattice thermal conductivity and electron-phonon superconductivity. 2015 , 5, 8446	6
1628	Quantum transport through 3D Dirac materials. 2015 , 359, 64-72	6
1627	Dirac semimetal films as spin conductors on topological substrates. 2015 , 91,	2
1626	Large Diamagnetic Susceptibility from Petit Fermi Surfaces in LaV ₂ Al ₂₀ . 2015 , 84, 113701	6
1625	Thermoelectric properties of materials with nontrivial electronic topology. 2015 , 3, 12130-12139	54

1624	Spin texture of the surface state of three-dimensional Dirac material Ca ₃ PbO. 2015 , 603, 012008	1
1623	Giant negative magnetoresistance induced by the chiral anomaly in individual Cd ₃ As ₂ nanowires. 2015 , 6, 10137	294
1622	Electrical-Controlled Transport for Surface States in a Dirac Semimetal Quantum Wire. 2015 , 32, 127302	2
1621	Stable compositions and structures in the Na-Bi system. 2015 , 17, 6933-47	16
1620	Unconventional localization transition in high dimensions. 2015 , 91,	64
1619	Topology and interactions in a frustrated slab: tuning from Weyl semimetals to C>1 fractional Chern insulators. 2015 , 114, 016806	52
1618	Chiral anomaly and transport in Weyl metals. 2015 , 27, 113201	223
1617	Topological flat bands in optical checkerboardlike lattices. 2015 , 91,	6
1616	Plasmon mode as a detection of the chiral anomaly in Weyl semimetals. 2015 , 91,	96
1615	Quasi one dimensional Dirac electrons on the surface of RuBn. 2014 , 4, 5168	20
1614	Classification of crystalline topological semimetals with an application to Na ₃ Bi. 2015 , 603, 012002	12
1613	Kondo effect and non-Fermi-liquid behavior in Dirac and Weyl semimetals. 2015 , 92,	26
1612	TOPOLOGICAL MATTER. Experimental observation of Weyl points. <i>Science</i> , 2015 , 349, 622-4	33.3 609
1611	Negative longitudinal magnetoresistance in Dirac and Weyl metals. 2015 , 91,	137
1610	Quantum-limited shot noise and quantum interference in graphene-based Corbino disk. 2015 , 95, 599-608	4
1609	Chiral Current in the Lattice Model of Weyl Semimetal. 2015 , 32, 057501	3
1608	Critical transport in weakly disordered semiconductors and semimetals. 2015 , 114, 166601	90
1607	Anisotropic quantum confinement effect and electric control of surface states in Dirac semimetal nanostructures. 2015 , 5, 7898	40

1606	Exchange Interaction Makes Superconductivity in 3D Dirac Semi-metal Triplet. 2015 , 179, 101-107	
1605	Unconventional transformation of spin Dirac phase across a topological quantum phase transition. 2015 , 6, 6870	28
1604	Magnetic impurities make superconductivity in 3D Dirac semi-metal triplet. 2015 , 109, 67006	2
1603	Microscopic study of vorticities in relativistic chiral fermions. 2015 , 2015, 1	2
1602	Na3Bi: A Robust Material Offering Dirac Electrons for Device Applications. 2015 , 44, 3215-3219	5
1601	The electronic and magnetic properties of transition-metal element doped three-dimensional topological Dirac semimetal in Cd3As2. 2015 , 3, 3547-3551	15
1600	Quantum transport in three-dimensional Weyl electron system in the presence of charged impurity scattering. 2015 , 91,	19
1599	Rich stoichiometries of stable Ca-Bi system: structure prediction and superconductivity. 2015 , 5, 9326	12
1598	Chiral universality class of normal-superconducting and exciton condensation transitions on surface of topological insulator. 2015 , 10, 303-320	2
1597	Bulk crystal growth and electronic characterization of the 3D Dirac semimetal Na3Bi. 2015 , 3, 041504	61
1596	Magneto-optics of massive dirac fermions in bulk Bi2Se3. 2015 , 114, 186401	55
1595	Anisotropic giant magnetoresistance in NbSb2. 2014 , 4, 7328	125
1594	Hybridization of Topological Surface States and Emergent States. 2015 , 11-30	2
1593	Topological Insulators, Topological Dirac semimetals, Topological Crystalline Insulators, and Topological Kondo Insulators. 2015 , 55-100	3
1592	Dirac semimetals A3Bi (A=Na,K,Rb) as Z2 Weyl semimetals. 2015 , 91,	29
1591	Quantum field theory in a magnetic field: From quantum chromodynamics to graphene and Dirac semimetals. 2015 , 576, 1-209	333
1590	Superpersistent currents and whispering gallery modes in relativistic quantum chaotic systems. 2015 , 5, 8963	15
1589	Topological insulators, topological superconductors and Weyl fermion semimetals: discoveries, perspectives and outlooks. 2015 , T164, 014001	94

1588	Kondo Effect in Dirac Systems. 2015 , 84, 074705	21
1587	Meissner Effect of Dirac Electrons in Superconducting State Due to Inter-Band Effect. 2015 , 84, 084704	7
1586	PHYSICS. Chiral anomaly without relativity. <i>Science</i> , 2015 , 350, 378-9	33-3 13
1585	2D MATERIALS. Observation of tunable band gap and anisotropic Dirac semimetal state in black phosphorus. <i>Science</i> , 2015 , 349, 723-6	33-3 597
1584	Infrared magneto-spectroscopy of two-dimensional and three-dimensional massless fermions: A comparison. 2015 , 117, 112803	5
1583	Carrier screening, transport, and relaxation in three-dimensional Dirac semimetals. 2015 , 91,	62
1582	Large linear magnetoresistance in the Dirac semimetal TlBiSSe. 2015 , 91,	109
1581	Chiral magnetic effect in a two-band lattice model of Weyl semimetal. 2015 , 91,	67
1580	Superconducting dome and crossover to an insulating state in $[Tl_4]Tl_1Sn_xTe_3$. 2015 , 3, 041507	9
1579	Quantum anomalous Hall effect and related topological electronic states. 2015 , 64, 227-282	251
1578	Landau level splitting in Cd ₃ As ₂ under high magnetic fields. 2015 , 6, 7779	98
1577	Electrically tunable multiple Dirac cones in thin films of the (LaO) ₂ (SbSe ₂) ₂ family of materials. 2015 , 6, 8517	22
1576	Optical magnetoplasmons in rhombohedral graphite with a three-dimensional Dirac cone structure. 2015 , 27, 125602	1
1575	Scalable Growth of High Mobility Dirac Semimetal Cd ₃ As ₂ Microbelts. 2015 , 15, 5830-4	34
1574	New perspectives for Rashba spin-orbit coupling. 2015 , 14, 871-82	970
1573	Weyl semimetal phase in the non-centrosymmetric compound TaAs. 2015 , 11, 728-732	649
1572	A new form of Ca ₃ P ₂ with a ring of Dirac nodes. 2015 , 3, 083602	244
1571	Generalized three-dimensional Dirac points and Z ₂ gapless surface states in a topological photonic crystal. 2015 ,	

1570	Evidence for the chiral anomaly in the Dirac semimetal NaBi. <i>Science</i> , 2015 , 350, 413-6	33.3	719
1569	Phonon-drag thermopower in 3D Dirac semimetals. 2015 , 27, 455801		4
1568	Gate-tunable quantum oscillations in ambipolar Cd ₃ As ₂ thin films. 2015 , 7, e221-e221		60
1567	Evidence of topological surface state in three-dimensional Dirac semimetal Cd ₃ As ₂ . 2014 , 4, 6106		131
1566	Triplet superconductivity in 3D Dirac semi-metal due to exchange interaction. 2015 , 27, 025701		6
1565	Observation of Fermi arc surface states in a topological metal. <i>Science</i> , 2015 , 347, 294-8	33.3	488
1564	Ultra-high mobility and giant magnetoresistance in the Dirac semimetal Cd ₃ As ₂ . 2015 , 14, 280-4		931
1563	Spectroscopic evidence for a type II Weyl semimetallic state in MoTe. 2016 , 15, 1155-1160		372
1562	Transport evidence for Fermi-arc-mediated chirality transfer in the Dirac semimetal Cd ₃ As ₂ . 2016 , 535, 266-70		212
1561	Electron cooling in three-dimensional Dirac fermion systems at low temperature: Effect of screening. 2016 , 10, 248-252		15
1560	Pressure-induced topological phases of KNa ₂ Bi. 2016 , 6, 24137		19
1559	Aharonov-Bohm oscillations in Dirac semimetal Cd ₃ As ₂ nanowires. 2016 , 7, 10769		111
1558	Quantum Oscillations at Integer and Fractional Landau Level Indices in Single-Crystalline ZrTe. 2016 , 6, 35357		25
1557	Monte Carlo study of Dirac semimetals phase diagram. 2016 , 94,		12
1556	Interplanar coupling-dependent magnetoresistivity in high-purity layered metals. 2016 , 7, 10903		36
1555	A robust relativistic quantum two-level system with edge-dependent currents and spin polarization. 2016 , 115, 20005		6
1554	Quantum oscillation and nontrivial transport in the Dirac semimetal Cd ₃ As ₂ nanodevice. 2016 , 108, 183103		10
1553	Linear magnetoconductivity in an intrinsic topological Weyl semimetal. 2016 , 18, 053039		54

1552	Chiral anomaly in real space from stable fractional charges at the edge of a quantum spin Hall insulator. 2016 , 94,	23
1551	Thickness-dependent quantum oscillations in Cd ₃ As ₂ thin films. 2016 , 18, 083003	29
1550	Amplification of terahertz frequency acoustic phonons by drifting electrons in three-dimensional Dirac semimetals. 2016 , 120, 125705	1
1549	Universal optical conductivity of a disordered Weyl semimetal. 2016 , 6, 32446	51
1548	Cerenkov emission of acoustic phonons electrically generated from three-dimensional Dirac semimetals. 2016 , 119, 195701	5
1547	On the search for the chiral anomaly in Weyl semimetals: the negative longitudinal magnetoresistance. 2016 , 18, 085006	104
1546	Observation of Fermi arc and its connection with bulk states in the candidate type-II Weyl semimetal WTe ₂ . 2016 , 94,	158
1545	Giant magnetoresistance, three-dimensional Fermi surface and origin of resistivity plateau in YSb semimetal. 2016 , 6, 38691	51
1544	Topological Nonsymmorphic Metals from Band Inversion. 2016 , 6,	48
1543	Magnetic-field-induced nonlinear optical responses in inversion symmetric Dirac semimetals. 2016 , 94,	20
1542	Collective modes in multi-Weyl semimetals. 2016 , 6, 34023	23
1541	Large linear magnetoresistance in a new Dirac material BaMnBi ₂ . 2016 , 25, 107503	19
1540	Negative magnetoresistance without well-defined chirality in the Weyl semimetal TaP. 2016 , 7, 11615	301
1539	Schwinger pair creation in Dirac semimetals in the presence of external magnetic and electric fields. 2016 , 94,	7
1538	Enhanced zero-bias conductance peak and splitting at mesoscopic interfaces between an s-wave superconductor and a 3D Dirac semimetal. 2016 , 109, 252602	2
1537	Large transverse Hall-like signal in topological Dirac semimetal Cd ₃ As ₂ . 2016 , 6, 27487	13
1536	Recent observations of negative longitudinal magnetoresistance in semimetal. 2016 , 25, 117204	9
1535	Observation of unusual topological surface states in half-Heusler compounds LnPtBi (Ln=Lu, Y). 2016 , 7, 12924	77

1534	Ising and Gross-Neveu model in next-to-leading order. 2016 , 94,	36
1533	Presence of exotic electronic surface states in LaBi and LaSb. 2016 , 94,	58
1532	Inhomogeneous Weyl and Dirac Semimetals: Transport in Axial Magnetic Fields and Fermi Arc Surface States from Pseudo-Landau Levels. 2016 , 6,	92
1531	On the disorder-driven quantum transition in three-dimensional relativistic metals. 2016 , 94,	27
1530	Signatures of evanescent transport in ballistic suspended graphene-superconductor junctions. 2016 , 6, 24274	11
1529	Molecular beam epitaxy of Cd ₃ As ₂ on a III-V substrate. 2016 , 4, 126110	47
1528	Weak antilocalization and interaction-induced localization of Dirac and Weyl Fermions in topological insulators and semimetals. 2016 , 25, 117202	13
1527	Dirac semimetal thin films in in-plane magnetic fields. 2016 , 6, 34882	5
1526	Electronic properties in a quantum well structure of Weyl semimetal. 2016 , 108, 163105	6
1525	Nearly massless Dirac fermions hosted by Sb square net in BaMnSb ₂ . 2016 , 6, 30525	46
1524	Dirac node arcs in PtSn ₄ . 2016 , 12, 667-671	167
1523	A topological semimetal model with f-wave symmetry in a non-Abelian triangular optical lattice. 2016 , 494, 49-52	1
1522	Two-Carrier Transport Induced Hall Anomaly and Large Tunable Magnetoresistance in Dirac Semimetal Cd ₃ As ₂ Nanoplates. 2016 , 10, 6020-8	47
1521	Uncovering the behavior of Hf ₂ Te ₂ P and the candidate Dirac metal Zr ₂ Te ₂ P. 2016 , 28, 14LT01	7
1520	Electronic Properties of High-Quality Epitaxial Topological Dirac Semimetal Thin Films. 2016 , 16, 3210-4	42
1519	Field emission from Dirac and Weyl semimetals. 2016 , 122, 1	
1518	ZnGeSb: a promising thermoelectric material with tunable ultra-high conductivity. 2016 , 18, 26275-26283	8
1517	Dirac-node arc in the topological line-node semimetal HfSiS. 2016 , 94,	100

1516	Topological semimetal to insulator quantum phase transition in the Zintl compounds Ba ₂ X(X=Si,Ge). 2016 , 94,	14
1515	Chiral magnetic effect in condensed matter systems. 2016 , 956, 107-111	7
1514	Relativistic Chiral Kinetic Theory. 2016 , 956, 657-660	
1513	Type-II Dirac fermions in the PtSe ₂ class of transition metal dichalcogenides. 2016 , 94,	187
1512	Strong Intrinsic Spin Hall Effect in the TaAs Family of Weyl Semimetals. 2016 , 117, 146403	98
1511	Topological magnon insulators: Chern numbers and surface magnons. 2016 ,	1
1510	Uncovering the hidden quantum critical point in disordered massless Dirac and Weyl semimetals. 2016 , 94,	31
1509	Spin-orbit semimetals in the layer groups. 2016 , 94,	73
1508	Weyl semimetal generated from Dirac semimetal using off-resonant light. 2016 , 503, 162-166	1
1507	Quantum phases of interacting electrons in three-dimensional dirty Dirac semimetals. 2016 , 94,	36
1506	Z ₂ and Chiral Anomalies in Topological Dirac Semimetals. 2016 , 117, 136602	50
1505	Magnon Dirac materials. 2016 , 94,	77
1504	Robust Type-II Weyl Semimetal Phase in Transition Metal Diphosphides XP ₂ (X=Mo, W). 2016 , 117, 066402	131
1503	Nature and topology of the low-energy states in ZrTe ₅ . 2016 , 94,	39
1502	New family of Dirac and Weyl semimetals in XAuTe (X = Na, K, Rb) ternary honeycomb compounds. 2016 , 59, 1	3
1501	Dirac fermions in an antiferromagnetic semimetal. 2016 , 12, 1100-1104	144
1500	Topological density-wave states in a particle-hole symmetric Weyl metal. 2016 , 94,	18
1499	Anomalous Phase Shift of Quantum Oscillations in 3D Topological Semimetals. 2016 , 117, 077201	68

1498	Classification of topological quantum matter with symmetries. 2016 , 88,	1093
1497	Dirac Node Lines in Pure Alkali Earth Metals. 2016 , 117, 096401	131
1496	Nodal-chain metals. 2016 , 538, 75-78	324
1495	Three-dimensional Dirac cone carrier dynamics in Na ₃ Bi and Cd ₃ As ₂ . 2016 , 94,	36
1494	Tunable Weyl Points in Periodically Driven Nodal Line Semimetals. 2016 , 117, 087402	132
1493	Asymmetric mass acquisition in LaBi: Topological semimetal candidate. 2016 , 94,	40
1492	Resonance states and beating pattern induced by quantum impurity scattering in Weyl/Dirac semimetals. 2016 , 6, 36106	9
1491	Observation of quasi-two-dimensional Dirac fermions in ZrTe ₅ . 2016 , 8, e325-e325	41
1490	Topological insulating phases from two-dimensional nodal loop semimetals. 2016 , 94,	12
1489	Observation of Weyl nodes and Fermi arcs in tantalum phosphide. 2016 , 7, 11006	224
1488	Monitoring Electron-Photon Dressing in WSe. 2016 , 16, 7993-7998	46
1487	Shot noise in NS junctions with a Weyl superconductor. 2016 , 94,	1
1486	Observation of Fermi arcs in the type-II Weyl semimetal candidate WTe ₂ . 2016 , 94,	215
1485	Blue Phosphorene Oxide: Strain-Tunable Quantum Phase Transitions and Novel 2D Emergent Fermions. 2016 , 16, 6548-6554	91
1484	Magnetic phases and unusual topological electronic structures of Weyl semimetals in strong interaction limit. 2016 , 94,	7
1483	Electronic structure, Dirac points and Fermi arc surface states in three-dimensional Dirac semimetal Na ₃ Bi from angle-resolved photoemission spectroscopy. 2016 , 25, 077101	14
1482	Optical Distinctions Between Weyl Semimetal TaAs and Dirac Semimetal Na ₃ Bi: An Ab Initio Investigation. 2016 , 45, 5867-5876	17
1481	Are the surface Fermi arcs in Dirac semimetals topologically protected?. 2016 , 113, 8648-52	84

1480	Quantum simulation of exotic PT-invariant topological nodal loop bands with ultracold atoms in an optical lattice. 2016, 93,	40
1479	Dirac and Weyl rings in three-dimensional cold-atom optical lattices. 2016, 93,	24
1478	Nernst and magnetothermal conductivity in a lattice model of Weyl fermions. 2016, 93,	97
1477	Long-range Coulomb interaction in nodal-ring semimetals. 2016, 93,	107
1476	Semimetal with both Rarita-Schwinger-Weyl and Weyl excitations. 2016, 93,	26
1475	Temperature-pressure phase diagram of cubic Laves phase Au ₂ Pb. 2016, 93,	10
1474	Strong topological metal material with multiple Dirac cones. 2016, 93,	13
1473	Visualizing the chiral anomaly in Dirac and Weyl semimetals with photoemission spectroscopy. 2016, 93,	34
1472	Quantum oscillations in Weyl and Dirac semimetal ultrathin films. 2016, 93,	25
1471	Disorder-driven itinerant quantum criticality of three-dimensional massless Dirac fermions. 2016, 93,	43
1470	Optical and transport properties in three-dimensional Dirac and Weyl semimetals. 2016, 93,	74
1469	Optical conductivity of Weyl semimetals and signatures of the gapped semimetal phase transition. 2016, 93,	56
1468	Hybridization and anisotropy in the exchange interaction in three-dimensional Dirac semimetals. 2016, 93,	18
1467	Spin textures and spin-wave excitations in doped Dirac-Weyl semimetals. 2016, 93,	19
1466	Transport evidence for the three-dimensional Dirac semimetal phase in ZrTe ₅ . 2016, 93,	105
1465	Drumhead surface states and topological nodal-line fermions in TlTaSe ₂ . 2016, 93,	201
1464	Competition of density waves and quantum multicritical behavior in Dirac materials from functional renormalization. 2016, 93,	25
1463	Unconventional spin Hall effect and axial current generation in a Dirac semimetal. 2016, 93,	1

1462	Thermoelectric transport in double-Weyl semimetals. 2016, 93,	41
1461	Topological crystalline semimetals in nonsymmorphic lattices. 2016, 93,	46
1460	Electromagnetic response of interacting Weyl semimetals. 2016, 93,	18
1459	Chiral wave-packet scattering in Weyl semimetals. 2016, 93,	25
1458	Topology of nonsymmorphic crystalline insulators and superconductors. 2016, 93,	95
1457	Photovoltaic chiral magnetic effect in Weyl semimetals. 2016, 93,	46
1456	Classification of stable Dirac and Weyl semimetals with reflection and rotational symmetry. 2016, 93,	45
1455	Ca ₃ P ₂ and other topological semimetals with line nodes and drumhead surface states. 2016, 93,	230
1454	Determining the chirality of Weyl fermions from circular dichroism spectra in time-dependent angle-resolved photoemission. 2016, 93,	19
1453	Floquet Weyl fermions in three-dimensional stacked graphene systems irradiated by circularly polarized light. 2016, 93,	30
1452	Origin of dissipative Fermi arc transport in Weyl semimetals. 2016, 93,	46
1451	Three-dimensional photonic Dirac points stabilized by point group symmetry. 2016, 93,	45
1450	Dielectric response and novel electromagnetic modes in three-dimensional Dirac semimetal films. 2016, 93,	155
1449	Stable Dirac semimetal in the allotropes of group-IV elements. 2016, 93,	11
1448	Resonant plasmon-axion excitations induced by charge density wave order in a Weyl semimetal. 2016, 93,	9
1447	Surface plasmon polaritons in topological Weyl semimetals. 2016, 93,	62
1446	Mott insulating states and quantum phase transitions of correlated SU(2N) Dirac fermions. 2016, 93,	43
1445	Renormalization of fermion velocity in finite temperature QED ₃ . 2016, 93,	2

1444	Double Dirac Semimetals in Three Dimensions. 2016 , 116, 186402	199
1443	Evidence of Topological Nodal-Line Fermions in ZrSiSe and ZrSiTe. 2016 , 117, 016602	270
1442	Colloquium: Topological band theory. 2016 , 88,	745
1441	Beyond Dirac and Weyl fermions: Unconventional quasiparticles in conventional crystals. <i>Science</i> , 2016 , 353, aaf5037	33-3 601
1440	Superconductivity in doped Dirac semimetals. 2016 , 94,	43
1439	Molecular Doping the Topological Dirac Semimetal Na ₃ Bi across the Charge Neutrality Point with F4-TCNQ. 2016 , 8, 16412-8	19
1438	Topological nematic phase in Dirac semimetals. 2016 , 93,	12
1437	Magnetic susceptibility in three-dimensional nodal semimetals. 2016 , 93,	56
1436	Collective modes in nodal line semimetals. 2016 , 93,	41
1435	Dirty Weyl semimetals: Stability, phase transition, and quantum criticality. 2016 , 93,	76
1434	Pressure-induced topological insulator in NaBaBi with right-handed surface spin texture. 2016 , 93,	15
1433	Electric-field-induced spin resonance in antiferromagnetic insulators: Inverse process of the dynamical chiral magnetic effect. 2016 , 93,	17
1432	Emergence of topological bands on the surface of ZrSnTe crystal. 2016 , 93,	50
1431	Observation of pseudo-two-dimensional electron transport in the rock salt-type topological semimetal LaBi. 2016 , 93,	69
1430	Self-organized charge puddles in a three-dimensional topological material. 2016 , 93,	30
1429	Novel Z(2) Topological Metals and Semimetals. 2016 , 116, 016401	15
1428	Macroscopic Degeneracy of Zero-Mode Rotating Surface States in 3D Dirac and Weyl Semimetals under Radiation. 2016 , 116, 156803	23
1427	Torsional Chiral Magnetic Effect in a Weyl Semimetal with a Topological Defect. 2016 , 116, 166601	62

1426	Emergence of a Fermionic Finite-Temperature Critical Point in a Kondo Lattice. 2016 , 116, 177002	6
1425	Rare-Region-Induced Avoided Quantum Criticality in Disordered Three-Dimensional Dirac and Weyl Semimetals. 2016 , 6,	64
1424	Universal conductance fluctuations in Dirac semimetal Cd ₃ As ₂ nanowires. 2016 , 94,	17
1423	Large anomalous magnetic moment in three-dimensional Dirac and Weyl semimetals. 2016 , 94,	4
1422	Dirac cone tilt on interband optical background of type-I and type-II Weyl semimetals. 2016 , 94,	41
1421	Photoexcitation of electron wave packets in quantum spin Hall edge states: Effects of chiral anomaly from a localized electric pulse. 2016 , 94,	22
1420	Zeeman splitting and dynamical mass generation in Dirac semimetal ZrTe ₅ . 2016 , 7, 12516	108
1419	Topologically stable gapless phases in nonsymmorphic superconductors. 2016 , 94,	31
1418	Tilted anisotropic Dirac cones in partially hydrogenated graphene. 2016 , 94,	22
1417	Disorder effects in topological states: Brief review of the recent developments. 2016 , 25, 117311	17
1416	Electromagnetic Signatures of the Chiral Anomaly in Weyl Semimetals. 2016 , 117, 217204	14
1415	Superconductivity in topologically nontrivial material Au ₂ Pb. 2016 , 1,	30
1414	Imaging electronic states on topological semimetals using scanning tunneling microscopy. 2016 , 18, 105003	17
1413	Electronic properties of SnTe-class topological crystalline insulator materials. 2016 , 25, 117313	9
1412	Quantum transport properties of the three-dimensional Dirac semimetal Cd ₃ As ₂ single crystals. 2016 , 25, 117105	10
1411	Anomalous conductivity tensor in the Dirac semimetal Na ₃ Bi. 2016 , 114, 27002	67
1410	Magnetic susceptibility of topological nodal semimetals. 2016 , 94,	19
1409	Nonadiabatic bulk-surface oscillations in driven topological insulators. 2016 , 94,	8

1408	Topological semimetals. 2016 , 15, 1145-1148	291
1407	Topological mirror insulators in one dimension. 2016 , 94,	37
1406	Hot dense magnetized ultrarelativistic spinor matter in a slab. 2016 , 94,	2
1405	Pressure-induced superconductivity in the three-dimensional topological Dirac semimetal Cd ₃ As ₂ . 2016 , 1,	97
1404	Strong nonlinear terahertz response induced by Dirac surface states in Bi ₂ Se ₃ topological insulator. 2016 , 7, 11421	85
1403	Magnetotransport properties of the type-II Weyl semimetal candidate Ta ₃ S ₂ . 2016 , 94,	21
1402	Tuning the scattering mechanism in the three-dimensional Dirac semimetal Cd ₃ As ₂ . 2016 , 94,	7
1401	Photovoltaic anomalous Hall effect in line-node semimetals. 2016 , 94,	36
1400	Chern numbers and chiral anomalies in Weyl butterflies. 2016 , 94,	9
1399	Chiral Anomaly from Strain-Induced Gauge Fields in Dirac and Weyl Semimetals. 2016 , 6,	107
1398	Dirac cone protected by non-symmorphic symmetry and three-dimensional Dirac line node in ZrSiS. 2016 , 7, 11696	423
1397	Topological node-line semimetal in compressed black phosphorus. 2016 , 94,	89
1396	Low Carrier Density Metal Realized in Candidate Line-Node Dirac Semimetals CaAgP and CaAgAs. 2016 , 85, 123701	28
1395	Magnetic torque anomaly in the quantum limit of Weyl semimetals. 2016 , 7, 12492	43
1394	Weyl Mott Insulator. 2016 , 6, 19853	32
1393	Magneto-optical conductivity of Weyl semimetals with quadratic term in momentum. 2016 , 6, 025312	8
1392	On the chiral separation effect in a slab. 2016 , 114, 61001	1
1391	Topological semimetals with helicoid surface states. 2016 , 12, 936-941	91

- 1390 Electromagnetic fields and anomalous transports in heavy-ion collisions-a pedagogical review. **2016**, 79, 076302 150
- 1389 Topological semimetals predicted from first-principles calculations. **2016**, 28, 303001 202
- 1388 The chiral anomaly and thermopower of Weyl fermions in the half-Heusler GdPtBi . **2016**, 15, 1161-1165 301
- 1387 Nernst-Ettingshausen effect at the trivial-nontrivial band ordering in topological crystalline insulator $\text{Pb}_{1-x}\text{Sn}_x\text{Se}$. **2016**, 18, 013047 3
- 1386 Novel three dimensional topological nodal line semimetallic carbon. **2016**, 98, 468-473 29
- 1385 Chiral magnetic effect in ZrTe_5 . **2016**, 12, 550-554 588
- 1384 Intrinsic diamagnetism in the Weyl semimetal TaAs . **2016**, 408, 73-76 11
- 1383 Phase diagrams of disordered Weyl semimetals. **2016**, 93, 67
- 1382 New type of Weyl semimetal with quadratic double Weyl fermions. **2016**, 113, 1180-5 199
- 1381 Pressure-induced superconductivity in a three-dimensional topological material ZrTe_5 . **2016**, 113, 2904-9 91
- 1380 Emergent gravity in the cubic tight-binding model of Weyl semimetal in the presence of elastic deformations. **2016**, 366, 45-56 32
- 1379 Quasiparticle interference of the Fermi arcs and surface-bulk connectivity of a Weyl semimetal. *Science*, **2016**, 351, 1184-7 33-3 130
- 1378 Negative magnetoresistance in Dirac semimetal Cd_3As_2 . **2016**, 7, 10301 289
- 1377 Symmetry-protected topological photonic crystal in three dimensions. **2016**, 12, 337-340 182
- 1376 Unconventional superconductivity at mesoscopic point contacts on the 3D Dirac semimetal Cd_3As_2 . **2016**, 15, 32-7 119
- 1375 Evolution of the Fermi surface of Weyl semimetals in the transition metal pnictide family. **2016**, 15, 27-31 202
- 1374 Spectroscopic evidence for bulk-band inversion and three-dimensional massive Dirac fermions in ZrTe_5 . **2017**, 114, 816-821 49
- 1373 Multiple Dirac cones at the surface of the topological metal LaBi . **2017**, 8, 13942 75

1372	Quantum oscillations without magnetic field. 2017 , 95,	49
1371	Topological Dirac nodal lines and surface charges in fcc alkaline earth metals. 2017 , 8, 14022	107
1370	Ultrafast relaxation dynamics of photoexcited Dirac fermions in the three-dimensional Dirac semimetal Cd ₃ As ₂ . 2017 , 95,	34
1369	Body-Centered Tetragonal C : A Novel Topological Node-Line Semimetallic Carbon Composed of Tetrarings. 2017 , 13, 1602894	49
1368	Room-temperature chiral charge pumping in Dirac semimetals. 2017 , 8, 13741	82
1367	Topological Materials: Weyl Semimetals. 2017 , 8, 337-354	659
1366	Creating stable Floquet-Weyl semimetals by laser-driving of 3D Dirac materials. 2017 , 8, 13940	155
1365	Emergence of topological nodal loops in alkaline-earth hexaborides XB (X = Ca, Sr, and Ba) under pressure. 2017 , 19, 8210-8215	16
1364	Modifying the band-structure and properties of zirconium telluride using phosphorus addition. 2017 , 146, 554-561	9
1363	Large nonsaturating magnetoresistance and signature of nondegenerate Dirac nodes in ZrSiS. 2017 , 114, 2468-2473	164
1362	Control of topological phase transitions in Dirac semimetal films by exchange fields. 2017 , 26, 017102	
1361	Hidden topological constellations and polyvalent charges in chiral nematic droplets. 2017 , 8, 14594	37
1360	Pressure-induced topological phase transitions and strongly anisotropic magnetoresistance in bulk black phosphorus. 2017 , 95,	24
1359	Distinct Evolutions of Weyl Fermion Quasiparticles and Fermi Arcs with Bulk Band Topology in Weyl Semimetals. 2017 , 118, 106406	23
1358	Topological nodal line semimetals in the CaP ₃ family of materials. 2017 , 95,	142
1357	Dynamic Chiral Magnetic Effect and Faraday Rotation in Macroscopically Disordered Helical Metals. 2017 , 118, 107401	7
1356	Topological semimetals protected by off-centered symmetries in nonsymmorphic crystals. 2017 , 95,	61
1355	Robust dual topological character with spin-valley polarization in a monolayer of the Dirac semimetal Na ₃ Bi. 2017 , 95,	27

1354	Correlation effects and quantum oscillations in topological nodal-loop semimetals. 2017 , 95,	56
1353	BaSn2: A wide-gap strong topological insulator. 2017 , 95,	13
1352	Nonlocal electrodynamics in Weyl semimetals. 2017 , 95,	6
1351	Quantum oscillations in a lead chalcogenide three-dimensional Dirac system. 2017 , 95,	4
1350	Excitonic pairing and insulating transition in two-dimensional semi-Dirac semimetals. 2017 , 95,	17
1349	Direct Observation of Landau Level Resonance and Mass Generation in Dirac Semimetal CdAs Thin Films. 2017 , 17, 2211-2219	28
1348	Tunneling conductance in a two-dimensional Dirac semimetal protected by nonsymmorphic symmetry. 2017 , 95,	5
1347	Discovery of Weyl Fermion Semimetals and Topological Fermi Arc States. 2017 , 8, 289-309	258
1346	Observation of surface superstructure induced by systematic vacancies in the topological Dirac semimetal Cd3As2. 2017 , 95,	3
1345	Anisotropic magnetotransport in Dirac-Weyl magnetic junctions. 2017 , 95,	8
1344	Topological transport in Dirac electronic systems: A concise review. 2017 , 26, 037301	8
1343	Heavy Weyl Fermion State in CeRu4Sn6. 2017 , 7,	30
1342	CaTe: a new topological node-line and Dirac semimetal. 2017 , 2,	87
1341	Angle-dependent magnetoresistance and quantum oscillations in high-mobility semimetal LuPtBi. 2017 , 29, 195501	7
1340	Experimental evidence of hourglass fermion in the candidate nonsymmorphic topological insulator KHgSb. 2017 , 3, e1602415	78
1339	Artificial gravity field, astrophysical analogues, and topological phase transitions in strained topological semimetals. 2017 , 2,	80
1338	Observation of three-component fermions in the topological semimetal molybdenum phosphide. 2017 , 546, 627-631	231
1337	Fractional charge oscillations in quantum dots with quantum spin Hall effect. 2017 , 95,	12

1336	Temperature-induced Lifshitz transition in topological insulator candidate HfTe5. 2017 , 62, 950-956	23
1335	Magneto-optical conductivity study in three-dimensional Dirac semimetals of ZrTe5. 2017 , 90, 1	7
1334	Quantum transport in Dirac and Weyl semimetals: a review. 2017 , 2, 518-544	57
1333	Relativistic Zitterbewegung in non-Hermitian photonic waveguide systems. 2017 , 19, 013017	
1332	Electronic evidence of temperature-induced Lifshitz transition and topological nature in ZrTe. 2017 , 8, 15512	131
1331	Two-dimensional arsenene oxide: A realistic large-gap quantum spin Hall insulator. 2017 , 110, 213101	100
1330	Two-Dimensional Node-Line Semimetals in a Honeycomb-Kagome Lattice *. 2017 , 34, 057302	59
1329	Omnidirectional spin Hall effect in a Weyl spin-orbit-coupled atomic gas. 2017 , 95,	4
1328	Route towards Dirac and Weyl antiferromagnetic spintronics. 2017 , 11, 1700044	34
1327	Angle-resolved photoemission spectroscopy for the study of two-dimensional materials. 2017 , 4,	24
1326	Accurate Determination of the Quasiparticle and Scaling Properties Surrounding the Quantum Critical Point of Disordered Three-Dimensional Dirac Semimetals. 2017 , 118, 146401	12
1325	Evidence of topological insulator state in the semimetal LaBi. 2017 , 95,	42
1324	Dirac line nodes and effect of spin-orbit coupling in the nonsymmorphic critical semimetals MSiS(M=Hf,Zr). 2017 , 95,	93
1323	Band splitting and Weyl nodes in trigonal tellurium studied by angle-resolved photoemission spectroscopy and density functional theory. 2017 , 95,	42
1322	Controllable synthesis and magnetotransport properties of Cd3As2 Dirac semimetal nanostructures. 2017 , 7, 17689-17696	18
1321	Nonlocal Coulomb drag in Weyl semimetals. 2017 , 95,	2
1320	Unusual magnetotransport from Si-square nets in topological semimetal HfSiS. 2017 , 95,	38
1319	Electron-hole pairing of Fermi-arc surface states in a Weyl semimetal bilayer. 2017 , 95,	2

1318	Electronic and optical properties of topological semimetal CdAs. 2017 , 7, 45500	27
1317	Semimetallic carbon allotrope with a topological nodal line in mixed sp ² -sp ³ bonding networks. 2017 , 9, e361-e361	14
1316	Anomalous Magneto-Transport Behavior in Transition Metal Pentatelluride HfTe ₅ . 2017 , 34, 037102	13
1315	Z2Pack: Numerical implementation of hybrid Wannier centers for identifying topological materials. 2017 , 95,	230
1314	Chiral magnetic plasmons in anomalous relativistic matter. 2017 , 95,	27
1313	Antiferromagnetic Dirac semimetals in two dimensions. 2017 , 95,	27
1312	Pseudomagnetic helicons. 2017 , 95,	20
1311	Engineering and Probing Topological Properties of Dirac Semimetal Films by Asymmetric Charge Transfer. 2017 , 17, 963-972	10
1310	Magnetotransport properties near the Dirac point of Dirac semimetal CdAs nanowires. 2017 , 29, 044003	3
1309	Topological Dirac semimetal phase in Pd and Pt oxides. 2017 , 95,	20
1308	Synthetically tuned structural variations in CePdxGe _{2-x} (x = 0.21, 0.32, 0.69) towards diverse physical properties. 2017 , 4, 241-255	2
1307	Prediction of topological crystalline insulators and topological phase transitions in two-dimensional PbTe films. 2017 , 19, 29647-29652	6
1306	Topological phase transition in layered XIn ₂ P ₂ (X = Ca, Sr). 2017 , 50, 465304	4
1305	Ab Initio Predictions of Hexagonal Zr(B,C,N) Polymorphs for Coherent Interface Design. 2017 , 121, 26007-26018	8
1304	Interdimensional effects in systems with quasirelativistic fermions. 2017 , 96,	30
1303	Unconventional quantum Hall effects in two-dimensional massive spin-1 fermion systems. 2017 , 96,	15
1302	Topological phase stability and transformation of bismuthene. 2017 , 119, 27002	24
1301	Designer Curved-Space Geometry for Relativistic Fermions in Weyl Metamaterials. 2017 , 7,	24

1300	Evolution of Weyl orbit and quantum Hall effect in Dirac semimetal CdAs. 2017 , 8, 1272	77
1299	Extremely large magnetoresistance and Kohler's rule in PdSn4: A complete study of thermodynamic, transport, and band-structure properties. 2017 , 96,	37
1298	Dissolution of topological Fermi arcs in a dirty Weyl semimetal. 2017 , 96,	34
1297	Numerical study of universal conductance fluctuations in three-dimensional topological semimetals. 2017 , 96,	8
1296	Robust doubly charged nodal lines and nodal surfaces in centrosymmetric systems. 2017 , 96,	99
1295	ARPES studies of the inverse perovskite Ca3PbO: Experimental confirmation of a candidate 3D Dirac fermion system. 2017 , 96,	29
1294	Evidence for magnetic Weyl fermions in a correlated metal. 2017 , 16, 1090-1095	263
1293	Unusual interlayer quantum transport behavior caused by the zeroth Landau level in YbMnBi. 2017 , 8, 646	26
1292	Charge Density Waves in Graphite: Towards the Magnetic Ultraquantum Limit. 2017 , 119, 136601	16
1291	Prediction of Triple Point Fermions in Simple Half-Heusler Topological Insulators. 2017 , 119, 136401	56
1290	3D Quantum Hall Effect of Fermi Arcs in Topological Semimetals. 2017 , 119, 136806	74
1289	Optical conductivity of an interacting Weyl liquid in the collisionless regime. 2017 , 96,	8
1288	Topological Hopf and Chain Link Semimetal States and Their Application to Co ₂ MnGa. 2017 , 119, 156401	125
1287	Effects of Cd vacancies and unconventional spin dynamics in the Dirac semimetal CdAs. 2017 , 147, 084706	4
1286	Spinless hourglass nodal-line semimetals. 2017 , 96,	27
1285	Magnetoresistance of compensated semimetals in confined geometries. 2017 , 95,	24
1284	Experimental realization of two-dimensional Dirac nodal line fermions in monolayer CuSi. 2017 , 8, 1007	138
1283	Quantum Materials: Where Many Paths Meet. 2017 , 42, 698-705	10

1282	Sea of Majorana fermions from pseudo-scalar superconducting order in three dimensional Dirac materials. 2017 , 7, 8221	6
1281	Thickness-tuned transition of band topology in ZrTe5 nanosheets. 2017 , 95,	16
1280	Hourglass semimetals with nonsymmorphic symmetries in three dimensions. 2017 , 96,	16
1279	Evidence for pressure-induced node-pair annihilation in Cd3As2. 2017 , 96,	7
1278	Electron tunneling through double magnetic barriers in Weyl semimetals. 2017 , 7, 13633	5
1277	Anomalous cyclotron mass dependence on the magnetic field and Berry's phase in (Cd Zn Mn)As solid solutions. 2017 , 29, 455701	7
1276	Circular Phonon Dichroism in Weyl Semimetals. 2017 , 119, 075301	21
1275	Theoretical study of the pressure-induced topological phase transition in LaSb. 2017 , 96,	17
1274	Anisotropic lattice thermal conductivity in three-fold degeneracy topological semimetal MoP: a first-principles study. 2017 , 29, 435704	12
1273	Large optical conductivity of Dirac semimetal Fermi arc surface states. 2017 , 96,	11
1272	Magneto-optical conductivity of double Weyl semimetals. 2017 , 96,	11
1271	Two-Dimensional Massless Dirac Fermions in Antiferromagnetic AFe_2As_2 ($A=Ba,Sr$). 2017 , 119, 096401	16
1270	Experimental evidence for type-II Dirac semimetal in PtSe2. 2017 , 96,	142
1269	Three-dimensional topological critical Dirac semimetal in $AMgBi$ ($A= K, Rb, Cs$). 2017 , 96,	26
1268	Large magnetoresistance and Fermi surface topology of PrSb. 2017 , 96,	23
1267	Topological Type-II Nodal Line Semimetal and Dirac Semimetal State in Stable Kagome Compound MgBi. 2017 , 8, 4814-4819	105
1266	Classification of accidental band crossings and emergent semimetals in two-dimensional noncentrosymmetric systems. 2017 , 96,	12
1265	Wigner function and kinetic phenomena for chiral plasma in a strong magnetic field. 2017 , 2017, 1	14

1264	Robust and Pristine Topological Dirac Semimetal Phase in Pressured Two-Dimensional Black Phosphorus. 2017 , 121, 20931-20936	12
1263	Dirac semimetal phase in hexagonal LiZnBi. 2017 , 96,	19
1262	Epitaxial thin films of Dirac semimetal antiperovskite Cu ₃ PdN. 2017 , 5, 096103	8
1261	Interplay between short-range correlated disorder and Coulomb interaction in nodal-line semimetals. 2017 , 96,	15
1260	Chiral response in lattice models of Weyl materials. 2017 , 96,	8
1259	Three-Dimensional Dirac Semimetal EPbO ₂ . 2017 , 11, 1700271	7
1258	Topological nodal points in two coupled Su-Schrieffer-Heeger chains. 2017 , 96,	23
1257	Phase transitions in three-dimensional Dirac semimetal induced by off-resonant circularly polarized light. 2017 , 381, 3499-3504	6
1256	Lorentz-violating type-II Dirac fermions in transition metal dichalcogenide PtTe. 2017 , 8, 257	239
1255	Anatomy of topological surface states: Exact solutions from destructive interference on frustrated lattices. 2017 , 96,	16
1254	Three-dimensional band structure of LaSb and CeSb: Absence of band inversion. 2017 , 96,	39
1253	Pseudomagnetic lens as a valley and chirality splitter in Dirac and Weyl materials. 2017 , 95,	10
1252	Topological quantum chemistry. 2017 , 547, 298-305	537
1251	Crystal-electric-field excitations and spin dynamics in Ce ₃ Co ₄ Sn ₁₃ semimetallic chiral-lattice phase. 2017 , 95,	4
1250	Nearly massless Dirac fermions and strong Zeeman splitting in the nodal-line semimetal ZrSiS probed by de Haas-van Alphen quantum oscillations. 2017 , 96,	87
1249	Floquet multi-Weyl points in crossing-nodal-line semimetals. 2017 , 96,	36
1248	A magnetic topological semimetal SrMnSb (y, z 2017, 16, 905-910	87
1247	Stability of Weyl points in magnetic half-metallic Heusler compounds. 2017 , 96,	27

1246	Kinetic derivation of generalized phase space Chern-Simons theory. 2017 , 95,	5
1245	Magnetotransport properties of the triply degenerate node topological semimetal tungsten carbide. 2017 , 95,	54
1244	Tunability of the topological nodal-line semimetal phase in ZrSiX-type materials (X=S, Se, Te). 2017 , 95,	85
1243	High-performance electronic transport in the plane of 3D type-II Dirac semimetals. 2017 , 29, 415701	1
1242	Second-order chiral kinetic theory: Chiral magnetic and pseudomagnetic waves. 2017 , 95,	22
1241	Optical phonon dynamics and electronic fluctuations in the Dirac semimetal Cd ₃ As ₂ . 2017 , 95,	25
1240	Super-Klein tunneling of massive pseudospin-one particles. 2017 , 96,	28
1239	Superconductivity in HfTe across weak to strong topological insulator transition induced via pressures. 2017 , 7, 44367	19
1238	Quantized chiral anomaly materials cloak. 2017 , 7, 3253	3
1237	Influence of Fermi arc states and double Weyl node on tunneling in a Dirac semimetal. 2017 , 7, 4030	6
1236	Electronic structure of SrSnAs near the topological critical point. 2017 , 7, 6133	13
1235	Observation of nodal line in non-symmorphic topological semimetal InBi. 2017 , 19, 065007	35
1234	Topological protection from exceptional points in Weyl and nodal-line semimetals. 2017 , 96,	53
1233	Chiral anomaly in Dirac semimetals due to dislocations. 2017 , 95,	25
1232	Manipulation of type-I and type-II Dirac points in PdTe ₂ superconductor by external pressure. 2017 , 96,	48
1231	Large spontaneous Hall effects in chiral topological magnets. 2017 , 97, 2815-2827	4
1230	Magnetotransport of Weyl semimetals due to the chiral anomaly. 2017 , 95,	36
1229	Strain-induced quantum topological phase transitions in Na ₃ Bi. 2017 , 96,	25

1228	Type-II nodal loops: Theory and material realization. 2017 , 96,	110
1227	Antiferromagnetic topological nodal line semimetals. 2017 , 96,	22
1226	Collapse of Landau levels in Weyl semimetals. 2017 , 96,	21
1225	Superuniversality of topological quantum phase transition and global phase diagram of dirty topological systems in three dimensions. 2017 , 95,	17
1224	Direct observation of topological surface-state arcs in photonic metamaterials. 2017 , 8, 97	76
1223	The Enabling Electronic Motif for Topological Insulation in ABO ₃ Perovskites. 2017 , 27, 1701266	17
1222	Temperature-dependent $n\beta$ transition in a three-dimensional Dirac semimetal Na ₃ Bi thin film. 2017 , 96,	7
1221	Hourglass Dirac chain metal in rhenium dioxide. 2017 , 8, 1844	79
1220	A simple and efficient criterion for ready screening of potential topological insulators. 2017 , 62, 1649-1653	9
1219	Type-II Dirac cone and Dirac cone protected by nonsymmorphic symmetry in the carbon-lithium compound C ₄ Li. 2017 , 96,	4
1218	From Multiple Nodal Chain to Dirac/Weyl Semimetal and Topological Insulator in Ternary Hexagonal Materials. 2017 , 121, 28587-28593	10
1217	Massive fermions with low mobility in antiferromagnet orthorhombic CuMnAs single crystals. 2017 , 96,	5
1216	Nodal-knot semimetals. 2017 , 96,	101
1215	Extremely high magnetoresistance and conductivity in the type-II Weyl semimetals WP and MoP. 2017 , 8, 1642	111
1214	Trigger of the Ubiquitous Surface Band Bending in 3D Topological Insulators. 2017 , 7,	15
1213	A New Dirac Semimetal in Hexagonal BaGaSnH. 2017 , 86, 124714	2
1212	Two-Dimensional Dirac Fermions Protected by Space-Time Inversion Symmetry in Black Phosphorus. 2017 , 119, 226801	50
1211	Magnetoresistance and robust resistivity plateau in MoAs. 2017 , 7, 15669	20

1210	Multiple Types of Topological Fermions in Transition Metal Silicides. 2017 , 119, 206402	176
1209	Topology of the momentum space, Wigner transformations, and a chiral anomaly in lattice models. 2017 , 106, 172-178	8
1208	Nernst effect in Dirac and inversion-asymmetric Weyl semimetals. 2017 , 96,	29
1207	Theoretical prediction of two-dimensional functionalized MXene nitrides as topological insulators. 2017 , 96,	50
1206	Coexistence of type-II Dirac point and weak topological phase in Pt ₃ Sn. 2017 , 96,	3
1205	Elastic and transport properties of topological semimetal ZrTe. 2017 , 19, 113044	10
1204	Fortune teller fermions in two-dimensional materials. 2017 , 9, 19337-19345	3
1203	Edge states of mechanical diamond and its topological origin. 2017 , 19, 035003	10
1202	Weyl semimetal induced from a Dirac semimetal by magnetic doping. 2017 , 96,	13
1201	Observation of the topological surface state in the nonsymmorphic topological insulator KHgSb. 2017 , 96,	11
1200	Evolution of the topologically protected surface states in superconductor BiPd from the three-dimensional to the two-dimensional limit. 2017 , 29, 325501	8
1199	Giant planar Hall effect in topological metals. 2017 , 96,	109
1198	Elemental Topological Dirac Semimetal: Bi on InSb(111). 2017 , 118, 146402	71
1197	Quantum oscillation studies of the topological semimetal candidate ZrGeM(M=S,Se,Te). 2017 , 95,	44
1196	Filling-Enforced Magnetic Dirac Semimetals in Two Dimensions. 2017 , 118, 186401	44
1195	Disruption of the Accidental Dirac Semimetal State in ZrTe ₅ under Hydrostatic Pressure. 2017 , 118, 206601	27
1194	Possible Weyl fermions in the magnetic Kondo system CeSb. 2017 , 2,	38
1193	Antibonding ground state of adatom molecules in bulk Dirac semimetals. 2017 , 96,	3

1192	Type-II Symmetry-Protected Topological Dirac Semimetals. 2017 , 119, 026404	112
1191	Two-dimensional topological nodal line semimetal in layered X ₂ Y (X=Ca, Sr, and Ba; Y=As, Sb, and Bi). 2017 , 95,	28
1190	Gate-tuned Aharonov-Bohm interference of surface states in a quasiballistic Dirac semimetal nanowire. 2017 , 95,	20
1189	Single-particle excitations in disordered Weyl fluids. 2017 , 95,	35
1188	Nontrivial Berry phase and type-II Dirac transport in the layered material PdTe ₂ . 2017 , 96,	135
1187	Narrow-gap semiconducting properties of KMgBi with multiband feature. 2017 , 95,	5
1186	Three-dimensional nature of the band structure of ZrTe ₅ measured by high-momentum-resolution photoemission spectroscopy. 2017 , 95,	53
1185	Topological semimetals with a double-helix nodal link. 2017 , 96,	120
1184	Nodal-link semimetals. 2017 , 96,	165
1183	Topological Anderson insulator phase in a Dirac-semimetal thin film. 2017 , 95,	13
1182	Effects of partial La filling and Sb vacancy defects on CoSb ₃ skutterudites. 2017 , 95,	16
1181	Interacting Weyl fermions: Phases, phase transitions, and global phase diagram. 2017 , 95,	72
1180	Nontrivial topology of cubic alkali bismuthides. 2017 , 95,	2
1179	Dirac nodal lines and induced spin Hall effect in metallic rutile oxides. 2017 , 95,	70
1178	Coexistence of four-band nodal rings and triply degenerate nodal points in centrosymmetric metal diborides. 2017 , 95,	101
1177	Magnetotransport properties of the single-crystalline nodal-line semimetal candidates CaTX (T=Ag, Cd; X=As, Ge). 2017 , 95,	46
1176	Predicted Realization of Cubic Dirac Fermion in Quasi-One-Dimensional Transition-Metal Monochalcogenides. 2017 , 7,	44
1175	Chiral anomaly factory: Creating Weyl fermions with a magnetic field. 2017 , 95,	56

1174	Effect of deformation on the electronic structure and topological properties of the $\text{AlIMg}_2\text{Bi}_2$ (Al = Mg,Ca,Sr,Ba) compounds. 2017 , 105, 502-507	4
1173	Current-voltage characteristics of Weyl semimetal semiconducting devices, Veselago lenses, and hyperbolic Dirac phase. 2017 , 95,	39
1172	Extremely Large Magnetoresistance in a Topological Semimetal Candidate Pyrite PtBi_2 . 2017 , 118, 256601	82
1171	Model Hamiltonian and time reversal breaking topological phases of antiferromagnetic half-Heusler materials. 2017 , 95,	31
1170	Molecular beam epitaxy of thin HfTe_2 semimetal films. 2017 , 4, 015001	47
1169	Breaking inversion symmetry induces excitonic peak in optical absorption of topological semimetal. 2017 , 100, 161-169	4
1168	Spectral function of the three-dimensional system of massless Dirac electrons. 2017 , 85, 199-205	1
1167	Topological nodal line semimetals predicted from first-principles calculations. 2017 , 12, 1	91
1166	Spectroscopic evidence for the gapless electronic structure in bulk ZrTe_5 . 2017 , 219, 45-52	14
1165	ARPES study of the epitaxially grown topological crystalline insulator $\text{SnTe}(111)$. 2017 , 219, 35-40	5
1164	Quantum transport in topological semimetals under magnetic fields. 2017 , 12, 1	78
1163	Kinetic theory and anomalous transports in the presence of nonabelian phase-space Berry curvatures. 2017 , 2017,	1
1162	Lifshitz transition mediated electronic transport anomaly in bulk ZrTe_5 . 2017 , 19, 015005	43
1161	Magnetotransport properties and evidence of a topological insulating state in LaSbTe . 2017 , 96,	30
1160	Tunable omnidirectional photonic band gap of one-dimensional photonic crystals containing Dirac semimetals. 2017 , 122, 223108	13
1159	Observation of open-orbit Fermi surface topology in the extremely large magnetoresistance semimetal MoAs_2 . 2017 , 96,	14
1158	Surface Floating 2D Bands in Layered Nonsymmorphic Semimetals: ZrSiS and Related Compounds. 2017 , 7,	31
1157	Transversal magnetoresistance and Shubnikov-de Haas oscillations in Weyl semimetals. 2017 , 96,	15

1156	Strong magnetic field induces superconductivity in a Weyl semimetal. 2017 , 96,	7
1155	Prediction of Ideal Topological Semimetals with Triply Degenerate Points in the NaCu ₃ Te ₂ Family. 2017 , 119, 256402	29
1154	Evidence for topological type-II Weyl semimetal WTe. 2017 , 8, 2150	160
1153	Gross-Neveu-Yukawa model at three loops and Ising critical behavior of Dirac systems. 2017 , 96,	44
1152	Magnetic order induces symmetry breaking in the single-crystalline orthorhombic CuMnAs semimetal. 2017 , 96,	14
1151	Quantum kinetic theory of the chiral anomaly. 2017 , 96,	23
1150	Topological gapless phase in Kitaev model on square lattice. 2017 , 7, 17179	5
1149	Spatial charge inhomogeneity and defect states in topological Dirac semimetal thin films of NaBi. 2017 , 3, eaa06661	9
1148	Quantum Hall states observed in thin films of Dirac semimetal CdAs. 2017 , 8, 2274	82
1147	Phase diagrams in materials science of topological insulators based on metal chalcogenides. 2017 , 62, 1703-1729	39
1146	Prediction of TiRhAs as a Dirac nodal line semimetal via first-principles calculations. 2017 , 96,	2
1145	Quantum oscillations in an anisotropic Weyl semimetal in crossed magnetic and electric fields. 2017 , 43, 1382-1386	1
1144	Magnonic triply-degenerate nodal points. 2017 , 120, 57002	10
1143	Intra-cone transition effect to magnetoconductivity in Dirac semimetal. 2017 , 2017, 1	
1142	Weak Localization and Antilocalization in Topological Materials with Impurity Spin-Orbit Interactions. 2017 , 10,	15
1141	Ultrahigh lattice thermal conductivity in topological semimetal TaN caused by a large acoustic-optical gap. 2018 , 30, 105701	5
1140	Experimental observation of photonic nodal line degeneracies in metacrystals. 2018 , 9, 950	42
1139	Observation of gapless Dirac surface states in ZrGeTe. 2018 , 97,	19

1138	Quantum Dots Formed in Three-dimensional Dirac Semimetal CdAs Nanowires. 2018 , 18, 1863-1868	11
1137	Tunable Weyl and Dirac states in the nonsymmorphic compound CeSbTe. 2018 , 4, eaar2317	61
1136	Topological nature of the node-arc semimetal PtSn probed by de Haas-van Alphen quantum oscillations. 2018 , 30, 155701	7
1135	Symmorphic Intersecting Nodal Rings in Semiconducting Layers. 2018 , 120, 106403	31
1134	Detection of sub-MeV dark matter with three-dimensional Dirac materials. 2018 , 97,	90
1133	Ternary Bismuthide SrPtBi ₂ : Computation and Experiment in Synergism to Explore Solid-State Materials. 2018 , 122, 5057-5063	2
1132	From nodal-ring topological superfluids to spiral Majorana modes in cold atomic systems. 2018 , 97,	4
1131	Towards the manipulation of topological states of matter: a perspective from electron transport. 2018 , 63, 580-594	13
1130	Experimental observation of node-line-like surface states in LaBi. 2018 , 97,	9
1129	Trivial topological phase of CaAgP and the topological nodal-line transition in CaAg(P $\bar{1}$ Asx). 2018 , 97,	14
1128	Quantum oscillation evidence for a topological semimetal phase in ZrSnTe. 2018 , 97,	12
1127	Pressure-induced organic topological nodal-line semimetal in the three-dimensional molecular crystal Pd(ddd _t) ₂ . 2018 , 97,	16
1126	Hopf-link topological nodal-loop semimetals. 2018 , 97,	25
1125	Deformation and stability of surface states in Dirac semimetals. 2018 , 97,	14
1124	Quantum anomalies in nodal line semimetals. 2018 , 97,	20
1123	Field theoretic renormalization study of reduced quantum electrodynamics and applications to the ultrarelativistic limit of Dirac liquids. 2018 , 97,	12
1122	Surface and 3D Quantum Hall Effects from Engineering of Exceptional Points in Nodal-Line Semimetals. 2018 , 120, 146601	45
1121	Comparative study of the compensated semi-metals LaBi and LuBi: a first-principles approach. 2018 , 30, 205501	3

1120	Probing the Fermi surface and magnetotransport properties of MoAs ₂ . 2018 , 97,	10
1119	Converting topological insulators into topological metals within the tetradymite family. 2018 , 97,	1
1118	Chemical Principles of Topological Semimetals. 2018 , 30, 3155-3176	96
1117	Fermiology and Superconductivity of Topological Surface States in PdTe ₂ . 2018 , 120, 156401	71
1116	Pressure-Induced Topological Phase Transitions in CdGeSb and CdSnSb. 2018 , 9, 2202-2207	9
1115	Hall effect in the presence of rotation. 2018 , 121, 47001	10
1114	Robustness of the semimetal state of Na ₃ Bi and Cd ₃ As ₂ against Coulomb interactions. 2018 , 97,	3
1113	Topological properties and functionalities in oxide thin films and interfaces. 2018 , 51, 143001	24
1112	Coexistence of Type-I and Type-II Weyl Points in the Weyl-Semimetal OsC ₂ . 2018 , 122, 3533-3538	15
1111	Excitonic instability in optically pumped three-dimensional Dirac materials. 2018 , 97,	14
1110	Quasiparticle scattering in type-II Weyl semimetal MoTe. 2018 , 30, 105703	3
1109	Measurement of the bulk and surface bands in Dirac line-node semimetal ZrSiS. 2018 , 27, 017105	3
1108	Coexistent three-component and two-component Weyl phonons in TiS, ZrSe, and HfTe. 2018 , 97,	41
1107	Saddle-like topological surface states on the TT ₂ X family of compounds (T, T ₂ = Transition metal, X=Si, Ge). 2018 , 97,	11
1106	Critical chiral Heisenberg model with the functional renormalization group. 2018 , 97,	25
1105	Magnetization of topological line-node semimetals. 2018 , 97,	11
1104	Topological Dirac Nodal-Line Structure in Orthorhombic-Ti ₃ N ₂ . 2018 , 1, 1700018	
1103	Role of four-fermion interaction and impurity in the states of two-dimensional semi-Dirac materials. 2018 , 30, 125401	6

1102	Nonsymmorphic symmetry protected node-line semimetal in the trigonal YH. 2018 , 8, 1467	8
1101	Pressure-induced topological phase transitions and structural transition in 1T-TiTe ₂ single crystal. 2018 , 112, 041907	19
1100	Pressure-induced superconductivity and topological quantum phase transitions in a quasi-one-dimensional topological insulator: Bi ₄ I ₄ . 2018 , 3,	22
1099	Symmetry demanded topological nodal-line materials. 2018 , 3, 1414631	77
1098	Nonsymmorphic-symmetry-protected hourglass Dirac loop, nodal line, and Dirac point in bulk and monolayer X ₃ SiTe ₆ (X = Ta, Nb). 2018 , 97,	71
1097	Cr doping induced negative transverse magnetoresistance in Cd ₃ As ₂ thin films. 2018 , 97,	7
1096	Weyl and Dirac semimetals in three-dimensional solids. 2018 , 90,	1759
1095	Temperature-driven topological transition in 1T'-MoTe ₂ . 2018 , 3,	29
1094	Dynamic conductivity modified by impurity resonant states in doping three-dimensional Dirac semimetals. 2018 , 13, 1	2
1093	Topological quantum catalyst: Dirac nodal line states and a potential electrocatalyst of hydrogen evolution in the TiSi family. 2018 , 61, 23-29	65
1092	Different Topological Quantum States in Ternary Zintl compounds: BaCaX (X = Si, Ge, Sn and Pb). 2018 , 122, 705-713	11
1091	Observation of Dirac-like energy band and ring-torus Fermi surface associated with the nodal line in topological insulator CaAgAs. 2018 , 3,	63
1090	Tunable anisotropic anomalous Nernst effect and orbital magnetization in Floquet Weyl semimetals. 2018 , 382, 729-733	6
1089	Massless Dirac Fermions in ZrTe Semimetal Grown on InAs(111) by van der Waals Epitaxy. 2018 , 12, 1696-1703	60
1088	Three-component fermions with surface Fermi arcs in tungsten carbide. 2018 , 14, 349-354	75
1087	Dynamic current-current susceptibility in three-dimensional Dirac and Weyl semimetals. 2018 , 97,	29
1086	Intermetallic Ca ₃ Pb: a topological zero-dimensional electride material. 2018 , 6, 575-581	27
1085	Double-Weyl Phonons in Transition-Metal Monosilicides. 2018 , 120, 016401	124

1084	Mirror Anomaly in Dirac Semimetals. 2018 , 120, 016603	21
1083	Holographic calculation of the magneto-transport coefficients in Dirac semimetals. 2018 , 2018, 1	7
1082	Inversion symmetry breaking induced triply degenerate points in orderly arranged PtSeTe family materials. 2018 , 30, 245502	4
1081	Relativistic quantum chaos-An emergent interdisciplinary field. 2018 , 28, 052101	20
1080	Topological Semimetals Studied by Ab Initio Calculations. 2018 , 87, 041002	27
1079	Topological Phases of Quantum Matter. 2018 , 141-169	0
1078	Charge/spin supercurrent and the Fulde-Ferrell state induced by crystal deformation in Weyl/Dirac superconductors. 2018 , 97,	11
1077	Predicting multiple Dirac-cones and ultrahigh Fermi velocity in perovskite R _c phase LaCuO ₃ . 2018 , 6, 6132-6137	20
1076	Soft phonon modes driven huge difference on lattice thermal conductivity between topological semimetal WC and WN. 2018 , 148, 144706	7
1075	Validity of Weyl fermion picture for transition metals monopnictides TaAs, TaP, NbAs, and NbP from ab initio studies. 2018 , 8, 3534	23
1074	Quantum oscillations and Dirac dispersion in the BaZnBi ₂ semimetal guaranteed by local Zn vacancy order. 2018 , 97,	8
1073	Lattice field theory simulations of Dirac semimetals. 2018 , 391, 278-292	6
1072	A class of topological nodal rings and its realization in carbon networks. 2018 , 97,	32
1071	Energy scale of Dirac electrons in Cd ₃ As ₂ . 2018 , 97,	12
1070	Alloy Engineering of Topological Semimetal Phase Transition in MgTa _{{2-x}Nb_{x}N_{3}} . 2018 , 120, 136403	24
1069	Recent Progress in the Study of Topological Semimetals. 2018 , 87, 041001	69
1068	Probing lattice dynamics and electron-phonon coupling in the topological nodal-line semimetal ZrSiS. 2018 , 97,	17
1067	Highly anisotropic type-II nodal line state in pure titanium metal. 2018 , 112, 122403	24

1066	Topological semimetal state and field-induced Fermi surface reconstruction in the antiferromagnetic monpnictide NdSb. 2018 , 97,	22
1065	Self-similar transmission patterns induced by magnetic field effects in graphene. 2018 , 101, 22-28	4
1064	Boosting the discovery of 3D topological materials: mixing chemistry with physics via a two-step computational screening strategy. 2018 , 5, 316-318	2
1063	Transport evidence of 3D topological nodal-line semimetal phase in ZrSiS. 2018 , 13, 1	22
1062	Topological materials discovery using electron filling constraints. 2018 , 14, 55-61	32
1061	Discovery of 2D Anisotropic Dirac Cones. 2018 , 30, 1704025	62
1060	Monoclinic C16: sp-sp hybridized nodal-line semimetal protected by PT-symmetry. 2018 , 127, 527-532	28
1059	Surface plasmon of three-dimensional Dirac semimetals. 2018 , 30, 045002	6
1058	Electronic properties of topological insulator candidate CaAgAs. 2018 , 30, 045501	10
1057	Perfect transmission of 3D massive Kane fermions in HgCdTe Veselago lenses. 2018 , 30, 035501	5
1056	High-Dimensional Disorder-Driven Phenomena in Weyl Semimetals, Semiconductors, and Related Systems. 2018 , 9, 35-58	36
1055	Hot carrier relaxation in three dimensional gapped Dirac semi-metals. 2018 , 51, 015101	6
1054	Chapter 12:Discovery of Novel Topological Materials Via High-throughput Computational Search. 2018 , 392-422	1
1053	Chemically driven surface effects in polar intermetallic topological insulators ABi. 2018 , 20, 26372-26385	3
1052	Enhanced Confinement of Terahertz Surface Plasmon Polaritons in Bulk Dirac Semimetal-Insulator-Metal Waveguides. 2018 , 13, 308	11
1051	Magnetic field-induced electronic phase transition in the Dirac semimetal state of black phosphorus under pressure. 2018 , 63, 1539-1544	1
1050	Magnetoresistance of a three-dimensional Dirac gas. 2018 , 98,	7
1049	Topological Hourglass Dirac Semimetal in the Nonpolar Phase of Ag ₂ BiO ₃ . 2018 , 121, 226401	20

1048	Coupled wire models of interacting Dirac nodal superconductors. 2018 , 98,	5
1047	Interacting Topological Insulators with Synthetic Dimensions. 2018 , 8,	4
1046	Upper critical magnetic field in superconducting Dirac semimetal. 2018 , 124, 27004	1
1045	Anatomy of the chiral vortical effect. 2018 , 98,	9
1044	Long range intrinsic ferromagnetism in two dimensional materials and dissipationless future technologies. 2018 , 5, 041105	77
1043	Layered Topological Insulators and Semimetals for Magnetoresistance Type Sensors. 2018 , 2, 1800039	6
1042	Topologically nontrivial phase in the hexagonal antiperovskites A_3BiB ($A=Ba,Sr$; $B=P,N$). 2018 , 98,	3
1041	Chiral effects in magnetized quantum spinor matter in particle and astroparticle physics. 2018 , 33, 1845020	
1040	Single-crystal investigation of the proposed type-II Weyl semimetal CeAlGe. 2018 , 98,	29
1039	Tunability and enlargement of omnidirectional transmission frequency range in a photonic heterostructure containing Dirac semimetal. 2018 , 8, 125312	1
1038	Chiral anomaly without Landau levels: From the quantum to the classical regime. 2018 , 98,	3
1037	Giant tunable nonreciprocity of light in Weyl semimetals. 2018 , 98,	50
1036	Dirac semimetal in type-IV magnetic space groups. 2018 , 98,	44
1035	Predicting Dirac semimetals based on sodium ternary compounds. 2018 , 4,	9
1034	Phase diagram and Chiral Magnetic Effect in Dirac Semimetals from Lattice Simulation. 2018 , 175, 03001	2
1033	Magnetotransport Properties of a Nodal Line Semimetal TiSi. 2018 , 35, 117101	
1032	NMR diagnosis of pseudo-scalar superconductivity in 3D Dirac materials. 2018 , 30, 50LT01	
1031	Electric-field-tuned topological phase transition in ultrathin NaBi. 2018 , 564, 390-394	85

1030	Bulk band inversion and surface Dirac cones in LaSb and LaBi: Prediction of a new topological heterostructure. 2018 , 8, 14867	9
1029	Surface termination dependent quasiparticle scattering interference and magneto-transport study on ZrSiS. 2018 , 20, 103025	11
1028	Topological Materials and Solid-State Chemistry Binding and Characterizing New Topological Materials. 2018 , 211-243	
1027	Black-hole horizon in the Dirac semimetal Zn ₂ In ₂ S ₅ . 2018 , 98,	40
1026	Observation of band crossings protected by nonsymmorphic symmetry in the layered ternary telluride Ta ₃ SiTe ₆ . 2018 , 98,	13
1025	Scaling of the chiral magnetic effect in quantum diffusive Weyl semimetals. 2018 , 97,	1
1024	Type-I and type-II nodal lines coexistence in the antiferromagnetic monolayer CrAs ₂ . 2018 , 98,	28
1023	Majorana States. 2018 , 357-412	
1022	Spin-momentum locking and spin-orbit torques in magnetic nano-heterojunctions composed of Weyl semimetal WTe. 2018 , 9, 3990	64
1021	Tunable two-dimensional Dirac nodal nets. 2018 , 98,	6
1020	Global Phase Diagram of a Dirty Weyl Liquid and Emergent Superuniversality. 2018 , 8,	31
1019	Quantitative evaluation of Dirac physics in PbTe. 2018 , 98,	6
1018	Quantum transport in a compensated semimetal W ₂ As ₃ with nontrivial Z ₂ indices. 2018 , 98,	7
1017	Giant planar Hall effect in the Dirac semimetal ZrTe ₅ 2018 , 98,	50
1016	Tunable electromagnetically induced reflection with a high Q factor in complementary Dirac semimetal metamaterials. 2018 , 5, 125804	14
1015	Topological Insulators versus Topological Dirac Semimetals in Honeycomb Compounds. 2018 , 140, 13687-13694	41
1014	Electronic structure of the topological superconductor candidate Au ₂ Pb. 2018 , 98,	6
1013	The type II Weyl semimetals at low temperatures: Chiral anomaly, elastic deformations, zero sound. 2018 , 399, 26-52	7

1012	Tunable magnetoresistance in thin-film graphite field-effect transistor by gate voltage. 2018 , 98,	4
1011	Electron transport in Dirac and Weyl semimetals. 2018 , 27, 107402	15
1010	Dynamical density response and optical conductivity in topological metals. 2018 , 98,	7
1009	Photoexcitation in two-dimensional topological insulators. 2018 , 227, 1323-1344	5
1008	Full counting statistics in the free Dirac theory. 2018 , 51, 475002	8
1007	Proposal for Detecting Nodal-Line Semimetal Surface States with Resonant Spin-Flipped Reflection. 2018 , 121, 166802	22
1006	Temperature-Driven Topological Phase Transition and Intermediate Dirac Semimetal Phase in ZrTe ₅ . 2018 , 121, 187401	61
1005	Chiral electric separation effect in Weyl semimetals. 2018 , 98,	8
1004	Disorder-Driven Quantum Transition in Relativistic Semimetals: Functional Renormalization via the Porous Medium Equation. 2018 , 121, 166402	7
1003	Strain-induced nonlinear spin Hall effect in topological Dirac semimetal. 2018 , 8, 15236	7
1002	Prediction of ideal triple degenerate points in HfIrAs and HfIrBi. 2018 , 98,	5
1001	4 π -periodic Andreev bound states in a Dirac semimetal. 2018 , 17, 875-880	52
1000	Maximal distant entanglement in Kitaev tube. 2018 , 8, 12202	1
999	Visualization of electronic topology in ZrSiSe by scanning tunneling microscopy. 2018 , 98,	6
998	Conversion Rules for Weyl Points and Nodal Lines in Topological Media. 2018 , 121, 106402	18
997	Dirac-Weyl Semimetal: Coexistence of Dirac and Weyl Fermions in Polar Hexagonal ABC Crystals. 2018 , 121, 106404	34
996	Dirac nodal line in bilayer borophene: Tight-binding model and low-energy effective Hamiltonian. 2018 , 98,	17
995	Band Topology and Linking Structure of Nodal Line Semimetals with Z ₂ Monopole Charges. 2018 , 121, 106403	81

994	Magnetotransport in Sr ₃ PbO antiperovskite. 2018 , 98,	15
993	Large intrinsic anomalous Hall effect in half-metallic ferromagnet CoSnS with magnetic Weyl fermions. 2018 , 9, 3681	240
992	Experimental observation of bulk nodal lines and electronic surface states in ZrB ₂ . 2018 , 3,	27
991	Drumhead surface states and their signatures in quasiparticle scattering interference. 2018 , 98,	3
990	Lattice thermal conductivity and bandgap engineering of a three-dimensional sp ² -hybridized Dirac carbon material: HS-C48. 2018 , 155, 293-297	6
989	Quadratic contact point semimetal: Theory and material realization. 2018 , 98,	33
988	Visualizing electronic structures of quantum materials by angle-resolved photoemission spectroscopy. 2018 , 3, 341-353	36
987	Spectroscopic evidence of topological phase transition in the three-dimensional Dirac semimetal Cd ₃ (As _{1-x} P _x) ₂ . 2018 , 98,	4
986	High-Pressure Synthesis: A New Frontier in the Search for Next-Generation Intermetallic Compounds. 2018 , 51, 1315-1323	19
985	Fermi arc mediated entropy transport in topological semimetals. 2018 , 97,	10
984	Bulk Fermi Surfaces of the Dirac Type-II Semimetallic Candidates MA ₃ (Where M=V, Nb, and Ta). 2018 , 120, 206401	19
983	Quasiparticle interference on type-I and type-II Weyl semimetal surfaces: a review. 2018 , 3, 1466661	26
982	Phase transition studies of NaBi system under uniaxial strain. 2018 , 30, 125502	2
981	Observation of Landau quantization and standing waves in HfSiS. 2018 , 97,	3
980	Engineering topological phases in the Luttinger semimetal Bi ₂ Se ₃ . 2018 , 97,	28
979	Thickness-Tunable Synthesis of Ultrathin Type-II Dirac Semimetal PtTe Single Crystals and Their Thickness-Dependent Electronic Properties. 2018 , 18, 3523-3529	103
978	Gate-tuned quantum Hall states in Dirac semimetal (Cd _{1-x} Zn _x)As. 2018 , 4, eaar5668	31
977	Magnetic field induced metal-insulator transition in single nodal ring topological semimetals. 2018 , 30, 285501	0

976	Pressure-induced superconductivity in MoP. 2018 , 3,	18
975	Generation of a Nernst Current from the Conformal Anomaly in Dirac and Weyl Semimetals. 2018 , 120, 206601	35
974	Tuning the topological nontrivial nature in a family of alkali-metal-based inverse Heusler compounds: A first-principles study. 2018 , 463, 44-49	5
973	Structural and transport properties of the topological semimetal TaSb ₂ at high pressures. 2018 , 265, 359-363	2
972	Relativistic quantum chaos. 2018 , 753, 1-128	24
971	Almost ideal nodal-loop semimetal in monoclinic CuTeO ₃ material. 2018 , 97,	20
970	Anomalous transport properties of Dirac and Weyl semimetals (Review Article). 2018 , 44, 487-505	26
969	Discovery of coexisting Dirac and triply degenerate magnons in a three-dimensional antiferromagnet. 2018 , 9, 2591	36
968	Nodal line fermions in magnetic oxides. 2018 , 97,	17
967	Surface states in Dirac semimetals and topological crystalline insulators. 2018 , 98,	5
966	Surface plasmons in Weyl semimetals. 2018 , 30, 365003	10
965	Non-Abelian properties of electron wave packets in the Dirac semimetals A ₃ Bi (A=Na,K,Rb). 2018 , 98,	6
964	Distinct multiple fermionic states in a single topological metal. 2018 , 9, 3002	8
963	Dirac semimetals based tunable narrowband absorber at terahertz frequencies. 2018 , 26, 11471-11480	70
962	Controlling terahertz surface plasmon polaritons in Dirac semimetal sheets. 2018 , 8, 884	22
961	Nodal-chain network, intersecting nodal rings and triple points coexisting in nonsymmorphic BaSi. 2018 , 20, 21177-21183	13
960	Alkali-metal-induced topological nodal line semimetal in layered XN ₂ (X = Cr, Mo, W). 2018 , 13, 1	7
959	Tip-induced or enhanced superconductivity: a way to detect topological superconductivity. 2018 , 63, 1141-1158	20

958	Magnetic states and Kondo screening in Weyl semimetals with chiral anomaly. 2018 , 98,	6
957	Nodeless superconductivity in the type-II Dirac semimetal PdTe ₂ : London penetration depth and pairing-symmetry analysis. 2018 , 98,	29
956	A smeared quantum phase transition in disordered holography. 2018 , 2018, 1	16
955	Anisotropic transverse magnetoresistance and Fermi surface in TaSb. 2018 , 8, 10527	8
954	Triply degenerate nodal points in RRh ₆ Ge ₄ (R=Y,La,Lu). 2018 , 98,	9
953	Thermal plasmon resonantly enhances electron scattering in Dirac/Weyl semimetals. 2018 , 98,	7
952	Effective lagrangian for axial anomaly and its applications in Dirac and Weyl semimetals. 2018 , 8, 11271	
951	Spin-1 topological monopoles in the parameter space of ultracold atoms. 2018 , 98,	7
950	Planar Hall effect in the type-II Dirac semimetal VAl ₃ . 2018 , 98,	44
949	Tunable electronic structure and surface states in rare-earth monobismuthides with partially filled f shell. 2018 , 98,	16
948	Large anomalous Hall current induced by topological nodal lines in a ferromagnetic van der Waals semimetal. 2018 , 17, 794-799	187
947	Topological spin excitations in a three-dimensional antiferromagnet. 2018 , 14, 1011-1015	46
946	Multiple topologically nontrivial bands in noncentrosymmetric YSn ₂ . 2018 , 98,	1
945	Observation of a Dirac nodal line in AlB ₂ . 2018 , 98,	14
944	Band Structure Perfection and Superconductivity in Type-II Dirac Semimetal Ir Pt Te. 2018 , 30, e1801556	28
943	Experimental Observation of Acoustic Weyl Points and Topological Surface States. 2018 , 10,	49
942	Dirac Semimetal Heterostructures: 3D Cd As on 2D Graphene. 2018 , 30, e1707547	23
941	Coherent terahertz SmithBurcell radiation from Dirac semimetals grating with very deep and narrow slits. 2018 , 11, 082801	5

940	Lattice quantum Monte Carlo study of chiral magnetic effect in Dirac semimetals. 2018 , 396, 78-86	5
939	Dynamical bulk-edge correspondence for degeneracy lines in parameter space. 2018 , 98,	4
938	Wallpaper fermions and the nonsymmorphic Dirac insulator. <i>Science</i> , 2018 , 361, 246-251	33-3 73
937	Ubiquitous formation of bulk Dirac cones and topological surface states from a single orbital manifold in transition-metal dichalcogenides. 2018 , 17, 21-28	89
936	Rotational strain in Weyl semimetals: A continuum approach. 2018 , 97,	25
935	Observation of a nodal chain with Dirac surface states in TiB ₂ . 2018 , 97,	26
934	Extremely large magnetoresistance and high-density Dirac-like fermions in ZrB ₂ . 2018 , 97,	10
933	Evidence for a Dirac nodal-line semimetal in SrAs ₃ . 2018 , 63, 535-541	21
932	Three-dimensional Dirac semimetal Cd ₃ As ₂ as a potential candidate for thermoelectric applications. 2018 ,	
931	Experimental Observation of Dirac Nodal Links in Centrosymmetric Semimetal TiB ₂ . 2018 , 8,	32
930	Thermionic energy conversion based on 3D Dirac semimetals. 2018 , 51, 405501	13
929	Magnetic field induced Weyl semimetal from Wannier-function-based tight-binding model. 2018 , 98,	5
928	Extremely large magnetoresistance in the nonmagnetic semimetal YBi. 2018 , 6, 10020-10029	6
927	Cryogenic amplifier with low input-referred voltage noise calibrated by shot noise measurement. 2018 , 27, 060702	3
926	Spindle nodal chain in three-dimensional α -boron. 2018 , 20, 23500-23506	13
925	MgTa ₂ N ₃ : A reference Dirac semimetal. 2018 , 98,	12
924	Topological Dirac semimetal Na ₃ Bi films in the ultrathin limit via alternating layer molecular beam epitaxy. 2018 , 6, 086103	3
923	Large magnetoresistance and superconductivity in α -gallium single crystals. 2018 , 3,	10

922	Type I superconductivity in Dirac materials. 2018 , 30, 335403	5
921	Quantum criticality with infinite anisotropy in topological phase transitions between Dirac and Weyl semimetals. 2018 , 98,	9
920	Two-dimensional type-II Dirac fermions in layered oxides. 2018 , 9, 3252	14
919	Spin-orbit coupling driven crossover from a starfruitlike nodal semimetal to Dirac and Weyl semimetal state in CaAuAs. 2018 , 98,	13
918	A possible candidate for triply degenerate point fermions in trigonal layered PtBi. 2018 , 9, 3249	33
917	3D Dirac Plasmons in the Type-II Dirac Semimetal PtTe ₂ . 2018 , 121, 086804	57
916	Symmetry protected topological Luttinger liquids and the phase transition between them. 2018 , 63, 753-758	18
915	Ferromagnetic Weyl fermions in CrO ₂ . 2018 , 97,	16
914	Long-range Coulomb interaction effects on the topological phase transitions between semimetals and insulators. 2018 , 97,	6
913	Negative magnetoresistance suppressed through a topological phase transition in (Cd _{1-x} Zn _x) ₃ As ₂ thin films. 2018 , 97,	14
912	Hot electron cooling in Dirac semimetal CdAs due to polar optical phonons. 2018 , 30, 265303	9
911	Inducing Strong Superconductivity in WTe by a Proximity Effect. 2018 , 12, 7185-7196	26
910	Coexistence of tunable Weyl points and topological nodal lines in ternary transition-metal telluride TaIrTe ₄ . 2018 , 97,	18
909	Klein tunneling and electron optics in Dirac-Weyl fermion systems with tilted energy dispersion. 2018 , 97,	29
908	Resonant electron tunneling spectroscopy of antibonding states in a Dirac semimetal. 2018 , 97,	1
907	Quantum oscillations in type-II Dirac semimetal PtTe ₂ . 2018 , 97,	17
906	Topological Triply Degenerate Points Induced by Spin-Tensor-Momentum Couplings. 2018 , 120, 240401	27
905	Topological Dirac semimetal phase in GexSny alloys. 2018 , 112, 251601	6

904	Spin susceptibility of three-dimensional Dirac-Weyl semimetals. 2018 , 97,	8
903	Catalysis of dynamical chiral symmetry breaking by chiral chemical potential in Dirac semimetals. 2019 , 100,	7
902	Magneto-optical conductance of Kane fermion gas in low frequencies. 2019 , 21, 083010	1
901	Field-effect transistors with the three-dimensional Dirac semimetal cadmium arsenide. 2019 , 115, 062101	6
900	Dimensional Crossover and Topological Phase Transition in Dirac Semimetal NaBi Films. 2019 , 13, 9647-9654	17
899	De Haas-van Alphen study on three-dimensional topological semimetal pyrite PtBi ₂ . 2019 , 64, 1496-1501	2
898	Time-reversal symmetry breaking type-II Weyl state in YbMnBi. 2019 , 10, 3424	73
897	Large Contribution of Fermi Arcs to the Conductivity of Topological Metals. 2019 , 123, 066804	10
896	Magnetic Susceptibility of Topological Semimetals. 2019 , 197, 272-309	7
895	Design triple points, nexus points, and related topological phases by stacking monolayers. 2019 , 115, 073105	1
894	Fermi surface nesting and intrinsic resistivity of beryllium: First-principles calculations. 2019 , 100,	2
893	Topological Lifshitz transitions and Fermi arc manipulation in Weyl semimetal NbAs. 2019 , 10, 3478	20
892	Chiral tunneling oscillations based on Weyl semimetals. 2019 , 133, 106213	2
891	Mixed topological semimetals driven by orbital complexity in two-dimensional ferromagnets. 2019 , 10, 3179	17
890	Spin fluctuation induced Weyl semimetal state in the paramagnetic phase of EuCdAs. 2019 , 5, eaaw4718	48
889	Exploring Topological Superconductivity in Topological Materials. 2019 , 2, 1800112	17
888	Straight nodal lines and waterslide surface states observed in acoustic metacrystals. 2019 , 100,	4
887	Topological nodal lines in three-dimensional single wall carbon nanotube network. 2019 , 169, 109123	1

886	Tunable ferromagnetic Weyl fermions from a hybrid nodal ring. 2019 , 5,	11
885	Structural, elastic, and electronic properties of topological semimetal WC-type MX family by first-principles calculation. 2019 , 28, 077105	5
884	Dynamically Stable Topological Phase of Arsenene. 2019 , 9, 7966	12
883	Topological Semimetals from First Principles. 2019 , 49, 153-183	67
882	Nonsaturating Magnetoresistance and Nontrivial Band Topology of Type-II Weyl Semimetal NbIrTe ₄ . 2019 , 5, 1900250	9
881	Anisotropic Landau level splitting and Lifshitz transition induced magnetoresistance enhancement in ZrTe ₅ crystals. 2019 , 21, 093009	3
880	Band structure engineering of chemically tunable LnSbTe (Ln = La, Ce, Pr). 2019 , 7, 101113	11
879	Phonon-limited mobility of Dirac fermions in three-dimensional Dirac semimetal Cd ₃ As ₂ . 2019 , 126, 135703	3
878	The study of magnetic topological semimetals by first principles calculations. 2019 , 5,	29
877	Topological nodal lines and hybrid Weyl nodes in YCoC ₂ . 2019 , 7, 101109	8
876	Composite Dirac semimetals. 2019 , 100,	6
875	Coexistence of Weyl and Type-II Triply Degenerate Fermions in a Ternary Topological Semimetal YPtP. 2019 , 13, 1900421	0
874	Magnetic and transport properties of Zr Nb CoSn. 2019 , 31, 275702	1
873	Phonon limited mobility in 3D Dirac semimetal Cd ₃ As ₂ . 2019 , 561, 012030	
872	A New Three-Dimensional Subsulfide IrInS with Dirac Semimetal Behavior. 2019 , 141, 19130-19137	17
871	Realization of interlayer ferromagnetic interaction in MnSbTe toward the magnetic Weyl semimetal state. 2019 , 100,	41
870	Weyl semimetal phase in the noncentrosymmetric superlattice W ₂ XY(X,Y=S,Se,Te,XIV). 2019 , 100,	2
869	Dual topological insulator and insulator-semimetal transition in mirror-symmetric honeycomb materials. 2019 , 100,	1

868	Transverse thermopower in Dirac and Weyl semimetals. 2019 , 100,	7
867	Photon-Induced Weyl Half-Metal Phase and Spin Filter Effect from Topological Dirac Semimetals. 2019 , 123, 206601	13
866	Thermoelectric transport coefficients of a Dirac electron gas in high magnetic fields. 2019 , 100,	0
865	Higher-Order Topology, Monopole Nodal Lines, and the Origin of Large Fermi Arcs in Transition Metal Dichalcogenides XTe_2 ($X=Mo,W$). 2019 , 123, 186401	116
864	Multifold nodal points in magnetic materials. 2019 , 7, 101125	24
863	Giant tunable Goos-Hänchen shifts based on surface plasmon resonance with Dirac semimetal films. 2019 , 53, 015107	6
862	Multifractality at the Weyl-semimetal-diffusive-metal transition for generic disorder. 2019 , 100,	5
861	Dirac-Weyl semimetal phase in noncentrosymmetric transition metal monochalcogenides $MoTe$ and WTe . 2019 , 7, 12151-12159	8
860	Angle-resolved photoemission spectroscopy and its application to topological materials. 2019 , 1, 609-626	91
859	Ultrafast nonlocal collective dynamics of Kane plasmon-polaritons in a narrow-gap semiconductor. 2019 , 5, eaau9956	10
858	Locally self-consistent embedding approach for disordered electronic systems. 2019 , 100,	1
857	Origin of the butterfly magnetoresistance in a Dirac nodal-line system. 2019 , 100,	6
856	Robust topological nodal lines in halide carbides. 2019 , 21, 20262-20268	6
855	Anomalous quantum oscillations and evidence for a non-trivial Berry phase in $SmSb$. 2019 , 4,	5
854	Selective control of surface spin current in topological pyrite-type OsX_2 ($X = Se, Te$) crystals. 2019 , 4,	5
853	Review of Electron-Electron Interaction Effects in Planar Dirac Liquids. 2019 , 200, 1222-1236	3
852	Quantum oscillations and nontrivial topological state in a compensated semimetal TaP_2 . 2019 , 100,	6
851	Large magnetothermopower and anomalous Nernst effect in $HfTe_5$. 2019 , 100,	11

850	Fully spin-polarized open and closed nodal lines in Borophene by magnetic proximity effect. 2019 , 100,	7
849	Nonlinear plasmonics of three-dimensional Dirac semimetals. 2019 , 4, 034402	32
848	Tunable topological semimetallic phases in Kondo lattice systems. 2019 , 99,	3
847	Quantum transport characteristics of heavily doped bismuth selenide nanoribbons. 2019 , 4,	20
846	Emergence of Topological insulator and Nodal line semi-metal states in $XX'Bi$ ($X = Na, K, Rb, Cs$; $X' = Ca, Sr$). 2019 , 9, 527	7
845	Bulk-boundary correspondence in a non-Hermitian system in one dimension with chiral inversion symmetry. 2019 , 99,	174
844	Extreme magnetoresistance and pressure-induced superconductivity in the topological semimetal candidate YBi. 2019 , 99,	8
843	Chiral anomaly and nontrivial Berry phase in the topological nodal-line semimetal $SrAs_3$. 2019 , 99,	13
842	Quaternary Heusler alloy: An ideal platform to realize triple point fermions. 2019 , 99,	14
841	Topological properties of the intermetallic compounds $Sc-TM$ ($TM = Cd, Ag, Cu, Hg, Au$). 2019 , 160, 275-278	4
840	Deformation-induced phase transition in Weyl semimetals: pseudo-field origin of effect. 2019 , 45, 107-112	0
839	Magnetism in Cu_2Si zigzag nanoribbon. 2019 , 161, 119-126	3
838	Probing the origin of extreme magnetoresistance in Pr/Sm mono-antimonides/bismuthides. 2019 , 99,	4
837	Two-dimensional spin-valley-coupled Dirac semimetals in functionalized $SbAs$ monolayers. 2019 , 6, 781-787	21
836	Observation of Three-Dimensional Photonic Dirac Points and Spin-Polarized Surface Arcs. 2019 , 122, 203903	31
835	Quantum and transport mobilities of a Na_3Bi -based three-dimensional Dirac system. 2019 , 99,	1
834	Topology on a new facet of bismuth. 2019 , 116, 13255-13259	32
833	Fermi surface topology and large magnetoresistance in the topological semimetal candidate PrBi. 2019 , 99,	9

832	Topologically nontrivial photonic nodal surface in a photonic metamaterial. 2019 , 99,	17
831	Singular angular magnetoresistance in a magnetic nodal semimetal. <i>Science</i> , 2019 , 365, 377-381	33.3 41
830	New topological semimetal candidate of nonsymmorphic PdSb ₂ with unique six-fold degenerate point. 2019 , 14, 1	3
829	Extremely high conductivity observed in the triple point topological metal MoP. 2019 , 10, 2475	28
828	Thermionic emission laws for general electron dispersion relations and band structure data. 2019 , 125, 215105	2
827	Chiral magnetic chemical bonds in molecular states of impurities in Weyl semimetals. 2019 , 9, 8452	2
826	Fermi-level Dirac crossings in 4d and 5d cubic metal oxides: NaPd ₃ O ₄ and NaPt ₃ O ₄ . 2019 , 99,	3
825	Observation of multiple types of topological fermions in PdBiSe. 2019 , 99,	15
824	Ultrafast photocarrier dynamics in a 3D Dirac semimetal Cd ₃ As ₂ film studied with terahertz spectroscopy. 2019 , 114, 221102	32
823	Spatial anisotropy of the Kondo screening cloud in a type-II Weyl semimetal. 2019 , 99,	2
822	High-throughput Discovery of Topologically Non-trivial Materials using Spin-orbit Spillage. 2019 , 9, 8534	24
821	Topological Phase Transition in SbMg Assisted by Strain. 2019 , 4, 8701-8706	5
820	Effective models for nearly ideal Dirac semimetals. 2019 , 14, 1	2
819	Dual topological nodal line and nonsymmorphic Dirac semimetal in three dimensions. 2019 , 99,	4
818	Universal Broadening of Cyclotron Absorption in Dirac Semimetals. 2019 , 109, 316-319	
817	Composite topological nodal lines penetrating the Brillouin zone in orthorhombic AgF ₂ . 2019 , 5,	7
816	Ab initio study of the electronic, elastic, vibrational and dielectric properties of KBaBi. 2019 , 276, 272-277	3
815	Dirac nodal surfaces and nodal lines in ZrSiS. 2019 , 5, eaau6459	53

814	Topological Semimetals in the SnTe Material Class: Nodal Lines and Weyl Points. 2019 , 122, 186801	14
813	Broken symmetry driven phase transitions from a topological semimetal to a gapped topological phase in SrAgAs. 2019 , 99,	5
812	Fate of superconductivity in disordered Dirac and semi-Dirac semimetals. 2019 , 3, 055006	0
811	Quantum transport in topological semimetals under magnetic fields (II). 2019 , 14, 1	12
810	Prediction of robust multiple Dirac-cones in newly designed perovskite R3Rc phase AgBO3 from first-principles. 2019 , 13, 102301	5
809	Emergence of topological electronic phases in elemental lithium under pressure. 2019 , 116, 9197-9201	3
808	Fragility of Fermi arcs in Dirac semimetals. 2019 , 99,	10
807	Electromagnetic fields induced by an electric charge near a Weyl semimetal. 2019 , 99,	6
806	Surface Reconstruction, Oxidation Mechanism, and Stability of Cd3As2. 2019 , 29, 1900965	9
805	Dirac fermions in the layered titanium-based oxypnictide superconductor BaTi2Bi2O. 2019 , 99,	3
804	Novel electric field effects on Landau levels in multi-Weyl semimetals. 2019 , 383, 2339-2345	0
803	Hopf-chain networks evolved from triple points. 2019 , 99,	7
802	Symmetry protected topological phases characterized by isolated exceptional points. 2019 , 99,	32
801	Anisotropic magnetoelectronic structures and magneto-transport properties of topological Dirac semimetal nanowires. 2019 , 484, 373-381	2
800	Fermions and bosons in nonsymmorphic PdSb2 with sixfold degeneracy. 2019 , 99,	13
799	Spin transport and spin pump in graphene-like materials: effects of tilted Dirac cone. 2019 , 92, 1	5
798	Shubnikov-de Haas oscillations in the three-dimensional Dirac fermion system Ca3PbO. 2019 , 99,	4
797	A Dirac semimetal phase diagram of the binary compound CuI(R-3m). 2019 , 131, 62-68	1

796	Observation of unconventional chiral fermions with long Fermi arcs in CoSi. 2019 , 567, 496-499	129
795	Relativistic suppression of Auger recombination in Weyl semimetals. 2019 , 99,	6
794	Tunable surface plasmons in Weyl semimetals TaAs and NbAs. 2019 , 99,	13
793	Non-saturating quantum magnetization in Weyl semimetal TaAs. 2019 , 10, 1028	16
792	From Dirac Semimetals to Topological Phases in Three Dimensions: A Coupled-Wire Construction. 2019 , 9,	11
791	Nonlinear chiral transport from holography. 2019 , 2019, 1	7
790	Nodal chain semimetal in geometrically frustrated systems. 2019 , 99,	11
789	Robustness of anomaly-related magnetoresistance in doped Weyl semimetals. 2019 , 99,	6
788	Shubnikov-de Haas and de Haas-van Alphen oscillations in the topological semimetal CaAl ₄ . 2019 , 99,	2
787	New type of hybrid nodal line semimetal in Be ₂ Si. 2019 , 21, 033018	12
786	Electronic properties of the parabolic Dirac system. 2019 , 383, 1795-1805	3
785	Fundamental insights to topological quantum materials: A real-space view of 13 cases by supersymmetry of valence bonds approach. 2019 , 6, 011304	4
784	Optically Driven Collective Spin Excitations and Magnetization Dynamics in the Néel-type Skyrmion Host GaV ₄ S ₈ . 2019 , 122, 107203	12
783	Topological massive Dirac fermions in Tungsten. 2019 , 99,	5
782	Effective spin-2 quasi-particles at linear dispersive five-fold degenerate points with tunable topological Chern numbers. 2019 , 383, 2139-2144	1
781	Thermoelectric energy conversion and topological materials based on heavy metal chalcogenides. 2019 , 275, 103-123	19
780	Broken cubic symmetry driven co-emergence of type-I and type-II Dirac points in topological crystalline insulator ThTaN. 2019 , 31, 295501	2
779	Transport of Topological Semimetals. 2019 , 49, 207-252	76

778	Topological magnon nodal lines and absence of magnon spin Nernst effect in layered collinear antiferromagnets. 2019 , 125, 36002	5
777	Electronic, elastic and lattice dynamic properties of the topological Dirac semimetal Na ₃ Bi. 2019 , 6, 076308	1
776	Transport properties of topological nodal-line semimetal candidate CaAs ₃ under hydrostatic pressure. 2019 , 28, 046202	3
775	One-dimensional topological metal. 2019 , 99,	5
774	Realization of low-energy type-II Dirac fermions in (Ir _{1-x} Pt _x)Te ₂ superconductors. 2019 , 28, 037103	4
773	Majorana flat band edge modes of topological gapless phase in 2D Kitaev square lattice. 2019 , 9, 4978	4
772	Theory for spin torque in Weyl semimetal with magnetic texture. 2019 , 9, 5365	20
771	RKKY interaction on the surface of three-dimensional Dirac semimetals. 2019 , 99,	10
770	Electronic properties of candidate type-II Weyl semimetal WTe ₂ . A review perspective. 2019 , 1, 014003	14
769	Experimental progress on layered topological semimetals. 2019 , 6, 032001	16
768	Mirror anomaly and anomalous Hall effect in type-I Dirac semimetals. 2019 , 99,	2
767	Robust Twin Pairs of Weyl Fermions in Ferromagnetic Oxides. 2019 , 122, 057205	6
766	Ideal Nodal Line Semimetal in a Two-Dimensional Boron Bilayer. 2019 , 123, 4977-4983	19
765	Axial-field-induced chiral channels in an acoustic Weyl system. 2019 , 15, 357-361	50
764	Topological phases in acoustic and mechanical systems. 2019 , 1, 281-294	219
763	Quantum transport properties of single-crystalline AgSeTe nanowires as a new topological material. 2019 , 11, 5171-5179	4
762	Zero chiral bulk modes in 3D Weyl metamaterials. 2019 , 64, 799-801	1
761	Evolution of Superconductivity with Sr-Deficiency in Antiperovskite Oxide SrSnO. 2019 , 9, 1831	10

760	Spin-orbit crossed susceptibility in topological Dirac semimetals. 2019 , 99,	10
759	Observation of Chiral Fermions with a Large Topological Charge and Associated Fermi-Arc Surface States in CoSi. 2019 , 122, 076402	109
758	Possible pressure-induced topological quantum phase transition in the nodal line semimetal ZrSiS. 2019 , 99,	10
757	Weyl points of mechanical diamond. 2019 , 99,	5
756	Transport Properties of Topological Semimetal Tungsten Carbide in the 2D Limit. 2019 , 5, 1800839	5
755	Single crystal growth of PtSe ₂ via CuSe flux method and its large magneto-resistance. 2019 , 785, 871-874	5
754	Non-Hermitian nodal-line semimetals with an anomalous bulk-boundary correspondence. 2019 , 99,	84
753	Weyl-loop half-metal in Li ₃ (FeO ₃) ₂ . 2019 , 99,	43
752	Electronic non-coplanar refraction and deflected diffraction of Weyl-node-mismatch junctions. 2019 , 21, 113057	6
751	Nontrivial topology in the layered Dirac nodal-line semimetal candidate SrZnSb ₂ with distorted Sb square nets. 2019 , 100,	11
750	Dual-Polarization, Tunable Breaking Window in the Polarization Conversion Pass Band in a Terahertz Dirac Semimetal-Based Metamaterial. 2019 , 11, 1-9	2
749	Topological dual double node-line semimetals NaAlSi(Ge) and their potential as cathode material for sodium ion batteries. 2019 , 7, 15375-15381	12
748	Molecular diamond lattice antiferromagnet as a Dirac semimetal candidate. 2019 , 99,	5
747	Two-dimensional Tunable Dirac/Weyl Semimetal in Non-Abelian Gauge Field. 2019 , 9, 18516	4
746	Semi-quantized Spin Pumping and Spin-Orbit Torques in Topological Dirac Semimetals. 2019 , 9, 19659	7
745	PT-symmetry-protected Dirac states in strain-induced hidden MoS ₂ monolayer. 2019 , 100,	6
744	Dirac fermions and possible weak antilocalization in LaCuSb ₂ . 2019 , 7, 121108	6
743	Cooper instability generated by attractive fermion-fermion interaction in the two-dimensional semi-Dirac semimetals. 2019 , 31, 275601	3

742	Robustness of the pumping charge to dynamic disorder. 2019 , 100,	2
741	Anisotropic planar Hall effect in the type-II topological Weyl semimetal WTe ₂ . 2019 , 100,	19
740	Chiral fermion reversal in chiral crystals. 2019 , 10, 5505	17
739	Theoretical and experimental evidence for the intrinsic three-dimensional Dirac state in Cu ₂ HgSnSe ₄ . 2019 , 100,	1
738	Observation of bulk states and spin-polarized topological surface states in transition metal dichalcogenide Dirac semimetal candidate NiTe ₂ . 2019 , 100,	28
737	Angle-dependent magnetoresistance and its implications for Lifshitz transition in W ₂ As ₃ . 2019 , 4,	3
736	Saddle-point Van Hove singularity and dual topological state in Pt ₂ HgSe ₃ . 2019 , 100,	15
735	Topological nodal line states in three-dimensional ball-and-stick sonic crystals. 2019 , 100,	7
734	Quantum oscillations and electronic structure in the large Chern number semimetal RhSn. 2019 , 100,	5
733	Type-II Dirac states in full Heusler compounds XInPd ₂ (X = Ti, Zr, and Hf). 2019 , 100,	6
732	Quasiparticle interference evidence of the topological Fermi arc states in chiral fermionic semimetal CoSi. 2019 , 5, eaaw9485	15
731	Singular low-energy states of tilted Dirac semimetals induced by the fermion-fermion interactions. 2019 , 92, 1	
730	Positive longitudinal spin magnetoconductivity in Z ₂ topological Dirac semimetals. 2019 , 100,	3
729	Out-of-plane transport in ZrSiS and ZrSiSe microstructures. 2019 , 7, 101116	5
728	PT-symmetric non-Hermitian Dirac semimetals. 2019 , 100,	25
727	Topological nodal lines and nodal points in the antiferromagnetic material Fe ₂ PO ₅ . 2019 , 7, 12657-12663	33
726	Topological semi-metal Na ₃ Bi as efficient spin injector in current driven magnetic tunnel junction. 2019 , 126, 233901	3
725	Dynamical polarization in a graphene-topological-insulator heterostructure. 2019 , 6, 045603	

724	Superconductivity in topological semimetals. 2019 , 6, 199-202	7
723	Higher-order topological phases: A general principle of construction. 2019 , 99,	97
722	Topological 'Luttinger' invariants for filling-enforced non-symmorphic semimetals. 2019 , 31, 104001	0
721	Observation of chiral zero mode in inhomogeneous three-dimensional Weyl metamaterials. <i>Science</i> , 2019 , 363, 148-151	33-3 71
720	Dynamically tunable plasmon-induced absorption in Dirac semimetal waveguide. 2019 , 437, 246-250	7
719	Prediction of a topological $p + ip$ excitonic insulator with parity anomaly. 2019 , 10, 210	8
718	Crystalline topological Dirac semimetal phase in rutile structure PtO_2 . 2019 , 99,	8
717	High Hole Mobility and Nonsaturating Giant Magnetoresistance in the New 2D Metal NaCuSe Synthesized by a Unique Pathway. 2019 , 141, 635-642	9
716	All-Silicon Topological Semimetals with Closed Nodal Line. 2019 , 10, 244-250	14
715	Topological Quantum Materials for Realizing Majorana Quasiparticles. 2019 , 31, 26-51	19
714	Multiple topological states in iron-based superconductors. 2019 , 15, 41-47	96
713	The effect of spin-orbit coupling on nonsymmorphic square-net compounds. 2019 , 128, 296-300	9
712	Topological properties of NaAuTe in the hexagonal and Heusler structures. 2020 , 171, 109206	1
711	Observations of nodal lines in the topological semimetal ZrSnTe. 2020 , 63, 1	2
710	Realization of predicted exotic materials: The burden of proof. 2020 , 32, 35-45	17
709	2D Boron Sheets: Structure, Growth, and Electronic and Thermal Transport Properties. 2020 , 30, 1904349	69
708	Magnetic Textures and Dynamics in Magnetic Weyl Semimetals. 2020 , 532, 1900287	14
707	Crystal growth of BaAgAs family topological materials via flux method. 2020 , 531, 125304	5

706	Enhancement of a tunable single-band metamaterial absorber based on bright modes coupling effect in terahertz range. 2020 , 95, 035508	3
705	Synthesis and resistivity of topological metal MoP nanostructures. 2020 , 8, 011103	7
704	High throughput study on magnetic ground states with Hubbard U corrections in transition metal dihalide monolayers. 2020 , 2, 495-501	9
703	Nano-makisu: highly anisotropic two-dimensional carbon allotropes made by weaving together nanotubes. 2020 , 12, 347-355	2
702	Designing Dirac semimetals with a honeycomb Na ₃ Bi-lattice via isovalent cation substitution. 2020 , 8, 1257-1264	2
701	Experimental evidence of a new class of massless fermions. 2020 , 5, 679-682	1
700	A family of all sp ² -bonded carbon allotropes of topological semimetals with strain-robust nodal-lines. 2020 , 8, 1548-1555	14
699	Quantum confinement effect induced topological phase transitions in anisotropic Weyl semimetal. 2020 , 138, 106386	0
698	Topological photonic crystals: a review. 2020 , 13, 50-72	19
697	Unconventional superconductivity in the topological semimetal MoP: Evidence from first-principles calculated electron-phonon coupling. 2020 , 173, 109466	5
696	Directional massless Dirac fermions in a layered van der Waals material with one-dimensional long-range order. 2020 , 19, 27-33	9
695	Novel topological nodal lines and exotic drum-head-like surface states in synthesized CsCl-type binary alloy TiOs. 2020 , 22, 137-144	26
694	Surface Nonlinear Optics on Centrosymmetric Dirac Nodal-Line Semimetal ZrSiS. 2020 , 32, e1904498	5
693	Three-dimensional Kagome graphene networks and their topological properties. 2020 , 173, 109406	1
692	Numerical analysis of DNA-based implementation for terahertz switchable metamaterial absorber. 2020 , 117, 113844	2
691	Effect of Mechanical Strain on the Optical Properties of Nodal-Line Semimetal ZrSiS. 2020 , 6, 1900860	5
690	Emergence of Type-I and Type-II Dirac line nodes in penta-octa-graphene. 2020 , 158, 210-215	8
689	Dirac fermions in antiferromagnetic FeSn kagome lattices with combined space inversion and time-reversal symmetry. 2020 , 102,	14

688	Strain-Tuned Nodal Ring in Two-Dimensional Zn ₃ C ₆ S ₆ Monolayers. 2020 , 2020, 1-6	1
687	Magneto-optical conductivity of nodal line semimetals. 2020 , 599, 412478	2
686	Three-dimensional Weyl hourglass networks in the nonsymmorphic half-metal Mg ₂ VO ₄ . 2020 , 102,	14
685	Large magnetoresistance and nonzero Berry phase in the nodal-line semimetal MoO ₂ . 2020 , 102,	6
684	Anomalous Thermodiffusion of Electrons in Graphene. 2020 , 125, 176802	0
683	Tunable electronic properties of the dynamically stable layered mineral PtHgSe (Jacutingaite). 2020 , 22, 24471-24479	14
682	First-principles theory of the Dirac semimetal Cd ₃ As ₂ under Zeeman magnetic field. 2020 , 102,	1
681	Chirality production with mass effects \mathbb{B} chwinger pair production and the axial Ward identity. 2020 , 35, 203005	3
680	A reconfigurable sandwich structure switchable DNA-based metamaterial. 2020 , 10, 17511	0
679	Type-III Dirac Cones from Degenerate Directionally Flat Bands: Viewpoint from Molecular-Orbital Representation. 2020 , 89, 103704	6
678	Topological Magnons with Nodal-Line and Triple-Point Degeneracies: Implications for Thermal Hall Effect in Pyrochlore Iridates. 2020 , 125, 047203	11
677	Novel electronic properties of monoclinic MP (M = Cr, Mo, W) compounds with or without topological nodal line. 2020 , 10, 11502	6
676	Observation of inverted band structure in the topological Dirac semimetal candidate CaAuAs. 2020 , 102,	2
675	Electronic structure of the Si-containing topological Dirac semimetal CaAl ₂ Si ₂ . 2020 , 102,	4
674	Eightfold fermionic excitation in a charge density wave compound. 2020 , 102,	7
673	Topological Fermi-arc surface resonances in bcc iron. 2020 , 102,	1
672	Dual topological insulator device with disorder robustness. 2020 , 102,	6
671	3D Quantum Hall Effect and a Global Picture of Edge States in Weyl Semimetals. 2020 , 125, 036602	12

670	Importance of interactions for the band structure of the topological Dirac semimetal Na ₃ Bi. 2020 , 102,	1
669	Gapless Criterion for Crystals from Effective Axion Field. 2020 , 125, 036401	5
668	Emerging Superconductivity and the Origin of Its Enhancement in Pressurized Topological Nodal-Line Semimetal SrAs ₃ . 2020 , 6, 2000293	1
667	Topological semimetals from the perspective of first-principles calculations. 2020 , 128, 191101	3
666	Atoms to topological electronic materials: a bedtime story for beginners. 2020 , 1	
665	Filling-enforced Dirac nodal loops in nonmagnetic systems and their evolutions under various perturbations. 2020 , 102,	1
664	Quantum-confinement-induced periodic surface states in two-dimensional metal-organic frameworks. 2020 , 117, 191601	0
663	The Synthesis and Investigation of the Electrical Properties of Tricadmium Diarsenide with MnAs Nanogranules. 2020 , 65, 1083-1086	1
662	Realization of photonic charge-2 Dirac point by engineering super-modes in topological superlattices. 2020 , 3,	5
661	Palladium oxide: an excellent topological electronic material with 0-D and 1-D band crossings and definite nontrivial surface states. 2020 , 22, 18447-18453	0
660	Trivial to nontrivial topology transition in rare-earth pnictides with epitaxial strain. 2020 , 102,	4
659	Recent Advances in Topological Quantum Materials by Angle-Resolved Photoemission Spectroscopy. 2020 , 3, 1114-1141	10
658	Evidence for topological semimetallicity in a chain-compound TaSe ₃ . 2020 , 5,	7
657	Unique topological nodal line states and associated exceptional thermoelectric power factor platform in NbGeTe monolayer and bulk. 2020 , 12, 16910-16916	11
656	Quantum Transport in Air-Stable NaBi Thin Films. 2020 , 12, 35542-35546	4
655	Symmetry-protected spinful magnetic Weyl nodal loops and multi-Weyl nodes in 5d _n cubic double perovskites (n=1,2). 2020 , 102,	3
654	Atomic frustrated impurity states in Weyl metals. 2020 , 102,	0
653	Possible instabilities in quadratic and cubic nodal-line fermion systems with correlated interactions. 2020 , 102,	3

- 652 Cubic ScPd topological metal: Closed nodal line, spin-orbit coupling-induced triply degenerate nodal point Dirac nodal point transition. **2020**, 19, 103553 0
- 651 Stability of two-dimensional asymmetric materials with a quadratic band crossing point under four-fermion interaction and impurity scattering. **2020**, 102, 1
- 650 Optical absorption window in Na₃Bi based three-dimensional Dirac electronic system. **2020**, 128, 155707
- 649 Antiferromagnetic transitions of Dirac fermions in three dimensions. **2020**, 102, 1
- 648 Role of f_d exchange interaction and Kondo scattering in the Nd-doped pyrochlore iridate (Eu_{1-x}Nd_x)₂Ir₂O₇. **2020**, 102, 0
- 647 Hidden-symmetry-enforced nexus points of nodal lines in layer-stacked dielectric photonic crystals. **2020**, 9, 176 4
- 646 Single-domain formation of SrMnBi₂ films on polar LaAlO₃ substrate. **2020**, 10, 105216 1
- 645 Magneto-Optical Tools to Study Effects in Dirac and Weyl Semimetals. **2020**, 12, 1412 1
- 644 Nontrivial topological states in the tantalum dipnictides TaX₂ (X = As, P). **2020**, 2, 251-260 2
- 643 Magnetotransport properties and topological phase transition in NaCd₄As₃. **2020**, 102, 1
- 642 Broken symmetries and the related interface-induced effects at Weyl-system TaAs in proximity of noble metals. **2020**, 10, 14438
- 641 A new protocol for the preparation of superconducting KBi. **2020**, 10, 26686-26692 0
- 640 Topological transitions of spin-excitations in insulating chiral antiferromagnets. **2020**, 131, 27001 1
- 639 Tunable Bragg reflector with parallel bulk Dirac semimetals at terahertz frequencies. **2020**, 67, 1010-1016 1
- 638 Topological Dirac states in a layered telluride TaPdTe₅ with quasi-one-dimensional PdTe₂ chains. **2020**, 102, 3
- 637 de Haas-van Alphen quantum oscillations and electronic structure in the large-Chern-number topological chiral semimetal CoSi. **2020**, 102, 1
- 636 Antiferromagnetism and spin density waves in three-dimensional Dirac metals. **2020**, 102, 0
- 635 Multiple Dirac nodes and symmetry protected Dirac nodal line in orthorhombic ERhSi. **2020**, 102, 1

634	Dirac fermions in the antiferromagnetic spintronics material CuMnAs. 2020 , 102,	2
633	Dirac and Weyl Semimetals in Sn _{1-x} In _x Te. 2020 , 14, 2000362	0
632	Recent advancements in the study of intrinsic magnetic topological insulators and magnetic Weyl semimetals. 2020 , 8, 090701	6
631	A nonsymmorphic-symmetry-protected hourglass Weyl node, hybrid Weyl node, nodal surface, and Dirac nodal line in PdX (X = S, Se) compounds. 2020 , 22, 22399-22407	7
630	The Tetragonal Monoxide of Platinum: A New Platform for Investigating Nodal-Line and Nodal-Point Semimetallic Behavior. 2020 , 8, 704	5
629	Enhanced anisotropic superconductivity in the topological nodal-line semimetal In _x Ta _{1-x} S ₂ . 2020 , 102,	4
628	A bi-tunable switchable polarization-independent dual-band metamaterial terahertz absorber using VO ₂ and Dirac semimetal. 2020 , 19, 103484	5
627	Influence of the degree of spatial coherence on the Goos-Hänchen shifts for a three-dimensional Dirac semimetal. 2020 , 599, 412469	
626	Lateral Gate and Magnetic Field Controlled Quantum Transport in a Topological Dirac Semimetal Nanowire. 2020 , 14,	1
625	Impurity-induced topological phase transitions in Cd ₃ As ₂ and Na ₃ Bi Dirac semimetals. 2020 , 102,	4
624	Topological electronic properties of silicon. 2020 , 102,	1
623	Prediction of nodal-line semimetals in two-dimensional black phosphorous films. 2020 , 10, 21351	1
622	Topological materials by molecular beam epitaxy. 2020 , 128, 210902	12
621	Coexistence of Rarita-Schwinger-Weyl fermion and spin-1 excitation in Bi ₄ Ni ₆ S ₄ . 2020 , 34, 2150003	
620	Photoinduced Floquet mixed-Weyl semimetallic phase in a carbon allotrope. 2020 , 102,	2
619	de Haas-van Alphen Quantum Oscillations in BaSn ₃ Superconductor with Multiple Dirac Fermions. 2020 , 37, 087101	4
618	Critical evaluation and thermodynamic modeling of the Pd ₃ Sn system. 2020 , 126, 106945	1
617	Photoinduced anomalous Hall and nonlinear Hall effect in borophene. 2020 , 322, 114092	3

616	Pnma metal hydride system LiBH: a superior topological semimetal with the coexistence of twofold and quadruple degenerate topological nodal lines. 2020 , 32, 365502	5
615	Topological Quantum States in Magnetic Oxides. 2020 , 11, 4036-4042	3
614	Non-Abelian topology of nodal-line rings in PT-symmetric systems. 2020 , 101,	16
613	Atomic Structure and Electronic Properties of Intermetallic CaBi Thin Films. 2020 , 11, 4385-4391	2
612	Mid-infrared transient reflectance study of the Dirac semimetal Cd3As2 under strong optical pumping. 2020 , 101,	3
611	Signature of Dirac semimetal states in gray arsenic studied by de Haas-van Alphen and Shubnikov-de Haas quantum oscillations. 2020 , 101,	1
610	Nodal Andreev spectra in multi-Majorana three-terminal Josephson junctions. 2020 , 101,	3
609	Anisotropic magnetic response of Weyl semimetals in a topological insulator multilayer. 2020 , 127, 163905	3
608	The de Haas-van Alphen Effect Study of the Fermi Surface of LaBi. 2020 ,	
607	Interlayer quantum transport in Dirac semimetal BaGa. 2020 , 11, 2370	4
606	Observation of sixfold degenerate fermions in PdSb2. 2020 , 101,	6
605	Band dispersion of graphene with structural defects. 2020 , 101,	5
604	Electrical Contact between an Ultrathin Topological Dirac Semimetal and a Two-Dimensional Material. 2020 , 13,	11
603	Broadband strong optical dichroism in topological Dirac semimetals with Fermi velocity anisotropy. 2020 , 29, 077802	3
602	Superconducting Interfaces between Weyl Semimetal and Normal Metal. 2020 , 3, 2000020	2
601	Electrically tunable Kondo effect as a direct measurement of the chiral anomaly in disordered Weyl semimetals. 2020 , 101,	2
600	Asymmetric Fermi velocity induced chiral magnetotransport anisotropy in the type-II Dirac semi-metal PtSe2. 2020 , 3,	4
599	Quantum criticality of the excitonic insulating transition in the nodal-line semimetal ZrSiS. 2020 , 101,	5

598	Vortex End Majorana Zero Modes in Superconducting Dirac and Weyl Semimetals. 2020 , 124, 257001	6
597	High pressure investigation of an organic three-dimensional Dirac semimetal candidate having a diamond lattice. 2020 , 101,	1
596	Strain tuning of closed topological nodal lines and opposite pockets in quasi-two-dimensional Φ phase FeSi. 2020 , 22, 13650-13658	10
595	Magnetotransport properties of compensated semimetal HfB with high-density light carriers. 2020 , 32, 015601	1
594	IrSi as a Superior Electronic Material with Novel Topological Properties and Nice Compatibility with Semiconductor Si. 2020 , 14, 2000178	2
593	Coexistence of nontrivial topological properties and strong ferromagnetic fluctuations in quasi-one-dimensional $A_2Cr_3As_3$. 2020 , 6,	10
592	Ternary compound HfCuP: An excellent Weyl semimetal with the coexistence of type-I and type-II Weyl nodes. 2020 , 24, 523-528	40
591	Symmetry-guaranteed ideal Weyl semimetallic phase in face-centered orthogonal C_6 . 2020 , 101,	1
590	Fermiology of ZrTe with triply degenerate nodes and highly anisotropic magnetization. 2020 , 101,	5
589	Ideal type-III nodal-ring phonons. 2020 , 101,	16
588	Electron-phonon interaction and zero-field charge carrier transport in the nodal-line semimetal ZrSiS. 2020 , 101,	1
587	Electric Control of Fermi Arc Spin Transport in Individual Topological Semimetal Nanowires. 2020 , 124, 116802	19
586	Coexistence of type-I and critical-type nodal line states in intermetallic compounds ScM ($M = Cu, Ag, Au$). 2020 , 32, 295502	3
585	Discovering Topological Surface States of Dirac Points. 2020 , 124, 104301	10
584	The Subchalcogenides $IrInQ$ ($Q = S, Se, Te$): Dirac Semimetal Candidates with Re-entrant Structural Modulation. 2020 , 142, 6312-6323	4
583	Symmetry-enforced three-dimensional Dirac phononic crystals. 2020 , 9, 38	13
582	Magneto-transport and Shubnikov-de Haas oscillations in the layered ternary telluride topological semimetal candidate Ta_3SiTe_6 . 2020 , 116, 092402	9
581	Crystal Structures, Electronic Structures, and Topological Signatures in Equiatomic $TT'X$ Compounds ($T = Sc, Zr, Hf$; $T' = Co, Pt, Pd, Ir, Rh$; $X = Al, Ga, Sn$). 2020 , 124, 7378-7385	13

580	Special topic on topological semimetals New directions. 2020 , 8, 030401	4
579	Intersecting nodal rings in orthorhombic-type BaLi ₂ Sn compound. 2020 , 8, 5461-5466	9
578	Topological Anderson insulator in two-dimensional non-Hermitian systems. 2020 , 29, 050502	9
577	Critical topological nodal points and nodal lines/rings in Kagome graphene. 2020 , 22, 8713-8718	2
576	Experimental demonstration of acoustic semimetal with topologically charged nodal surface. 2020 , 6, eaav2360	24
575	Tunable mid-infrared refractive index sensor with high angular sensitivity and ultra-high figure-of-merit based on Dirac semimetal. 2020 , 17, 103035	2
574	Dynamical Time-Reversal and Inversion Symmetry Breaking, Dimensional Crossover, and Chiral Anomaly in \mathbb{Z}_2 (BEDT-TTF) ₂ I ₃ . 2020 , 89, 073705	2
573	Acoustic spin-1 Weyl semimetal. 2020 , 63, 1	5
572	Collective excitations and universal broadening of cyclotron absorption in Dirac semimetals in a quantizing magnetic field. 2020 , 101,	2
571	Examining the validity of the two-dimensional conical model to describe the three-dimensional ZrTe ₅ . 2020 , 101,	4
570	Topological Dirac Semimetal Phase in Bismuth Based Anode Materials for Sodium-Ion Batteries. 2020 , 5, 39	1
569	Stability of Weyl semimetals with quasiperiodic disorder. 2020 , 102,	4
568	Anomalous gravitational TTT vertex, temperature inhomogeneity, and pressure anisotropy. 2020 , 802, 135236	3
567	Quasiparticle interference and impurity resonances on WTe ₂ . 2020 , 13, 2534-2540	0
566	Quantum Simulation for Three-Dimensional Chiral Topological Insulator. 2020 , 125, 020504	19
565	Three-terminal Weyl complex with double surface arcs in a cubic lattice. 2020 , 6,	5
564	Semimetals for high-performance photodetection. 2020 , 19, 830-837	70
563	Signatures of Sixfold Degenerate Exotic Fermions in a Superconducting Metal PdSb. 2020 , 32, e1906046	15

562	Photoemission Spectroscopic Evidence for the Dirac Nodal Line in the Monoclinic Semimetal SrAs ₃ . 2020 , 124, 056402	12
561	Magnetic exchange induced Weyl state in a semimetal EuCd ₂ Sb ₂ . 2020 , 8, 011109	13
560	Ab initio approach to the elastic, electronic, and optical properties of MoTe ₂ topological Weyl semimetal. 2020 , 829, 154522	15
559	Rich novel zero-dimensional (0D), 1D, and 2D topological elements predicted in the P6/m type ternary boride HfIrB. 2020 , 12, 8314-8319	14
558	Planar Hall effect in PtSe ₂ . 2020 , 127, 054306	11
557	Transport evidence of mass-less Dirac fermions in (Cd _{1-x} Zn _x Mny) ₃ As ₂ (x + y = 0.4). 2020 , 7, 015918	2
556	Surface and bulk Landau levels in thin films of Weyl semimetals. 2020 , 101,	3
555	Giant photonic spin Hall effect near the Dirac points. 2020 , 101,	11
554	Tunable Massive Dirac Fermions in Ferromagnetic Fe ₃ Sn ₂ Kagome Lattice. 2020 , 14, 1900705	5
553	Chiral vortical and Chiral torsional effects. 2020 , 1435, 012009	0
552	Dynamically tunable Fano resonance with high Q factor based on asymmetric Dirac semimetal split-ring structure. 2020 , 7, 025041	7
551	Creation of the Dirac Nodal Line by Extrinsic Symmetry Engineering. 2020 , 20, 2157-2162	1
550	Active control of narrowband total absorption based on terahertz hybrid Dirac semimetal-graphene metamaterials. 2020 , 53, 205106	11
549	Quantum oscillations in acoustic phonons in Weyl semimetals. 2020 , 101,	6
548	Emergence of Nontrivial Low-Energy Dirac Fermions in Antiferromagnetic EuCd As. 2020 , 32, e1907565	14
547	Electronic structure, doping effect and topological signature in realistic intermetallics LiNaM (x = 3, 2, 1, 0; M = N, P, As, Sb, Bi). 2020 , 22, 5847-5854	9
546	Emerging edge states on the surface of the epitaxial semimetal CuMnAs thin film. 2020 , 116, 061603	
545	Effect of Environment on the Scattering of Electrons by a Junction of Different Topological Materials. 2020 , 532, 1900399	1

544	Risk Methodology for SEE Caused by Proton- Induced Fission of High-Z Materials in Microelectronic Packaging. 2020 , 67, 1152-1160	0
543	Flux Synthesis of MgNiBi and Its Structural Relationship to NiBi. 2020 , 59, 3452-3458	1
542	Evidence from transport measurements for YRh ₆ Ge ₄ being a triply degenerate nodal semimetal. 2020 , 101,	1
541	Photoprotected spin Hall effect on graphene with substrate induced Rashba spin-orbit coupling. 2020 , 32, 205701	1
540	Rashba spin-orbit coupling in two-dimensional systems. 2020 , 25-64	0
539	Controllable p-n junctions in three-dimensional Dirac semimetal CdAs nanowires. 2020 , 31, 205001	2
538	Cherenkov terahertz radiation from Dirac semimetals surface plasmon polaritons excited by an electron beam. 2020 , 29, 034101	4
537	Dirac terahertz plasmonics in two and three dimensions. 2020 , 462, 125319	5
536	Recent Advances in Tin: From Two-Dimensional Quantum Spin Hall Insulator to Bulk Dirac Semimetal. 2020 , 11, 1317-1329	9
535	Angle-dependent nontrivial phase in the Weyl semimetal NbAs with anisotropic Fermi surface. 2020 , 101,	1
534	Rich topological nodal line bulk states together with drum-head-like surface states in NaAlGe with -PbFCl type structure. 2020 , 23, 95-100	21
533	Novel Undamped Gapless Plasmon Mode in a Tilted Type-II Dirac Semimetal. 2020 , 124, 046803	18
532	Observation of giant spin-split Fermi-arc with maximal Chern number in the chiral topological semimetal PtGa. 2020 , 11, 2033	19
531	Multifunction tunable broadband terahertz device for polarization rotation and linear asymmetric transmission based on Dirac semimetals. 2020 , 468, 125802	10
530	Emergence of d-orbital magnetic Dirac fermions in a MoS ₂ monolayer with squared pentagon structure. 2020 , 101,	3
529	Direct observation of sixfold exotic fermions in the pyrite-structured topological semimetal PdSb ₂ . 2020 , 101,	12
528	Two-dimensional topological semimetal states in monolayer Cu ₂ Ge, Fe ₂ Ge, and Fe ₂ Sn. 2020 , 101,	5
527	Surface-state Coulomb repulsion accelerates a metal-insulator transition in topological semimetal nanofilms. 2020 , 6, eaaz5015	5

526	The Electronic, Optical, and Thermoelectric Properties of Monolayer PbTe and the Tunability of the Electronic Structure by External Fields and Defects. 2020 , 257, 2000182	28
525	The de Haas-van Alphen quantum oscillations in a three-dimensional Dirac semimetal TiSb ₂ . 2020 , 116, 142103	6
524	Topological Semimetal Nanostructures: From Properties to Topotronics. 2020 , 14, 3755-3778	19
523	Differential entropy per particle in Dirac semimetals in external magnetic field. 2020 , 46, 264-268	1
522	Observation of quadratic Weyl points and double-helicoid arcs. 2020 , 11, 1820	10
521	Strong and Weak 3D Topological Insulators Probed by Surface Science Methods. 2021 , 258, 2000060	0
520	Two-dimensional Weyl semimetal with coexisting fully spin-polarized type-I and type-II Weyl points. 2021 , 540, 148318	8
519	Topological Quantum Materials from the Viewpoint of Chemistry. 2021 , 121, 2780-2815	19
518	Emerging Spintronics Phenomena and Applications. 2021 , 57, 1-34	6
517	An Ab Initio study of electronic, mechanical, thermoelectric and vibrational properties of Dirac Semimetals Ca ₃ PbO and Ca ₃ SnO. 2021 , 26, 101741	2
516	Six-membered-ring inorganic materials: definition and prospects. 2021 , 8, nwa248	4
515	Experimental investigation and thermodynamic modeling of the binary PtBn system. 2021 , 854, 157064	2
514	Bandwidth convertible mid-infrared absorption of one-dimensional quasi-periodic system containing Dirac semimetals. 2021 , 482, 126603	1
513	Tunable quantum Shubnikov-de Hass oscillations in antiferromagnetic topological semimetal Mn-doped Cd ₃ As ₂ . 2021 , 76, 247-253	2
512	Angle, Spin, and Depth Resolved Photoelectron Spectroscopy on Quantum Materials. 2021 , 121, 2816-2856	3
511	Irvsp: To obtain irreducible representations of electronic states in the VASP. 2021 , 261, 107760	52
510	Strain effect on the mechanical and electronic properties of graphene-like B ₄ P ₄ C ₄ and B ₂ P ₂ C ₈ : First-principles calculation. 2021 , 128, 114583	1
509	Dynamically Tunable Plasmon-induced Transparency in a T-shaped Cavity Waveguide Based on Bulk Dirac Semimetals. 2021 , 16, 323-332	1

508	The topology of electronic band structures. 2021 , 20, 293-300	25
507	Two-dimensional topological insulators exfoliated from NaBi-like Dirac semimetals. 2021 , 23, 10545-10550	1
506	Superconductivity in topological insulator PbBi under pressure. 2021 ,	1
505	Nonequilibrium states in quantum materials under time-period driving. 2021 , 0-0	0
504	Tunable 3D Dirac-semimetals supported mid-IR hybrid plasmonic waveguides. 2021 , 46, 472-475	29
503	Superconducting properties of BaBi at ambient and high pressures. 2021 , 23, 23014-23023	1
502	Impurity effects in a two-dimensional nonsymmorphic Dirac semimetal. 2021 , 133, 27003	
501	Kondo screening regimes in multi-Dirac and Weyl systems. 2021 , 103,	0
500	Quantum oscillations of the magnetic torque in the nodal-line Dirac semimetal ZrSiS . 2021 , 103,	0
499	Emergent chiral symmetry in a three-dimensional interacting Dirac liquid. 2021 , 2021, 1	3
498	Magnetoresistance and Kondo Effect in Nodal-Line Semimetal VAs_2 *. 2021 , 38, 017202	3
497	The 2021 quantum materials roadmap. 2020 , 3, 042006	48
496	Three-band perfect absorber with high refractive index sensing based on an active tunable Dirac semimetal. 2021 , 23, 17374-17381	28
495	Abundant topological phases in hydrogenated group-IV binary alloy compounds.. 2021 , 11, 14434-14440	
494	Sixfold fermion near the Fermi level in cubic PtBi_2 . 2021 , 10,	3
493	Complex Dirac-like Electronic Structure in Atomic Site-Ordered $\text{Rh}_3\text{In}_{3.4}\text{Ge}_{3.6}$. 2021 , 33, 1218-1227	
492	Type-III Dirac fermions in $\text{Hf}_x\text{Zr}_{1-x}\text{Te}_2$ topological semimetal candidate. 2021 , 129, 075104	5
491	Progress in Epitaxial Thin-Film Na Bi as a Topological Electronic Material. 2021 , 33, e2005897	10

490	Picoscale Magnetoelasticity Governs Heterogeneous Magnetic Domains in a Noncentrosymmetric Ferromagnetic Weyl Semimetal. 2021 , 4, 2000101	3
489	Fermi arcs and surface criticality in dirty Dirac materials. 2021 , 103,	1
488	Rashba coupling and spin switching through surface states of Dirac semimetals. 2021 , 23, 023008	
487	Coexistence of type-II and type-IV Dirac fermions in SrAgBi. 2021 , 35, 2150181	0
486	Nonspecular effects in the vicinity of a photonic Dirac point. 2021 , 103,	2
485	Colossal Terahertz Photoresponse at Room Temperature: A Signature of Type-II Dirac Fermiology. 2021 , 15, 5138-5146	6
484	Tunable chiral symmetry breaking in symmetric Weyl materials. 2021 , 103,	0
483	Two-dimensional Dirac dispersion in the layered compound BaCdSb ₂ . 2021 , 103,	0
482	Spectroscopic evidence for the realization of a genuine topological nodal-line semimetal in LaSbTe. 2021 , 103,	4
481	Gapped Dirac semimetal with mixed linear and parabolic dispersions. 2021 , 103,	1
480	Tunable double Weyl phonons driven by chiral point group symmetry. 2021 , 103,	4
479	Probing mirror anomaly and classes of Dirac semimetals with circular dichroism. 2021 , 3,	0
478	Anisotropic Berry phase in the Dirac nodal-line semimetal ZrSiS: The effect of spin-orbit coupling. 2021 , 103,	2
477	From triple-point materials to multiband nodal links. 2021 , 103,	7
476	Room-Temperature Spin Transport in CdAs. 2021 , 15, 5459-5466	1
475	Quasi-two-dimensional relativistic fermions probed by de Haas-van Alphen quantum oscillations in LuSn ₂ . 2021 , 103,	0
474	Anisotropic magnetotransport in tilted magnetic topological semimetals. 2021 ,	2
473	Anomaly Non-renormalization in Interacting Weyl Semimetals. 2021 , 384, 997-1060	2

472	Strain engineering the topological type-II Dirac semimetal NiTe ₂ . 2021 , 103,	4
471	Modify Cd ₃ As ₂ nanowires with sulfur to fabricate self-powered NIR photodetectors with enhanced performance. 2021 , 14, 3379-3385	3
470	Prediction of two-dimensional Cu ₂ C with polyacetylene-like motifs and Dirac nodal line. 2021 , 5,	3
469	Tunable terahertz Dirac semimetal metamaterials. 2021 , 54, 235103	31
468	Highly tunable dual bound states in the continuum in bulk Dirac semimetal metasurface. 2021 , 14, 042002	3
467	Double band inversion in the topological phase transition of Ge _{1-x} Sn _x alloys. 2021 , 133, 57001	0
466	Rare regions and avoided quantum criticality in disordered Weyl semimetals and superconductors. 2021 , 168455	0
465	Switchable Fano Resonance Based on Cut-Induced Asymmetric Split-Ring Resonators with Dirac Semimetal Film. 2021 , 16, 1405	2
464	2D-Berry-Curvature-Driven Large Anomalous Hall Effect in Layered Topological Nodal-Line MnAlGe. 2021 , 33, e2006301	3
463	Surface charge induced Dirac band splitting in a charge density wave material (TaSe ₄) ₂ I. 2021 , 3,	4
462	Anomalous negative longitudinal magnetoresistance and violation of Ohm's law deep in the topological insulating regime in Bi[Formula: see text]Sb[Formula: see text]. 2021 , 11, 8756	2
461	Moiré superlattice on the surface of a topological insulator. 2021 , 103,	4
460	Weyl, Dirac and high-fold chiral fermions in topological quantum matter. 2021 , 6, 784-803	13
459	An Insightful Picture of Nonlinear Photonics in 2D Materials and their Applications: Recent Advances and Future Prospects. 2021 , 9, 2001671	2
458	Observation of topological Dirac fermions and surface states in superconducting BaSn ₃ . 2021 , 103,	2
457	Inherited weak topological insulator signatures in the topological hourglass semimetal Nb ₃ XTe ₆ (X=Si, Ge). 2021 , 103,	4
456	Omnipresence of Weak Antilocalization (WAL) in BiSe Thin Films: A Review on Its Origin. 2021 , 11,	6
455	Tunable plasmonic filter based on parallel bulk Dirac semimetals at terahertz frequencies. 2021 , 60, 3634-3640	2

454	Novel electric field effects on magneto-optical conductivity in eight-borophene. 2021 , 33,	2
453	Topological gimbals phonons in T-carbon. 2021 , 103,	7
452	Experimental perspective on three-dimensional topological semimetals. 2021 , 93,	35
451	Quantum spin Hall and quantum anomalous Hall states in magnetic TiTeO single layer. 2021 , 33,	0
450	Interacting spin-32 fermions in a Luttinger semimetal: Competing phases and their selection in the global phase diagram. 2021 , 103,	3
449	Atomically Thin Quantum Spin Hall Insulators. 2021 , 33, e2008029	8
448	A Raman probe of phonons and electron-phonon interactions in the Weyl semimetal NbIrTe. 2021 , 11, 8155	3
447	Extremely large magnetoresistance from electron-hole compensation in the nodal-loop semimetal ZrP2. 2021 , 103,	5
446	Electronic correlation effect on nontrivial topological fermions in CoSi. 2021 , 94, 1	1
445	Modulating Near-Field Radiative Heat Transfer through Thin Dirac Semimetal Films. 2021 , 25, 101-115	0
444	Kramers nodal line metals. 2021 , 12, 3064	3
443	Angle-resolved photoemission studies of quantum materials. 2021 , 93,	45
442	Evidence of nontrivial Berry phase and Kondo physics in SmBi. 2021 , 5,	1
441	Adsorption of gas molecules on 2D Na3Bi monolayer: A first-principles study. 2021 , 399, 127280	0
440	Chiral filtration of light by Weyl-semimetal medium. 2021 , 399, 127294	0
439	Noncentrosymmetric topological Dirac semimetals in three dimensions. 2021 , 103,	1
438	Three-Dimensional Dirac Phonons with Inversion Symmetry. 2021 , 126, 185301	8
437	Experimental Observation and Spin Texture of Dirac Node Arcs in Tetradymite Topological Metals. 2021 , 126, 196407	0

436	Triply degenerate nodal lines in topological and nontopological metals. 2021 , 103,	1
435	Lattice dynamics and topological surface phonon states in cuprous oxide Cu ₂ O. 2021 , 103,	2
434	Fermion-fermion interaction driven instability and criticality of quadratic band crossing systems with the breaking of time-reversal symmetry. 2021 , 966, 115371	1
433	Vortex states in an acoustic Weyl crystal with a topological lattice defect. 2021 , 12, 3654	8
432	Novel 2D PC 5 with a Dirac Cone and Edge-Size Dependence. 2100203	1
431	Observation of the critical state to multiple-type Dirac semimetal phases in KMgBi. 2021 , 129, 235109	
430	Real-space topological invariant and higher-order topological Anderson insulator in two-dimensional non-Hermitian systems. 2021 , 103,	4
429	2D weak anti-localization in thin films of the topological semimetal Pd[Formula: see text]Bi[Formula: see text]S[Formula: see text]. 2021 , 11, 12618	4
428	Observation of Negative Terahertz Photoconductivity in Large Area Type-II Dirac Semimetal PtTe ₂ . 2021 , 126, 227402	8
427	Signature of topological nontrivial band structure in Ta ₃ SiTe ₆ . 2021 , 5,	3
426	Coexistence of Surface Superconducting and Three-Dimensional Topological Dirac States in Semimetal KZnBi. 2021 , 11,	1
425	Quantum-limit Hall effect with large carrier density in topological semimetals. 2021 , 103,	1
424	Long-range spin transport on the surface of topological Dirac semimetal. 2021 , 3,	1
423	Electronic structure examination of the topological properties of CaMnSb ₂ by angle-resolved photoemission spectroscopy. 2021 , 103,	1
422	Negative Magnetoresistance in the GeSn Strip. 2021 , 13, 29960-29964	1
421	Dual Dirac points and odd-even oscillated energy gap in zigzag chlorinated stanene nanoribbon. 2021 , 33,	1
420	Symmetry-protected nodal points and nodal lines in magnetic materials. 2021 , 103,	2
419	Topologically nontrivial type-I and type-II nodal-line states in magnetic configurations of square-net pnictide CeCuBi ₂ . 2021 , 194, 110434	0

418	Critical behavior of the magnetic Weyl semimetal PrAlGe. 2021 , 103,	7
417	Chiralities of nodal points along high-symmetry lines with screw rotation symmetry. 2021 , 103,	1
416	Perovskite-type YRh3B with multiple types of nodal point and nodal line states. 2021 , 103,	6
415	Lattice-fermionic Casimir effect and topological insulators. 2021 , 3,	2
414	Magnetic monopole in a chiral plasma: Chiral dyon. 2021 , 103,	
413	Topological insulators and semimetals in classical magnetic systems. 2021 , 915, 1-64	11
412	Chiral transport of pseudospinors induced by synthetic gravitational field in photonic Weyl metamaterials. 2021 , 104,	0
411	Potential antiferromagnetic Weyl nodal line state in LiTi2O4 material. 2021 , 104,	2
410	Sixfold, fourfold, and threefold excitations in the rare-earth metal carbide R2C3. 2021 , 104,	2
409	As2Te3: Pressure-induced three-dimensional Dirac semimetal with ultralow room-pressure lattice thermal conductivity. 2021 , 104,	0
408	Strain-induced topological charge control in multifold fermion systems. 2021 , 33,	0
407	Cycling Fermi arc electrons with Weyl orbits. 2021 , 3, 660-670	0
406	Tip-induced superconductivity. 2021 , 33,	1
405	Topological quantum matter to topological phase conversion: Fundamentals, materials, physical systems for phase conversions, and device applications. 2021 , 145, 100620	8
404	Ferromagnetic-electrodes-induced Hall effect in topological Dirac semimetals. 2021 , 3,	1
403	Anisotropic superconductivity in the topological crystalline metal Pb1/3TaS2 with multiple Dirac fermions. 2021 , 104,	1
402	Pressure-Induced Electronic and Structural Transition in Nodal-Line Semimetal ZrSiSe. 2021 , 60, 11140-11146	
401	Multiple Dirac cones and Lifshitz transition in a two-dimensional Cairo lattice as a Hawking evaporation analogue. 2021 , 33,	0

400	Theory-Guided Discovery of Novel Materials. 2021 , 12, 6499-6513	6
399	Magnetization Signature of Topological Surface States in a Non-Symmorphic Superconductor. 2021 , 33, e2103257	
398	Valley-dependent electron scattering in Weyl semimetals. 2021 , 334-335, 114387	
397	2D Metallic Transition-Metal Dichalcogenides: Structures, Synthesis, Properties, and Applications. 2105132	17
396	Electron scattering by magnetic impurity in Weyl semimetals. 2021 , 23, 083003	0
395	Double-bowl state in photonic Dirac nodal line semimetal. 2021 , 10, 170	1
394	Nonperturbative Dyson-Schwinger equation approach to strongly interacting Dirac fermion systems. 2021 , 104,	1
393	Generation of tunable terajet via a dielectric rod covered with Dirac semimetal. 2021 , 130, 083103	0
392	Microscopic Theory of Electrically Induced Spin Torques in Magnetic Weyl Semimetals. 2021 , 90, 084702	3
391	Room-Temperature Topological Phase Transition in Quasi-One-Dimensional Material Bi4I4. 2021 , 11,	4
390	Charge-four Weyl point: Minimum lattice model and chirality-dependent properties. 2021 , 104,	4
389	Evolving Devil's Staircase Magnetization from Tunable Charge Density Waves in Nonsymmorphic Dirac Semimetals. 2021 , 33, e2103476	0
388	Photoexcited carrier dynamics of thin film Cd3As2 grown on a GaAs(111)B substrate by molecular beam epitaxy. 2021 , 104,	0
387	Cubic Dirac and quadruple Weyl points in screw-symmetric materials. 2021 , 104,	1
386	Magnetic proximity effects in topological insulator heterostructures: Implementation and characterization. 2021 , 5,	2
385	Strong suppression of electron convection in Dirac and Weyl semimetals. 2021 , 104,	1
384	Three-dimensional Dirac material anode enables concentrated solar thermionic converters. 2021 , 46, 4530-4533	2
383	Band-gap formation and morphing in \mathbb{Z}_3 superlattices. 2021 , 104,	1

- 382 Multiple Dirac nodal lines in an in-plane anisotropic semimetal TaNiTe5. **2021**, 104, 1
- 381 Nodal Lines and Boundary Modes in Topological Dirac Semimetals with Magnetism. **2021**, 90, 094702 0
- 380 Nontopological chiral chemical potential due to the Zeeman field in magnetic Weyl semimetals. **2021**, 104, 0
- 379 Spin susceptibilities in magnetic type-I and type-II Weyl semimetals. **2021**, 104, 0
- 378 Emergence of topological superconductivity in doped topological Dirac semimetals under symmetry-lowering lattice distortions. **2021**, 11, 18539 0
- 377 Highly tunable plasmon-induced transparency with Dirac semimetal metamaterials*. **2021**, 30, 096103 0
- 376 A study of topological and transport properties of YAuPb. **2021**, 33, 0
- 375 Topological Aspects of Antiferromagnets. 6
- 374 Alloying-induced enhancement of thermopower in the Dirac-semimetal system $Cd_{3-x}Zn_xAs_2$. **2021**, 5, 0
- 373 Extremely large magnetoresistance in the ordinary metal ReO_3 . **2021**, 104, 0
- 372 Strain-Induced Ideal Topological Semimetal in $Ort-B32$ Holding Parallel Arc-Like Nodal Lines and Anisotropic Multiple Weyl Fermions. 2100324
- 371 Tunneling in an anisotropic cubic Dirac semi-metal. **2021**, 432, 168563 1
- 370 Reconstructed conventional bulk-boundary correspondence in the non-Hermitian s-wave nodal-ring superconductor. **2021**, 104, 0
- 369 Predicting MnB_6 monolayer with room temperature ferromagnetism and high magnetic anisotropy. **2021**, 134, 114930 1
- 368 Highly stable full Heusler order $Cs(Na, K)_2Bi$ with diverse topological phases controlled by strain engineering. **2021**, 273, 115430 1
- 367 Broadband terahertz absorber based on hybrid Dirac semimetal and water. **2021**, 143, 107274 13
- 366 Enhanced second-order nonlinearity and tunable plasmon induced transparency in noncoplanar Dirac semimetal system. **2021**, 340, 114510 1
- 365 Epitaxial fabrication of topological Bi-Sb alloy films by surface alloying of Sb nanofilms. **2021**, 714, 121921 2


364	Dynamically controlled terahertz coherent absorber engineered with VO ₂ -integrated Dirac semimetal metamaterials. 2022 , 503, 127443	1
363	Evidence of Weyl fermions in RuCl ₃ . 2021 , 103,	0
362	Structural, electronic and elastic properties of topological pyrite-type OsSe ₂ semimetal. 2021 , 46, 5823-5826	
361	Spin-polarized quantized electronic structure of Fe(001) with symmetry breaking due to the magnetization direction. 2021 , 103,	3
360	Anomalous planar Hall effect in two-dimensional trigonal crystals. 2021 , 3,	4
359	Phase transition and topological transistors based on monolayer NaBi nanoribbons. 2021 , 13, 15048-15057	3
358	Quantum Transport in Topological Matters under Magnetic Fields. 2021 , 70, 1-30	0
357	Anisotropic lattice thermal conductivity in topological semimetal ZrGeX (X=S, Se, Te): A first-principles study. 2021 ,	0
356	Physical problems and experimental progress in layered magnetic topological materials. 2021 , 70, 127302-127302	
355	Charge density wave and weak Kondo effect in a Dirac semimetal CeSbTe. 2021 , 64, 1	4
354	Assessing the stability of Cd ₃ As ₂ Dirac semimetal in humid environments: the influence of defects, steps and surface oxidation. 2021 , 9, 1235-1244	2
353	Topological carbon materials: A new perspective. 2020 , 868, 1-32	14
352	Dual-controlled tunable terahertz coherent perfect absorption using Dirac semimetal and vanadium dioxide. 2020 , 19, 103688	14
351	Computationally Directed Discovery of MoBi. 2021 , 143, 214-222	9
350	Wonders of flat physics now seen in 3D.	1
349	Dirac points and the transition towards Weyl points in three-dimensional sonic crystals. 2020 , 9, 201	6
348	Linear and nonlinear optical responses in the chiral multifold semimetal RhSi. 2020 , 5,	14
347	Scars in Dirac fermion systems: the influence of an AharonovBohm flux. 2017 , 19, 013018	7

346	Weyl fermions in ferromagnetic high-temperature phase of K ₂ Cr ₈ O ₁₆ . 2020 , 22, 073062	0
345	Topological carbon allotropes: knotted molecules, carbon-nano-chain, chainmails, and Hopfene. 2020 , 7, 056301	2
344	Magnetotransport and ab initio calculation studies on the layered semimetal CaAl ₂ Si ₂ hosting multiple nontrivial topological states. 2020 , 101,	4
343	Prediction of Dirac semimetals and hourglass surface states in stacked hydrogenated Xenes (X=Sn and Pb). 2020 , 102,	2
342	Quantum transport in Weyl semimetal thin films in the presence of spin-orbit coupled impurities. 2017 , 96,	11
341	Robustness of persistent currents in two-dimensional Dirac systems with disorder. 2017 , 96,	8
340	Coupling of magnetic order and charge transport in the candidate Dirac semimetal EuCd ₂ As ₂ . 2018 , 97,	26
339	Momentum-dependent spin selection rule in photoemission with glide symmetry. 2018 , 98,	4
338	Ternary wurtzite CaAgBi materials family: A playground for essential and accidental, type-I and type-II Dirac fermions. 2017 , 1,	47
337	Towards diluted magnetism in TaAs. 2017 , 1,	1
336	Electrostatic modulation of the electronic properties of Dirac semimetal Na ₃ Bi thin films. 2017 , 1,	10
335	Evolution of band topology by competing band overlap and spin-orbit coupling: Twin Dirac cones in Ba ₃ SnO as a prototype. 2017 , 1,	9
334	Topological origin of the type-II Dirac fermions in PtSe ₂ . 2017 , 1,	30
333	Topological Dirac nodal-net fermions in AlB ₂ -type TiB ₂ and ZrB ₂ . 2018 , 2,	74
332	Quantum oscillations and coherent interlayer transport in a new topological Dirac semimetal candidate YbMnSb ₂ . 2018 , 2,	21
331	Observation of topological surface states and strong electron/hole imbalance in extreme magnetoresistance compound LaBi. 2018 , 2,	7
330	Nexus networks in carbon honeycombs. 2018 , 2,	13
329	Nonsymmorphic cubic Dirac point and crossed nodal rings across the ferroelectric phase transition in LiOsO ₃ . 2018 , 2,	24

328	Enhancement of the superconducting transition temperature by Re doping in Weyl semimetal MoTe ₂ . 2018 , 2,	16
327	Type-II Dirac line node in strained Na ₃ N. 2018 , 2,	7
326	Type-II Dirac semimetal candidates ATe ₂ (A= Pt, Pd): A de Haas-van Alphen study. 2018 , 2,	13
325	Fermi surface of the flat-band intermetallics APd ₃ (A=Pb,Sn). 2019 , 3,	0
324	High-pressure lithium as an elemental topological semimetal. 2019 , 3,	3
323	Topological and superconducting properties in YD ₃ (D=In, Sn, Tl, Pb). 2019 , 3,	8
322	Dirac nodal lines protected against spin-orbit interaction in IrO ₂ . 2019 , 3,	15
321	Topological semimetal features in the multiferroic hexagonal manganites. 2019 , 3,	5
320	Prediction of threefold fermions in a nearly ideal Dirac semimetal BaAgAs. 2019 , 3,	9
319	Topological band crossings in epitaxial strained SnTe. 2019 , 3,	4
318	Enormous electron-electron scattering in the filled-cage cubic compound Ba ₁₀ Ti ₂₄ Bi ₃₉ . 2019 , 3,	1
317	Symmetry-driven topological phases in XAgBi (X=Ba,Sr): An ab initio hybrid functional calculation. 2020 , 4,	4
316	Topological electronic structure and Weyl points in nonsymmorphic hexagonal materials. 2020 , 4,	1
315	Direct measurement of a beta function and an indirect check of the Schwinger effect near the boundary in Dirac semimetals. 2019 , 1,	7
314	Curved spacetime theory of inhomogeneous Weyl materials. 2019 , 1,	13
313	Chiral sound waves in strained Weyl semimetals. 2019 , 1,	11
312	Parabolic Hall effect due to copropagating surface modes. 2020 , 2,	1
311	Diagnosis scheme for topological degeneracies crossing high-symmetry lines. 2020 , 2,	9

310	Momentum-dependent mass and AC Hall conductivity of quantum anomalous Hall insulators and their relation to the parity anomaly. 2020 , 2,	4
309	Chiral-anomaly-induced angular narrowing of the positive longitudinal magnetoconductivity in Weyl semimetals. 2020 , 2,	1
308	Efficient generation of extreme terahertz harmonics in three-dimensional Dirac semimetals. 2020 , 2,	13
307	Photoinduced renormalization and electronic screening of quasi-two-dimensional Dirac states in BaNiS ₂ . 2020 , 2,	3
306	Angle-Resolved Photoemission Spectroscopy Study of Topological Quantum Materials. 2020 , 50, 131-153	4
305	Tunable terahertz metamaterial absorber based on Dirac semimetal films. 2018 , 57, 9555-9561	20
304	Tunable defect modes of one-dimensional photonic crystals containing a Dirac semimetal-based metamaterial defect layer. 2019 , 58, 94-101	20
303	Tunable narrow terahertz absorption of one-dimensional photonic crystals embedded with Dirac semimetal-dielectric defect layers. 2019 , 58, 8486-8494	3
302	Tunable bifunctional polarization-independent metamaterial device based on Dirac semimetal and vanadium dioxide. 2020 , 37, 1340-1349	9
301	Tunable Fano resonance with ultrahigh peak by bright-dark mode coupling in Dirac semimetal. 2019 , 36, 2461	3
300	Dynamically tunable coherent perfect absorption based on bulk Dirac semimetal. 2020 , 37, 1987	1
299	Ultrasensitive tunable terahertz sensor based on five-band perfect absorber with Dirac semimetal. 2019 , 27, 20165-20176	27
298	Bidirectional and dynamically tunable THz absorber with Dirac semimetal. 2019 , 27, 31062-31074	27
297	Controllable broadband asymmetric transmission of terahertz wave based on Dirac semimetals. 2019 , 27, 35784-35796	21
296	Optical Kerr effect and third harmonic generation in topological Dirac/Weyl semimetal. 2019 , 27, 38270-38280	11
295	Tunable bifunctional terahertz metamaterial device based on Dirac semimetals and vanadium dioxide. 2020 , 28, 17434-17448	44
294	Optical materials for maximal nanophotonic response [Invited]. 2020 , 10, 1561	10
293	Bifunctional tunable terahertz circular polarization converter based on Dirac semimetals and vanadium dioxide. 2020 , 10, 2289	13

292	Dynamically tunable broadband linear-to-circular polarization converter based on Dirac semimetals. 2018 , 8, 3238	32
291	Tunable polarization-nonsensitive electromagnetically induced transparency in Dirac semimetal metamaterial at terahertz frequencies. 2019 , 9, 1562	23
290	Tunable multiple plasmon-induced transparency in a simple terahertz Dirac semimetal based metamaterial. 2019 , 9, 3325	8
289	Dynamically tunable coherent perfect absorption and transparency in Dirac semimetal metasurface. 2019 , 9, 3649	5
288	Gap Generation in Weyl Semimetals in a Model with Local Four-Fermion Interaction. 2014 , 59, 696-705	6
287	Electronic structure of the candidate 2D Dirac semimetal SrMnSb ₂ : a combined experimental and theoretical study. 2018 , 4,	16
286	Detect axial gauge fields with a calorimeter. 2020 , 3,	1
285	Observation of planar Hall effect in topological semimetal ZrSiSe device. 2019 , 68, 227203	2
284	Electronic structures of topological quantum materials studied by ARPES. 2021 , 108, 1-42	0
283	Quantum transport study in three-dimensional topological insulator BiSbTeSe ₂ . 2021 , 108, 73-124	
282	Oxygen-vacancy-induced magnetism in anti-perovskite topological Dirac semimetal BaSnO. 2021 , 23, 24878-24891	0
281	Ultrafast photocarrier dynamics in Dirac semimetal PtTe ₂ thin film. 2021 ,	
280	Shubnikov-de Haas oscillations and electronic structure in the Dirac semimetal SrAgAs. 2021 , 104,	0
279	Elemental Topological Dirac Semimetal E_n with High Quantum Mobility. 2021 , e2104645	2
278	Quantum oscillations and quasilinear magnetoresistance in the topological semimetal candidate ScSn ₂ . 2021 , 104,	
277	Thickness dependence of magnetotransport properties of tungsten ditelluride. 2021 , 104,	0
276	Manipulation of Dirac Fermions in Nanochain-Structured Graphene. 2021 , 38, 097101	1
275	Planar Hall effect in the quasi-one-dimensional topological superconductor TaSe ₃ . 2021 , 104,	2

- 274 Theoretical Model for a Highly Sensitive Near Infrared Biosensor Based on Bloch Surface Wave with Dirac Semimetal. **2021**, 11, 1
- 273 Weyl nodal-ring semimetallic behavior and topological superconductivity in crystalline forms of Su-Schrieffer-Heeger chains. **2021**, 104, 0
- 272 Ideal topological phononic nodal chain in K2O materials class. **2021**, 23, 103043 3
- 271 Epitaxial HfTe2 Dirac semimetal in the 2D limit. **2021**, 9, 101103 1
- 270 What is a Weyl Semimetal. **2016**, 37, 625-630
- 269 Introduction. **2017**, 1-31
- 268 Dirac cones and topological states: Dirac and Weyl semimetals. **2018**, 535-545
- 267 Spectroscopic studies of plasmons in topological materials. **2019**, 68, 227801
- 266 Optical properties of topological semimetals. **2019**, 68, 227804 0
- 265 Angle resolved photoemission spectroscopy studies on three dimensional strong topological insulators and magnetic topological insulators. **2019**, 68, 227901 0
- 264 Progress of ARPES study on topological semimetals. **2019**, 68, 227102
- 263  **2019**, 200, 343-360
- 262 Topological materials discovery from crystal symmetry. 10
- 261 Three-Dimensional Dirac Semimetal Antennas for Telecommunications in the Terahertz Spectrum. **2020**,
- 260 Unified ballistic transport relation for anisotropic dispersions and generalized dimensions. **2020**, 2,
- 259 Linear and Nonlinear Terahertz Three-Dimensional Dirac Nano-Plasmonic Waveguides. **2020**, 1
- 258 Broadband terahertz absorber based on Dirac semimetal with tunable working bandwidth. **2020**, 19, 103683 1
- 257 High-order one-dimensional (1D) fermion in ferromagnetic RbFeF3. **2022**, 201, 110944

256	Manifestation of a topological gapless phase in a two-dimensional chiral symmetric system through Loschmidt echo. 2020 , 101,	
255	Eightfold Degenerate Fermions in Two Dimensions. 2021 , 127, 176401	0
254	Dirac semimetal phase and switching of band inversion in XMgBi (X = Ba and Sr). 2021 , 11, 21937	1
253	Topology of a parity-time symmetric non-Hermitian rhombic lattice.	1
252	Nonlinear Ballistic Response of Quantum Spin Hall Edge States. 2021 , 127, 206801	0
251	Maximal terahertz emission in high harmonic generation from 3D Dirac semimetals. 2021 , 4,	2
250	Electrically controlled spin polarized current in Dirac semimetals. 2021 , 11, 21509	
249	Magnetometric Studies of Composite Alloys of the Cd ₃ As ₂ MnAs System. 2021 , 66, 1544-1548	0
248	Ideal type-II Weyl points in twisted one-dimensional dielectric photonic crystals. 2021 , 29, 40606-40616	1
247	Engineering exotic second-order topological semimetals by periodic driving. 2021 , 104,	0
246	Three-dimensional topological plasmons in Weyl semimetals. 2021 , 104,	0
245	Tunable terahertz Dirac-semimetal hybrid plasmonic waveguides.	3
244	Large magnetoresistance and de Haas-van Alphen oscillations in the topological semimetal candidates BaX ₄ (X=Ga, In). 2021 , 104,	
243	Magnetic field effect on topological properties of Dirac semimetals PdTe/PtTe/PtSe. 2021 , 34,	
242	Electron transport probing the electrically tunable topological phase transition in a Dirac semimetal. 2021 , 104,	
241	Magnetic-field-induced nonlinear transport in HfTe ₅ .	0
240	Classification of Dirac points with higher-order Fermi arcs. 2021 , 104,	1
239	Degenerate topological line surface phonons in quasi-1D double helix crystal SnIP. 2021 , 7,	4

238	A four-band and polarization-independent BDS-based tunable absorber with high refractive index sensitivity. 2021 , 23, 26864-26873	65
237	Ultrafast time- and angle-resolved photoemission spectroscopy with widely tunable probe photon energy of 5.3-7.0 eV for investigating dynamics of three-dimensional materials.. 2022 , 93, 013902	4
236	Ultrafast photocarrier and coherent phonon dynamics in type-II Dirac semimetal PtTe ₂ thin films probed by optical spectroscopy.	3
235	3D Dirac Semimetal Supported Tunable TE Modes. 2100355	5
234	Topological phase transition associated with structural phase transition in ternary half Heusler compound LiAuBi.. 2022 ,	
233	Anisotropic nodal loop in NiB monolayer with nonsymmorphic configuration.. 2022 ,	0
232	Topological signatures in nodal semimetals through neutron scattering. 2022 , 24, 013016	1
231	Switchable coding metasurface for flexible manipulation of terahertz wave based on Dirac semimetal. 2022 , 33, 105204	3
230	Alkali-metal induced electronic structure evolution in Sn ₄ Sb ₃ studied by angle-resolved photoemission spectroscopy. 2022 , 162, 110526	
229	Interaction of the Dirac Electron Located in a Potential Well with a Plane Wave Field. 2020 ,	0
228	Anisotropic surface state in a topological semimetal candidate Ta ₃ SiTe ₆ . 2022 , 120, 041602	
227	Topology, Symmetry, and Band Theory of Materials. 2022 , 7-49	
226	Anisotropic Dirac cone and slow edge states in a photonic Floquet lattice. 2022 , 105,	
225	Strain-induced circular photogalvanic current in Dirac semimetal CdAs films epitaxied on a GaAs(111)B substrate.. 2022 ,	1
224	Interlayer exchange interaction driven topological phase transition in antiferromagnetic electride Gd ₂ O. 2022 , 105,	0
223	Dynamically controlled asymmetric transmission of linearly polarized waves in VO ₂ -integrated Dirac semimetal metamaterials.	0
222	Direct observation of the spin-orbit coupling effect in magnetic Weyl semimetal Co ₃ Sn ₂ S ₂ . 2022 , 7,	1
221	Type-II quadratic and cubic Weyl fermions. 2022 , 105,	0

220	Berry curvature induced anisotropic magnetotransport in a quadratic triple-component fermionic system.. 2022 ,	0
219	Synthetic Topological Nodal Phase in Bilayer Resonant Gratings.. 2022 , 128, 053002	2
218	Higher-order Dirac semimetal in a photonic crystal. 2022 , 105,	2
217	Systematic investigation of emergent particles in type-III magnetic space groups. 2022 , 105,	2
216	Kohler's rule and anisotropic Berry-phase effect in nodal-line semimetal ZrSiSe. 2022 , 131, 065106	1
215	Thickness-dependent topological phase transition and Rashba-like preformed topological surface states of $\text{Sn}(001)$ thin films on $\text{InSb}(001)$. 2022 , 105,	2
214	A comparative study of the structural, electronic, vibrational, dielectric and elastic properties of the two phases CaAgBi through first-principles calculations. 2022 , 555, 111449	0
213	Theoretical study of compounds XSb ($\text{X}=\text{La, Pr, Nd}$): Realization of inner nodal chains, nodal line frame, and Dirac points. 2022 , 206, 111231	0
212	Tunable topological phase transition from nodal-line semimetal to Weyl semimetal by breaking symmetry. 2021 , 104,	0
211	Type-II nodal line fermions in the Z2 topological semimetals AV_6Sb_6 ($\text{A}=\text{K, Rb, and Cs}$) with a kagome bilayer. 2021 , 104,	2
210	Dynamic Rashba-Dresselhaus Effect.. 2021 , 127, 237601	1
209	A high-efficiency wideband tunable polarization conversion metasurface assisted by the localized surface plasmon resonances. 2022 ,	
208	Pressure dependence of superconductivity in alkali-Bi compounds KBi and RbBi .. 2022 ,	1
207	An ideal Weyl nodal ring with a large drumhead surface state in the orthorhombic compound TiS .. 2022 ,	0
206	Challenges to magnetic doping of thin films of the Dirac semimetal Cd_3As_2 . 2022 , 6,	1
205	Large-area fabrication of 2D layered topological semimetal films and emerging applications. 2022 , 7,	2
204	Active modulation of quasi-bound state in the continuum based on bulk Dirac semimetals metamaterial. 2022 , 15, 032006	1
203	Threefold Fermions, Weyl Points, and Superconductivity in the Mirror Symmetry Lacking Semiconductor TlCdTe .. 2022 , 12,	0

- 202 Effect of Cu Doping on Structure and Physical Properties in the Antiferromagnetic Dirac Semimetal CaMnBi.. **2022**,
- 201 Optical forces in photonic Weyl system. 1
- 200 Squeezing the periodicity of Néel-type magnetic modulations by enhanced Dzyaloshinskii-Moriya interaction of 4d electrons. **2022**, 7, 2
- 199 Relativistic collapse of Landau levels of Kane fermions in crossed electric and magnetic fields. **2022**, 105, 0
- 198 Mid-Infrared Sensor Based on Dirac Semimetal Coupling Structure.. **2022**, 22,
- 197 Quantum Oscillations in Noncentrosymmetric Weyl Semimetal SmAlSi. **2022**, 39, 047501 0
- 196 Prediction of topological Dirac semimetal in Ca-based Zintl layered compounds CaMX (M = Zn or Cd; X = N, P, As, Sb, or Bi).. **2022**, 12, 4582 0
- 195 Experimental Demonstration of Bulk-Hinge Correspondence in a Three-Dimensional Topological Dirac Acoustic Crystal.. **2022**, 128, 115701 1
- 194 Strain-controlled evolution of electronic structure indicating topological phase transition in the quasi-one-dimensional superconductor TaSe3. **2022**, 105, 0
- 193 Measurement of the electronic structure of a type-II topological Dirac semimetal candidate VAl3 using angle-resolved photoelectron spectroscopy. 1
- 192 Topological Materials for Functional Optoelectronic Devices. 2110655 0
- 191 Electronic structure and open-orbit Fermi surface topology in isostructural semimetals NbAs2 and W2As3 with extremely large magnetoresistance. **2022**, 120, 123101 1
- 190 Candidate entanglement invariants for two Dirac spinors. **2022**, 105, 0
- 189 Searching for Band-Dispersive and Defect-Tolerant Semiconductors from Element Substitution in Topological Materials.. **2022**, 0
- 188 Dirac nodal-line semimetal zinc polynitride at high pressure. **2022**, 105, 0
- 187 Emergence of a Two-Dimensional Topological Dirac Semimetal Phase in a Phthalocyanine-Based Covalent Organic Framework. 2
- 186 Growth of F_n on silicon by a reversed F_n to F_n phase transformation for quantum material integration. **2022**, 3,
- 185 Tunneling properties in B_3 lattices: Effects of symmetry-breaking terms. **2022**, 105, 1

- 184 Dynamical polarization, optical conductivity and plasmon mode of a linear triple component fermionic system.. **2022**, 0
- 183 RKKY interaction of magnetic impurities in nodal-line semimetals. **2022**, 553, 169164
- 182 Thermal-field electron emission from three-dimensional Dirac and Weyl semimetals. **2021**, 104, 5
- 181 Half-Metallic Ferromagnets, Spin Gapless Semiconductors, and Topological Semimetals Based on Heusler Alloys: Theory and Experiment. **2021**, 122, 1133-1157 0
- 180 Anisotropic magnetoresistance and planar Hall effect in type-II Dirac semimetal PtTe₂. **2021**, 130, 233901 0
- 179 Topological states in the noncentrosymmetric superconductors LaPtSi and LaPtGe. **2021**, 104,
- 178 Surface atomic manipulation of low-dimensional structures. **2022**,
- 177 Unusual Electrical and Magnetic Properties in Layered EuZn₂As₂. 2200012 0
- 176 Angle dependent field-driven reorientation transitions in uniaxial antiferromagnet MnBi₂Te₄ single crystal. **2022**, 120, 163102 0
- 175 Berry phase in quantum oscillations of topological materials. **2022**, 7, 0
- 174 Robust non-integer conductance in disordered 2D Dirac semimetals.. **2022**,
- 173 Table_1.DOCX. **2020**,
- 172 Theory of topological superconductivity in doped IV-VI semiconductors. **2022**, 105,
- 171 Anisotropic magnetoresistance and possible weak antilocalization in Mg₃Bi₂ single crystal. 2
- 170 A semiclassical approach to surface Fermi arcs in Weyl semimetals. **2022**, 65, 0
- 169 Materials under high pressure: a chemical perspective. **2022**, 128, 1 2
- 168 Superconducting properties of the spin Hall candidate Ta₃Sb with eightfold degeneracy. **2022**, 105, 0
- 167 Robust structure symmetry and electronic band structure of the chiral topological semimetal CoSi against high pressure. **2022**, 103667

166	Possible realization of optical Dirac points in woodpile photonic crystals. 2022 , 30, 17204	0
165	Tunable mid-infrared ultra-narrowband plasmonic absorber and sensor based on bulk Dirac semimetal metamaterials.	
164	Enabling 100C Fast-Charging Bulk Bi Anodes for Na-Ion Batteries.. 2022 , e2201446	6
163	A Review: The Functional Materials-Assisted Terahertz Metamaterial Absorbers and Polarization Converters. 2022 , 9, 335	1
162	Embedded topological semimetals. 2022 , 105,	1
161	Novel Emerging Materials: Introduction and Evolution. 2022 , 3-36	
160	Magnetically tunable Dirac and Weyl fermions in the Zintl materials family. 2022 , 6,	1
159	The topological nodal lines and drum-head-like surface states in semimetals CrSi ₂ , MoSi ₂ and WSi ₂ . 2022 , 413928	0
158	Robust and tunable Weyl phases by coherent infrared phonons in ZrTe ₅ . 2022 , 8,	1
157	All topological bands of all nonmagnetic stoichiometric materials.. <i>Science</i> , 2022 , 376, eabg9094	33.3 8
156	The ultra-low lattice thermal conductivity dominated by the quartic anharmonicity in Bi-based binary compounds A ₃ Bi (A =K,Rb).	0
155	Dirac nodal lines in the quasi-one-dimensional ternary telluride TaPtTe ₅ . 2022 , 105,	0
154	A Class of Magnetic Topological Material Candidates with Hypervalent Bi Chains.	0
153	Tunable Angle-Selective Optical Transparency Induced by Photonic Topological Transition in Dirac Semimetals-based Hyperbolic Metamaterials.	2
152	Doubled quantum spin Hall effect with high-spin Chern number in \mathbb{H} antimonene and \mathbb{H} -bismuthene. 2022 , 105,	0
151	Effect of relativity and vacuum fluctuations on quantum measurement. 2022 , 105,	
150	Low threshold optical bistability based on topological edge state in photonic crystal heterostructure with Dirac semimetal. 2022 , 30, 20847	2
149	Enhanced spin Hall effect of reflected light due to optical Tamm states with Dirac semimetal at the terahertz range. 2022 , 128468	1

- 148 A high-efficiency wideband tunable polarization conversion metasurface assisted by localized surface plasmon resonances. **2022**, 71, 128101
- 147 Gapless vortex bound states in superconducting topological semimetals. ○
- 146 Ln₃MBi₅ (Ln=Pr, Nd, Sm; M=Zr, Hf): Intermetallics with Hypervalent Bismuth Chains.
- 145 ThreeFold Weyl Points for the Schrödinger Operator with Periodic Potentials. **2022**, 54, 3654-3695
- 144 Berry phase in the phase space worldline representation: The axial anomaly and classical kinetic theory. **2022**, 105, ○
- 143 The Structural, Mechanical, Lattice Dynamical, and Thermal Properties of 3D Dirac Semimetals BaXBi (X=Cu, Ag, Au) from First-Principles Calculations. 2200132
- 142 Evidence of topological surface states in dysprosium monpnictides compounds. **2022**, 283, 115774 ○
- 141 Tunable terahertz Bloch surface waves in one-dimensional photonic crystals with a Dirac semimetal cap layer. **2022**, 265, 169538 ○
- 140 Molecular beam epitaxy of antiperovskite oxides. **2022**, 10, 060904
- 139 First-principles calculations for structural, elastic, electronic, and phonon properties of topological WC-type TMO (TM =Ti, Zr and Hf; O) family. **2022**,
- 138 Angle-resolved photoemission spectroscopy. **2022**, 2, 3
- 137 3D Dirac semimetals-dielectric elliptical fiber supported tunable terahertz hybrid waveguide. **2022**, 61, 6152
- 136 Prediction of negative refraction in dirac semimetal metamaterial.
- 135 Magnetotransport properties of the topological semimetal SrAgBi. **2022**, 106, ○
- 134 Controlling SpinOrbit Coupling to Tailor Type-II Dirac Bands. ○
- 133 Topological quantum materials for energy conversion and storage. 3
- 132 Effect of spin-orbit coupling on the high harmonics from the topological Dirac semimetal Na₃Bi. **2022**, 8, ○
- 131 Unpaired topological triply degenerate point for spin-tensor-momentum-coupled ultracold atoms. **2022**, 4, ○

- 130 Weyl-type nodal chains in X_2MnO_4 ($X = Li, Na$). **2022**, 213, 111613
- 129 Structural, electronic and topological properties of 3D TmBi compound. **2022**, 137, 0
- 128 Highly Efficient Terahertz Generation Using 3D Dirac Semimetals. 2100279
- 127 Easily accessible topologically protected charge carriers in pure and robust Bi_2Se_3 films.
- 126 Magnetic field and strain effects in Janus-like Weyl semimetals MoTeSe with four Weyl points. **2022**, 213, 111617
- 125 Selective CO₂ reduction on topological Chern magnet TbMn₆Sn₆. **2022**, 24, 18600-18607 1
- 124 Generalized fermion doubling theorems: Classification of two-dimensional nodal systems in terms of wallpaper groups. **2022**, 106,
- 123 Advances in Bismuth-Based Topological Quantum Materials by Scanning Tunnelling Microscopy. 0
- 122 Triple nodal points characterized by their nodal-line structure in all magnetic space groups. **2022**, 106, 0
- 121 Two-Dimensional Topological States. **2022**, 81-122
- 120 Topological properties of CsCl type superconducting materials. **2022**, 128385 0
- 119 Coexistence of charge-2 Dirac and Weyl phonons in chiral space groups. **2022**, 106, 0
- 118 Connection between topological pumping effect and chiral anomaly in Weyl semimetals. **2022**, 106, 0
- 117 Nanomolding of topological nanowires. **2022**, 10, 080904 0
- 116 Topological acoustics. 2
- 115 Fermi surface of the chiral topological semimetal PtGa. **2022**, 34, 425502 0
- 114 Large nonsaturating magnetoresistance, weak anti-localization, and non-trivial topological states in SrAl₂Si₂. **2022**, 106,
- 113 Landau levels and magneto-optical responses in Weyl semimetal quantum wells in a non-uniform magnetic field. **2022**, 106,

- 112 Crystal chemistry at high pressure. **2022**, ○
- 111 A predicted orthogonal semimetallic carbon with negative thermal expansion and compressibility. **2022**, 24, 23497-23506 ○
- 110 A two-dimensional Be₂Au monolayer with planar hexacoordinate s-block metal atoms: a superconducting global minimum Dirac material with two perfect Dirac node-loops. **2022**, 13, 11099-11109 ○
- 109 Robust ferromagnetism and Weyl half-semimetal in a two-dimensional vanadium boride monolayer. **2022**, 14, 12491-12497 ○
- 108 Z₂ Dirac points with topologically protected multihelicoid surface states. **2022**, 4, ○
- 107 A first-principles study on the effect of Cr, Mn, and Co substitution on Fe-based normal- and inverse-Heusler compounds: Fe₃XY_xZ (x=0, 1, 2, 3; Y= Cr, Mn, Co; Z=Al, Ga, Si). 10, ○
- 106 Linear-in-frequency optical conductivity over a broad range in the three-dimensional Dirac semimetal candidate Ir₂In₈Se. **2022**, 106, ○
- 105 Spinor GW /Bethe-Salpeter calculations in BerkeleyGW: Implementation, symmetries, benchmarking, and performance. **2022**, 106, 1
- 104 Tunneling Phase Diagrams in Anisotropic Multi-Weyl Semimetals. 2200267 ○
- 103 Atomic-scale study of type-II Dirac semimetal PtTe₂ surface. **2022**, 5, 044003 ○
- 102 Ultrafast Optical Probe of Coherent Acoustic Phonons in Dirac Semimetal Cd₃As₂ Film Epitaxied on GaAs(111)B Substrate. **2022**, 13, 8783-8792 ○
- 101 Inverse Faraday effect in massive Dirac electrons. **2022**, 106, ○
- 100 High-Temperature Nodal Ring Semimetal in 2D Honeycomb-Kagome Mn₂N₃ Lattice. ○
- 99 High-order harmonic generation in three-dimensional Weyl semimetals with broken time-reversal symmetry. **2022**, 106, ○
- 98 Unremovable linked nodal structures protected by crystalline symmetries in stacked bilayer graphene with Kekulé texture. **2022**, 106, ○
- 97 Observation of Dirac Hierarchy in Three-Dimensional Acoustic Topological Insulators. **2022**, 129, 1
- 96 Analysis of unconventional chiral fermions in a noncentrosymmetric chiral crystal PtAl. **2022**, 106, ○
- 95 Emergent topological states via digital (001) oxide superlattices. **2022**, 8, ○

- 94 Discovery of the kagome superconductor in the Half-Heusler NbRhSb **2022**, 137, ○
- 93 High-mobility two-dimensional carriers from surface Fermi arcs in magnetic Weyl semimetal films. **2022**, 7, 1
- 92 Chemical bonding principles in magnetic topological quantum materials. **2022**, ○
- 91 Berry curvature induced anomalous Hall conductivity in the magnetic topological oxide double perovskite $\text{Sr}_2\text{FeMoO}_6$. **2022**, 106, ○
- 90 Spin pumping into anisotropic Dirac electrons. **2022**, 106, ○
- 89 Observation of Planar Hall Effect in a Strong Spin-Orbit Coupling Superconductor $\text{LaO}_{0.5}\text{F}_{0.5}\text{BiSe}_2$. ○
- 88 TM₂B₃ monolayers: Intrinsic anti-ferromagnetism and Dirac nodal line semimetal. **2022**, 121, 183103 ○
- 87 First-principles calculations for the effect of energetic point defect formation on electronic properties of the Weyl MX family (M = Nb, Ta; X = P, As). **2022**, ○
- 86 Multiple Dirac points including potential spin-orbit Dirac points in nonsymmorphic $\text{HfGe}_{0.92}\text{Te}$. **2023**, 66, ○
- 85 Semiconductorlike photocarrier dynamics in Dirac-semimetal Cd_3As_2 films probed with transient terahertz spectroscopy. **2022**, 106, ○
- 84 Phononic nodal point in two dimensions: A mini-review. 10, ○
- 83 Fermiology of a topological line-nodal compound CaSb_2 and its implication to superconductivity: Angle-resolved photoemission study. **2022**, 6, ○
- 82 Electronic structures and stability investigation of large band gap topological insulators MTl_4Te_3 (M = Cd, Hg). **2022**, 6, ○
- 81 Two-dimensional antiferromagnetic nodal-line semimetal and quantum anomalous Hall state in the van der Waals heterostructure germanene/ Mn_2S_2 . **2022**, 34, 505702 ○
- 80 Integer quantum Hall effect and enhanced g factor in quantum-confined Cd_3As_2 films. **2022**, 106, ○
- 79 Lifshitz transitions and hybrid Weyl points in RbAg_5Se_3 . ○
- 78 Chiral Dirac-like fermion in spin-orbit-free antiferromagnetic semimetals. **2022**, 3, 100343 ○
- 77 Degenerate line modes in the surface and bulk phonon spectra of orthorhombic NaMgF_3 perovskite. **2022**, 121, 192201 ○

- 76 Topologically protected surface states in TaPdTe5. **2022**, 1,
- 75 A newly designed femtosecond KBe₂BO₃F₂ device with pulse duration down to 55 fs for time- and angle-resolved photoemission spectroscopy. **2022**, 93, 113910
- 74 Tunable interface states between Floquet-Weyl semimetals. **2022**, 106,
- 73 Fine details of sixfold Dirac fermions in pyrite-structured PdSb₂. **2022**, 106,
- 72 Topological hinge modes in Dirac semimetals. **2023**, 18,
- 71 Recent advances in photonics of three-dimensional Dirac semimetal Cd₃As₂. **2022**, 1,
- 70 Magneto-optical conductivity of nodal link semimetals. **2022**, 132, 193903
- 69 Investigation of 3D Dirac semimetal supported terahertz dielectric-loaded plasmonic waveguides. **2022**, 74, 125702
- 68 Dirac Nodal Line in Hourglass Semimetal Nb₃SiTe₆.
- 67 Enhanced and tunable Goos-Hänchen shift of reflected light due to Tamm surface plasmons with Dirac semimetals. **2022**, 43, 106105
- 66 Two -dimensional semimetal AlSb monolayer with multiple nodal-loops and extraordinary transport properties under uniaxial strain.
- 65 Single crystal growth of topological semimetals and magnetic topological materials. **2023**, 0
- 64 A dispersion-corrected DFT method for zeolite-based CO₂/N₂ separation: Assessment and application. **2023**, 11, 109052
- 63 First-principles study of topological surface states and pressure induced phase transitions in a novel noncentrosymmetric superconductor PbTiSe₂. **2023**, 218, 111982
- 62 Topology and Symmetry in Quantum Materials. 2201058
- 61 ??????????????????. **2022**,
- 60 Wire construction of class DIII topological crystalline superconductors in two dimensions. **2022**, 106,
- 59 On the Z₂ topological invariant.

- 58 Electronic and magnetic properties of the topological semimetal SmMg₂Bi₂. **2022**, 106, ○
- 57 Enhanced photonic spin Hall effect in Dirac semimetal metamaterial enabled by zero effective permittivity. **2023**, 34, 105201 ○
- 56 Enhanced Absorption in One Dimensional Photonic Crystal with Three Dimensional Dirac Semimetals. ○
- 55 Triple hourglass Weyl phonons. **2022**, 106, ○
- 54 Symmetry-enforced planar nodal chain phonons in non-symmorphic materials. **2022**, 132, 224401 1
- 53 Nodal higher-order topological superconductivity from a C₄-symmetric Dirac semimetal. **2022**, 106, ○
- 52 Observation of Spin-Tensor Induced Topological Phase Transitions of Triply Degenerate Points with a Trapped Ion. **2022**, 129, ○
- 51 Anomalous symmetry breaking in the Weyl semimetal CeAlGe. **2022**, 106, ○
- 50 Multiple-symmetry-protected lantern-like nodal walls in lithium-rich compound LiRuO₂. 10, ○
- 49 Spin-momentum locking from topological quantum chemistry: Applications to multifold fermions. **2022**, 106, ○
- 48 Unraveling nodal-line semimetallic phase in SrIrO₃ by terahertz quasiparticle dynamics. **2022**, 106, ○
- 47 Charge instability of topological Fermi arcs in chiral crystal CoSi. **2023**, ○
- 46 Single crystal growth of topological semimetals and magnetic topological materials. **2023**, 72, 038101 ○
- 45 Spin-Lattice and Magnetoelectric Couplings Enhanced by Orbital Degrees of Freedom in Polar Multiferroic Semiconductors. **2023**, 130, ○
- 44 Engineering second-order nodal-line semimetals by breaking PT symmetry and periodic driving. **2023**, 107, ○
- 43 Signatures of Topological Surface State and Unconventional Magnetotransport Properties in Elemental Ruthenium. 2200116 ○
- 42 Tunable bi-direction terahertz vortex beam generator based on Dirac semimetals. **2023**, 129279 ○
- 41 Exceptional point in tunable terahertz metasurface based on bulk Dirac semimetal. **2023**, 16, 012011 ○

- 40 Topological properties of half Heusler compounds: Tuned by the spin-orbit coupling and p-d hybridization. **2023**, 460, 128612
- 39 Dirac semimetal like transport features in high-quality Bi_{0.96}Sb_{0.04} thin films. **2023**, 768, 139691
- 38 High-throughput first-principle prediction of collinear magnetic topological materials. **2022**, 8,
- 37 Signature of weakly coupled f electrons and conduction electrons in magnetic Weyl semimetal candidates PrAlSi and SmAlSi. **2023**, 107,
- 36 Topogivity: A Machine-Learned Chemical Rule for Discovering Topological Materials. **2023**, 23, 772-778
- 35 Ni-Intercalation-Induced Topological Nodal Line States and Superconductivity in NiTe. **2023**, 127, 4303-4309
- 34 Superconducting properties and gap structure of the topological superconductor candidate Ti₃Sb. **2023**, 107,
- 33 Engineering a pure Dirac regime in ZrTe₅. **2023**, 14,
- 32 Magneto-optical conductivity of nodal loop semimetals. **2023**, 466, 128694
- 31 Quantum transport in topological semimetals under magnetic fields (III). **2023**, 18,
- 30 Topological semimetal phases in a family of monolayer X₃YZ₆(X=Nb,Ta, Y=Si,Ge,Sn, Z=S,Se,Te) with abundant nodal lines and nodes. **2023**, 149, 115679
- 29 Reversal of the chiral anomaly bulk states with periodically staggered potential. **2023**, 107,
- 28 Photonic Band Inversion and Absorption Enhancement in Dirac Semi-Metal Tamm Plasmon Multilayer System. **2023**, 11,
- 27 Topological nature of large bulk band gap materials Sr₃Bi₂ and Ca₃Bi₂. **2023**, 98, 035813
- 26 Synthesis and Crystal Structure of the Zintl Phases NaSrSb, NaBaSb and NaEuSb. **2023**, 16, 1428
- 25 Anomalous magnetotransport behavior in single-crystal VSb₂. **2023**, 107,
- 24 Topology of three-dimensional Dirac semimetals and quantum spin Hall systems without gapless edge modes. **2023**, 5,
- 23 Quantum oscillations as a robust fingerprint of chiral anomaly in nonlinear response in Weyl semimetals. **2023**, 107,

- 22 First-principles theoretical analysis of magnetically tunable topological semimetallic states in antiferromagnetic DyPdBi. **2023**, 107, ○
- 21 Non-Hermitian Weyl fermions of types III and IV: Hamiltonian, topological protection, and Landau levels. **2023**, 107, ○
- 20 Magnetic tuning of band topology evidenced by exotic quantum oscillations in the Dirac semimetal EuMnSb₂. **2023**, 107, ○
- 19 Intrinsic magnetic topological materials. **2023**, 18, ○
- 18 Transverse Peierls Transition. **2023**, 13, ○
- 17 First Principles Computation of New Topological B₂X₂Zn (X = Ir, Rh, Co) Compounds. **2023**, 6, 152-163 ○
- 16 Strategies to break the trade-off between infrared transparency and conductivity. **2023**, 136, 101112 ○
- 15 Anomalous Positron Lifetime in Single Crystal of Weyl Semimetal CoSi. **2023**, 13, 509 ○
- 14 Symmetry-Enforced 2D Hourglass Phononic Nodal Net. ○
- 13 Single crystal synthesis and low-lying electronic structure of V₃S₄. **2023**, 949, 169776 ○
- 12 Attosecond magnetization dynamics in non-magnetic materials driven by intense femtosecond lasers. **2023**, 9, ○
- 11 Multi-Dimensional Topological Fermions in Electrides. ○
- 10 Tunable multichannel Fibonacci one-dimensional terahertz photonic crystal filter. **2023**, 13, ○
- 9 Quantum magnetoresistance of Weyl semimetals with strong Coulomb disorder. **2023**, 107, ○
- 8 High sensitivity HgTe room temperature terahertz photodetector. **2023**, 8, 046109 ○
- 7 First-principles calculations to investigate optical properties of topological semimetal MX compounds (M = Ti, Zr, Hf and X = S, Se, Te). **2023**, 106001 ○
- 6 Quantum kinetic theory of nonlinear optical currents: Finite Fermi surface and Fermi sea contributions. **2023**, 107, ○
- 5 Multiple Magnetic Topological Phases in the van der Waals Crystal Mn(Bi,Sb)₄Se₇. 3913-3919 ○

- 4 Electromagnetic Metamaterials: From Classical to Quantum. **2023**, 1, 1-33 ○
- 3 Observation of gapless nodal-line states in NdSbTe. **2023**, 7, ○
- 2 Unconventional Charge-Two Weyl Phonons in High-Symmetry Lines. ○
- 1 Robust three-dimensional type-II Dirac semimetal state in SrAgBi. **2023**, 8, ○